2020

Quantitative Imaging of Cell-Level Auxin Cytokinin Outputs in Soybean and Model Plants

Paul Gaillard
South Dakota State University

QUANTITATIVE IMAGING OF CELL-LEVEL AUXIN-CYTOKININ OUTPUTS IN SOYBEAN AND MODEL PLANTS

BY

PAUL GAILLARD

A dissertation submitted in partial fulfillment of the requirements for the

Doctor of Philosophy

Major in Plant Science

South Dakota State University

2020

DISSERTATION ACCEPTANCE PAGE

Paul Gaillard

This dissertation is approved as a creditable and independent investigation by a candidate for the Doctor of Philosophy degree and is acceptable for meeting the dissertation requirements for this degree. Acceptance of this does not imply that the conclusions reached by the candidate are necessarily the conclusions of the major department.

Senthil Subramanian
Advisor Date

David Wright
Department Head Date

Dean, Graduate School Date

To my family, friends, mentors, and inspiration…

He arrived in this world full of wonder and curiosity. He was told, “Winter is harsh here. Stay away from the snow that buries and the frost that bites”. All he could see was suns like dogs, snows like dunes and flakes like crystals. All he could hear was the silence; no breath in the plains. He sat, contemplated, and waited. Suspended at the fragility of time, he fainted in the dark. Words floated and soon surrounded him. Words became sentences and sentences became songs. All he could feel was the earth beating on his feet, in his hands, and through his heart. He knew his time had arrived. He stood up, gathered his thoughts, and stepped. How long did he stay? He could not tell.

All he could remember was the warmth in his heart. He started to hear again the voices of his people, the smells of food roasting on the fire, the games late into the night, the laughs, the hugs and the smiles. He was now able to read in the sky and breath among the stars. Soon, his whole body was fired by memories and irradiated with gratitude. As he recalled the beloved faces, his full heart burst into tears. Joy flowed from his eyes and flooded the plains. Soon, all the ice melted, and the sun started to rise. As the water receded, deer started to jump, pheasants flew, rabbits ran, and slugs crawled. All were celebrating the return of Spring. He was now ready to leave. He looked back, acknowledged the moments, and started to walk away. He felt pure joy and ecstasy. He was filled with wonder and curiosity. “

ACKNOWLEDGMENTS

I would like to acknowledge that South Dakota State University is located within the ancestral territory of the Oceti Sakowin (Seven Council Fires), an alliance that consists of the Santee-Dakota,Yankton-Nakota, and Teton-Lakota peoples. By offering this land acknowledgement, I affirm Indigenous sovereignty, history, and heritage.

I would like to express my gratitude towards my advisor, Assoc. Pr. Senthil Subramanian for his continual help, support, and encouragement. We not only had a very successful scientific collaboration, but we also savored an enriching human adventure ("should we say symbiotic interaction?! Haha"). To you I say "I will always be grateful for the offer of PhD training and your presence in the good and bad moments. Thank you, Sen."

I would like to express my hearty thanks to our close collaborators from South Dakota School of Mines & Technology: Pr. Steve Smith, Dr. Jon Fisher and Ni Putu Dewi Nurmalasari for their contributed expertise and unique perspective. "Without you this dissertation wouldn't have been possible."

I would like to express thanks to my committee members Pr. Anne Fennell, Pr. Michael Hildreth and Assoc. Pr. Gregory Michna. "Thank you for your advice and assistance."

I would like to thank my teachers for knowledge provided, their pedagogy and their time and effort invested.

I would like to thank SDSU Genomics lab, my funding agency, and Assis. Pr. Darci Fink for supporting my work and contributing to its excellence.

I offer reverent and hearty thanks to Dr. Carl Fellbaum for being a friend, a collaborative labmate and project initiator. “I hope that you’re proud of the work we invested and landmark discoveries we achieved.”

I could not write this acknowledgment without mentioning my labmates-friends! Thank you to Dr. Sajag Adhikari, Dr Shuchi Smita, Dr. Carl Fellbaum, Dr Laura White, Dr Suresh Damodaran, Spencer Schreier, Sunita Patak, Sadikshya Aryal, Pratiksha Kc, Dr. Bhanu Prakash Petla, Dr. Kevin Cope, Jaya Yakha, Jesus Loya, Nadee Kalawahandi, Dr. Marina Johnson, Dr. Sonya Erlandson, Mucahid Bozkus, Lilia Montañez, Athira Nair and Saeid Khaleghi. I’m also including Dwarika Bhattarai. “You might not have worked for Sen’s Lab, but you’ve always been intrinsic to it and you’re definitely a friend. Thank you for all the good times, parties, games, movies, trips, and memories we created together. I might not be the best at Rummikub but I’m sure my Biryani is darn delicious! Thank you so much for your laughs and support. Symbiosis Soirée 2019 was awesome, I can’t wait for Symbiosis Soirée 2020. No worry Bhanu, we will meet again, perhaps on a new continent this time!

I would like to recognize undergraduate students Kaitlyn Cihoski, Quinn Hunter, and Ian Hastings for helping me in this work.

I express my appreciation towards the community of Brookings for their support and hospitality and to the organizations I’ve been part of. Thanks to the Brookings

Toastmasters Club 3712. “We had such a fun time learning and growing together; it was a privilege to meet every one of you.” Also, thanks to the Satyagraha Institute. “Carl Kline, your program changed my life and I will always remember your kindness.”

I would like to express my gratitude to Assoc. Pr. Melissa Hauschild-Mork. “Your art enlightened my heart and deepened my soul. Thank you for sharing your passion and offering me the space to meet with and express my true self.”

I would also like to express my hearty thanks to Bill and Julie Ross for welcoming me to Good Roots Farm & Gardens, LLC. We had such a great time together and thanks to you my stay was very fruitful and “veggieful”. “Thank you for inviting me into your family; now it’s your turn to visit mine in France!” I also want to express my affection towards Good Roots community and specially Louise Snodgrass and Evan Ross for being such amazing friends. “I can’t wait to see you again!” I also want to thank my Kaj Lynoe. “Spending these days of confinements with you was quite an adventure!”

I want to thank my friends Momo and Romain. “How did you manage to have a baby while I was gone?”, “Rouges, I would have never expected you to visit me. You did it twice. Kudos to you!”, Annick Berbesson, “Thank you for your continuous support, your friendship and our commons dreams” and Noëlle Truehart “Thanks for believing in me and sharing endless laughs and conversations”.

I want to thank everyone that was present during my Final Oral Exam PhD. That was quite an adventure to do it over Zoom and having you all was such an honor.

Finally, I would like to express love and gratitude towards my parents. “Thank you for your presence, your encouragement and affection; No worries, I’m coming soon!”

TABLE OF CONTENTS

LIST OF FIGURES

ABSTRACT

QUANTITATIVE IMAGING OF CELL-LEVEL AUXIN-CYTOKININ OUTPUTS IN SOYBEAN AND MODEL PLANTS

PAUL GAILLARD

2020

Auxin and cytokinin are major plant hormones that orchestrate plant development. These hormones are involved in cell division and differentiation and their spatio-temporal balance controls organ initiation and maturation. Even though independent transcriptional responses to these hormones have been characterized, their concomitant outputs have not been described. We developed methodology to determine auxin-cytokinin relative output (ACRO) ratios at cellular resolution. Hormone-specific fluorescent markers that localize to the nucleus were used to report transcriptional outputs of auxin and cytokinin. Multiphoton microscopy and image data processing were used to quantify their relative ratio at cellular level in three-dimensional tissue volumes. This strategy was successfully applied to soybean (*Glycine max*) and two model plant species, *Arabidopsis thaliana* and *Medicago truncatula* to evaluate ACRO ratios in different organs of interest. The ACRO ratios estimated in soybean and Medicago root tips and lateral roots in this study agreed with previously reported outputs for each fluorescent reporter individually, suggesting that the method is reliable and accurate. Soybean and Medicago are legumes that can produce root nodules through a symbiotic partnership with nitrogen-fixing bacteria. Six soybean nodule developmental stages were studied and presented exclusive ACRO ratios patterns indicating a fine cell-specific regulation. We hypothesize that auxin bursts promote pattern initiation and cytokinin bursts promote cell differentiation. Based on ACRO ratios in

nodules of soybean roots with reduced sensitivity to auxin, we speculated that lower auxin-cytokinin balance in nodule initials allows development of more primordia into nodules but delay their maturation. Similar ACRO ratios in infection zones and vascular bundles of soybean and Medicago nodules suggested a conserved role for auxin and cytokinin in these species that produce two different types of nodules. Evaluation of ACRO ratios in Arabidopsis roots treated with different concentrations of auxin or cytokinin revealed that the sensor responds to auxin in a dose-dependent manner and to cytokinin in a cell type-specific manner. Understanding the role of auxin and cytokinin balance in organ development can help improve plant productivity. For example, creating plants with more nodules that fix for a for a longer period could increase the soybean production in an ecofriendly manner.

CHAPTER I

1. Introduction

1.1. Plant nodule a reliable source of nitrogen

1.1.1. Biological nitrogen fixation

Nitrogen, being a component of major biomolecules such as nucleotides and amino acids, is essential for the survival of all living organisms. While heterotrophic organisms (e.g animals) can find nitrogen in their diet, autotrophic organisms (e.g. plants) uptake nitrogen primarily from the soil and water. However, the availability of nitrogen in the environment is highly variable and can be a crucial limiting factor. To overcome this restriction, plants have developed multiple strategies over their evolution. One of these is biological nitrogen fixation (BNF) that appeared 3.3 billion years ago in a group of prokaryotic organisms in response to a high ammonium (NH_4^+) deficiency in the environment, reviewed by (Towe 2002). Plants obtain nitrogen from these prokaryotes through different means.

These interactions can be divided into three different categories: free-living nitrogen fixation, associative nitrogen fixation and symbiotic nitrogen fixation.

Azotobacter, *Beijerinckia*, and *Clostridium* are examples of free-living bacteria in soil. These diazotrophic bacteria encode for nitrogenase, an enzyme that converts dinitrogen gas to ammonia (NH_3) (Santi, Bogusz et al. 2013). Nitrogenase is inhibited by dioxygen, and free-living nitrogen-fixers have adopted several strategies to overcome this oxygen restriction. Some are anaerobic while others are associated to create micro-colonies containing heterocyst, a specific cell type with thick cell walls that prevent oxygen diffusion. Associative nitrogen fixing organisms include diazotrophic bacteria that live in contact with plants. These forms can be classified into different groups based on their degree of sophistication and closeness.

The most rudimentary types are represented by diazotrophic bacteria that live either outside (i.e. epiphyte) or inside (i.e. endophyte) of the plant in an extracellular fashion. This association is often correlated with higher plant biomass when nitrogen availability is limited (James 2020). The most elaborate and efficient BNF form is encountered in the endosymbiotic relation between plants and compatible bacteria that result in formation of root nodules, specialized organs dedicated to symbiotic N fixation.

Root nodules provide an oxygen-regulated environment for efficient functioning of nitrogenase and plants provide carbohydrates to the bacteria in exchange for nitrogen (Oldroyd, Murray et al. 2011). Nodule symbiosis falls in two categories, the legume family (*Fabaceae*) associated with rhizobia bacteria and eight angiosperm families (*Betulaceae*, *Casuarinaceae*, *Elaegnaceae*, *Myriaceae*, *Rhamnacea*, *Rosacea*, *Datiscaceae* and

Coriariaceae) interacting with *Frankia* filamentous bacteria in the context of actinorhizal symbiosis.

1.1.2. Different nodule types

Legume nodules can be divided into two main categories based on their site of primordium initiation and meristem persistence:(i) determinate nodules that initiate in the outer cortex and have a transient meristem resulting in a spherical nodule in which most of the tissues are at the same developmental stages; and (ii) indeterminate nodules that initiate in the inner cortex and have a persistent meristem, engendering an oblong nodule shape where the apex has mitotic activity. Each young cell produced by the meristem enter in a differentiation program and each differentiation stages are present in a mature indeterminate nodule, reviewed by (Ferguson, Indrasumunar et al. 2010). Determinate nodules are present in plants such as soybean (*Glycine max*) and the model plant *Lotus japonicus*, whereas indeterminate nodules are produced by plants such as barrel clover (*Medicago truncatula*) and white cover (*Trifolium repens*).

1.2. Nodule development

1.2.1. Early responses and rhizobia infection

The association between legumes and the diazotrophic bacteria rhizobia begins with a chemical dialog between the symbiotic partners and is determined by their respective spectra of specificity. During this process, nitrogen-deficient legumes release flavonoids in their rhizosphere. These flavonoids induce the production of lipochitooligosaccharide molecules termed Nod Factors (Lerouge, Roche et al. 1990, Abdel-Lateif, Bogusz et al. 2012) in compatible rhizobia bacteria in close proximity to plant root hairs. These NFs are perceived by plant receptors Nod factor receptor 1 and 5 (NFR1 and NFR5), and the signal is transduced to Symbiosis Receptor Kinase (SYMRK), a leucine-rich repeat (LRR) receptor kinase. It triggers the action of two potassic channels located on the nuclear membrane (CASTOR and POLLUX) and two nucleoporins (NUP85 and NUP133) inducing a specific calcium spiking signature. This calcium signaling is decoded by a Calcium/calmodulin-dependent protein kinase (CCaMK, Marsh et al., 2007) induces two parallel responses involving two related signaling cascades.

The first one results in the formation of an “infection thread” (IT) that transports rhizobia into the root cortex and primarily involves the phosphorylation of the transcription factor CYCLOPS by CCaMK. During this process, root hairs follow a deformation and curling that confine the micro-colony into an infection pocket. Plant and bacteria enzymes degrade plant cell walls and invagination of the plant plasma membrane forms an IT that carries rhizobia to root cortex cells that are diving to form the incipient nodule primordium (Capoen, Den Herder et al. 2007).

The second one involves LHK1 (Lotus Histidine Kinase 1), a cytokinin receptor and transcription factors (TFs) such as NSP1, NSP2, ERN1 and NIN (NODULATION SIGNALING PATHWAY 1, NODULATION SIGNALING PATHWAY 2, ETHYLENE RESPONSE FACTOR REQUIRED FOR NODULATION1 and NODULE INCEPTION) that initiates nodule organogenesis, reviewed by (Kouchi, Imaizumi-Anraku et al. 2010, Suzaki, Ito et al. 2013). Therefore, in parallel to the progression of the IT containing rhizobacteria in the epidermis, a nodule primordium forms at the root cortex. Infection and organogenesis responses and most of the signaling components involved are highly conserved between determinate and indetermination nodule forming legumes, reviewed by (Kouchi, Imaizumi-Anraku et al. 2010).

1.2.2. Primordium development, nodule and bacteria maturation

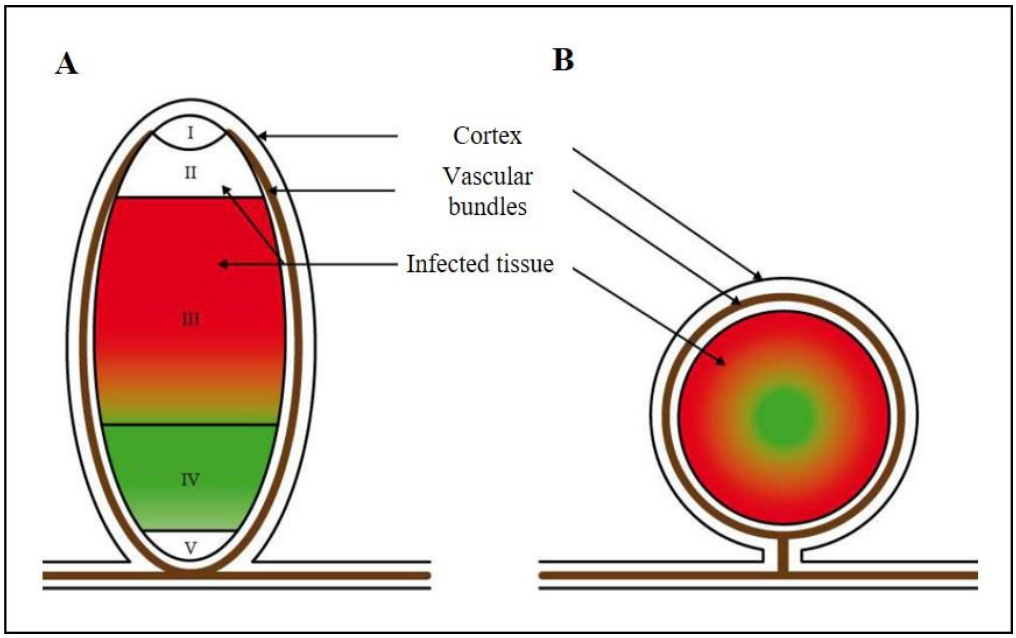

Figure 1.2.2-1: Comparison of indeterminate and determinate nodule morphology. *(A): representation of indeterminate nodule comprising five different tissues zones. I: apical meristem, II: infection and differentiation zone, III: fixation zone, IV: senescent zone and V: saprophytic zone. (B): representation of determinate nodule. Both nodule types are surrounded by a cortical cell layer, have vascular bundles represented with a brown line and central infected tissues. Red color represents zones of high nitrogen fixation and green indicates the absence of fixation as the nodules enter in a senescence program. Adapted from Dupont et al. 2012.*

Once the IT has reached the primordium, bacteria are release via endocytosis into plant membrane-derived vesicles called symbiosomes. There, rhizobia are differentiated into bacteroids via endoreduplication and undergo morphological changes to more efficiently convert atmospheric dinitrogen into NH_3. The morphological differences observed between determinate and indeterminate nodule result from a different cell fate programming during organogenesis. In determinate nodules, anticlinal cell division initiates in the outer cortex and later in the pericycle and inner cortex to form the primordia, reviewed by (Ferguson, Indrasumunar et al. 2010). Outer cortical cells give rise to the central tissue and the pericycle and inner cortex cells differentiate into the parenchyma surrounding the central zone. Nodule vasculature forms from the root vasculature towards the base of the nodule parenchyma and branches out in the mature nodule periphery.

As meristematic activity ceases at the primordia stage, nodule maturation is the consequence of primordia cell elongation and results in a spherical nodule. Mature

determinate nodule can be divided into the central and the peripheral regions (Figure 1.2.2-1). The central zone or infection zone consists of rhizobia-infected cells where the atmospheric nitrogen is fixed. The peripheral region is composed of the vasculature embedded in a parenchyma, surrounded by the endodermis and a nodule cortex. The nodule vasculature is connected to the root vasculature to provide the fixed nitrogen to the plant.

Indeterminate nodule organogenesis involves anticlinal cell divisions in the inner cortex and later in the pericycle, reviewed by (Ferguson, Indrasumunar et al. 2010). The apical persistent meristem allows cell division at the mature stage which results in an elongated oblong structure comprised of different zones (Figure 1.2.2-1). Zone I represents the meristematic zone in which cells are continuously dividing. Zone II correspond to the infection zone, in zone III rhizobia are differentiated into bacteroids, this is the nitrogen fixation zone. Zone IV is the senescence zone, and Zone V is the saprophytic zone (Figure 1.2.2-1), reviewed by (Gage 2004, Ferguson, Indrasumunar et al. 2010). These zones are in the nodule central zone and surrounded by parenchyma traversed by vascular bundles (Bond 1948, Newcomb 1976). Once determinate nodules start senescence the entire nodule senesce, and it then replaced by a nodulation event. Interestingly, indeterminate nodule has a relatively less branched vasculature system than determinate nodule and determinate nodules can be covered by lenticels which helps in gas exchange. Over the course of infection, nodule organogenesis and nodule growth, hormones like auxin and cytokinin play a central role in both nodule types.

1.3. Auxin during nodulation

Auxin plays a significant role at every step of the nodulation process including, the early epidermal and root hair response, the initial cortical cell division and nodule maturation.

During rhizobia invasion auxin-responsive marker gene expression patterns suggest a rapid auxin response in the root hair cells. This induction is necessary for successful infection in Medicago and *L. japonicus* and can also be induced by Nod factor treatment (Breakspear, Liu et al. 2014, Nadzieja, Kelly et al. 2018). It is followed by a local auxin accumulation in the root cortex at the site of an incipient nodule primordium in both nodule types (Wasson, Pellerone et al. 2006, Suzaki, Ito et al. 2013). In mature determinate and indeterminate nodules, auxin response is absent/undetectable in the infection zone but is clearly detected in the vascular bundles. In the case of indeterminate nodule, auxin response has also been detected in the meristem, reviewed by (Kohlen, Ng et al. 2017). There are multiple ways to regulate the auxin action, 1. auxin biosynthesis, 2. auxin inactivation, 3. auxin signaling, 4. auxin signaling regulation via microRNA and 5. auxin transport.

1.3.1. Auxin biosynthesis

The major auxin biosynthesis pathway in plants involves the conversion of tryptophan into indole-3-pyruvic acid (IPA) by the TRYPTOPHAN AMINO-

TRANSFERASE RELATED (TAR) genes family members, followed by conversion of IPA into Indole-3-acetic acid (IAA) by members of the YUCCA (YUC) gene family (Mashiguchi, Tanaka et al. 2011). IAA is the prevalent chemical form of auxin, however other forms like phenyl acetic acid (PAA) and indole butyric acid (IBA) have been identified. Interestingly, LjTAR1 expression is Nod factor dependent and transcriptome data reported its induction after bacteria inoculation and Nod factor treatment (Nadzieja, Kelly et al. 2018). MtTAR2 is also up-regulated following Nod factor treatment (Herrbach, Chirinos et al. 2017).

In soybean, GmYUC2A expression is also induced by *Bradyrhizobium diazoefficiens* infection and observed in nodule tissues. Lines overexpressing GmYUC2A produce more auxin and have a defect in root hair development, delayed nodule maturation and a reduced nodule number (Wang, Yang et al. 2019). In Medicago YUCCA expression is also induced early after *Sinorhizobium meliloti* (*S. meliloti*) inoculation. The two keys steps involved in auxin biosynthesis are induced during the legume/rhizobia interaction and proper auxin production is required for nodule formation.

1.3.2. Auxin inactivation

The pool of active auxin is regulated by conjugation and/or degradation involving genes like GRETCHEN HAGEN 3 (GH3), UDP-GLUCOSYLTRANSFERASES (UGT), and DIOXYGENASE FOR AUXIN OXIDATION1 (DAO1), reviewed by (Staswick,

Serban et al. 2005, Muller and Leyser 2011). DAO1 is involved in IAA oxidation and UGT in IAA-amino acid conjugation. GH3 enzymes catalyze IAA-amino acid conjugation and alter the free (active) IAA pool (Staswick, Serban et al. 2005). Indeed, in Medicago GH3 genes are synergistically upregulated by Nod Factors and auxin treatments (Herrbach, Chirinos et al. 2017).

It is proposed that auxin can be inactivated in the root epidermis by GmGH3-14 and in the nodule primordium by GmGH3-15 (Damodaran, Westfall et al. 2017). Silencing GH3 genes impacts nodule numbers, maturity, and size. Symbiotic bacteria can also modify auxin's pool; however, their role is still unclear (Torres, Benavidez et al. 2018). Even though rhizobial auxin is essential for proper infection for at least determinate nodules (Fukuhara, Minakawa et al. 1994), *B. diazoefficiens* may also be able to degrade IAA and could potentially negatively regulates auxin pool in the infection zone of mature nodule (Torres, Benavidez et al. 2018). It appears that auxin level is controlled by inactivation during the infection and nodule primordium formation. Auxin biosynthesis and inactivation being observed at similar stages, this indicates a very tight regulation of the active pool of auxin to enable proper nodulation.

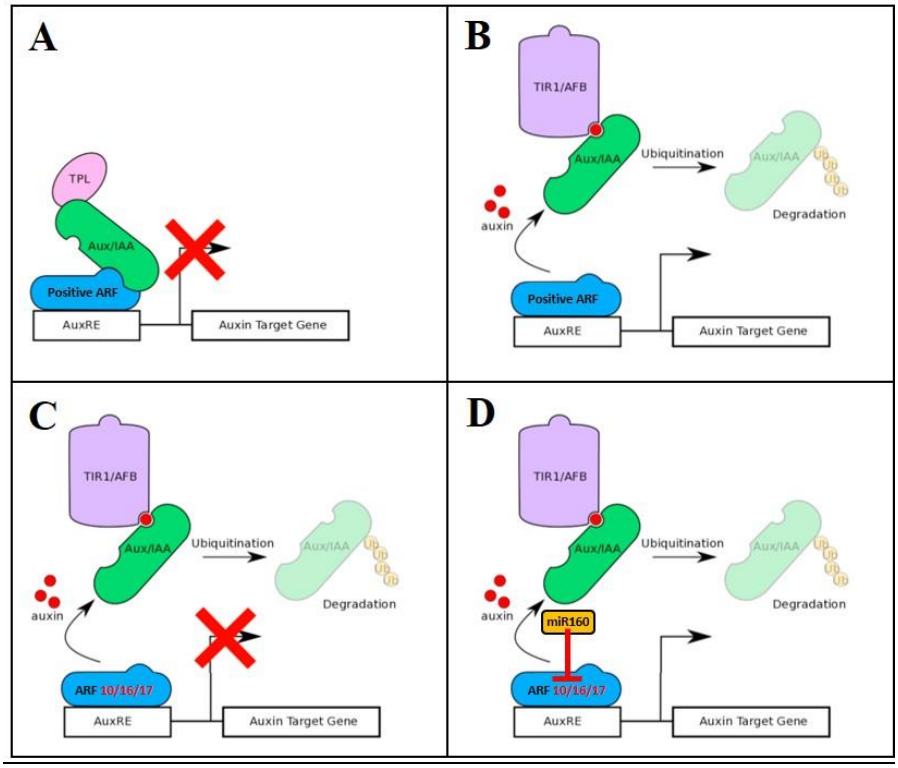

Figure 1.3.2-1: Auxin signaling pathway's regulation by ARF 10/16/17 and miR160. *(A) In absence of auxin positive ARF activity is suppressed by Aux/IAA and TPL. (B) In presence of auxin Aux/IAAs is ubiquitinated to TIR1/AFBs and degraded by the proteasome activity. Hence, positive ARF can induce the transcription of auxin response genes. (C) ARF 10/16/17 are negative regulators preventing the expression of auxin response genes in presence of auxin. (D) miR160 can target and repress ARF 10/16/17 to promote auxin response genes transcription in presence of auxin. Adapted from (Taylor-Teeples, Lanctot et al. 2016).*

1.3.3. Auxin signaling

The response to auxin is mediated by three groups of proteins: AUXIN RESPONSE FACTORs (ARFs), AUXIN/INDOLE-3- ACETIC ACID (Aux/IAA) and TRANSPORT INHIBITOR RESISTANT 1/AUXIN SIGNALING F-BOX (TIR1/AFB). ARFs are transcriptional activators or repressors that can respectively induce or inhibit the expression of early auxin response genes (Figure 1.3.2-1b and 1.3.2-1c). The Aux/IAA family includes repressors proteins that can act in association with the co-repressor TOPLESS (TPL) and inhibit ARF activity through dimerization and repress the expression of auxin response genes (Figure 1.3.2-1a). In presence of auxin, the Aux/IAA proteins are be degraded by the auxin receptor F-box proteins such as TRANSPORTER INHIBITOR RESPONSE1 (TIR1) to regulate plant development. Altering auxin signaling can result in nodulation phenotypes.

For example, overexpression of the soybean GmTIR1/GmAFB3 genes increases the number of infection events and nodules (Cai, Wang et al. 2017). During early infection of Medicago by *S. meliloti*, ten ARFs are suppressed, while ten others are upregulated (Shen, Yue et al. 2015). In Medicago, auxin signaling components like ARF16a and IAA9, are induced at infection sites and nodule primordia by Nod Factors, or *S. meliloti* and a mutation in MtARF16a reduces the number of infection threads (Breakspear, Liu et al. 2014). In soybean, GmARF8a/b silenced plants have less nodules (Wang, Li et al. 2015). ARFs are major actors of the auxin signaling pathway and positives and negative auxin response regulators are controlling nodulation. Moreover, other component of the auxin

signaling regulation such as TIR1 and IAAs are also implicated in this regulation, emphasizing the crucial role of proper and flexible auxin response during nodulation.

1.3.4. Auxin signaling regulation via microRNA

microRNAs (miRNAs) are 21 to 22 nucleotides long sequences that regulate transcripts in cleaving mRNA or inhibiting their translation reviewed by (Axtell 2013). They regulate plant development by fine-tuning expression levels of different transcription factors and other target genes. miRNAs that regulate auxin signaling have been identified in both determinate and indeterminate nodule-forming legumes. Specific auxin signaling actors are also regulated by microRNA to provide in a very fine and adaptable control of auxin responses during nodule development. Additionally, the miR390/TAS3 pathway relies on miR390 to produce Trans-Acting small interfering RNA (siRNA) and repress ARF2/ARF3/ARF4 (Marin, Jouannet et al. 2010).

GmmiR167 represses the expression of positive auxin response factors GmARF8a and GmARF8b and is expressed in the infection zone of soybean to positively regulate nodule number (Wang, Li et al. 2015). While miR160 represses the negative ARF10/16/17 family, is expressed in the majority of soybean mature nodule and its action is required for proper nodule maturation (Figure 1.3.2-1d). Taken together, in determinate nodule, auxin action is repressed via miRNA167 in the infection zone and miR160's partial and indirect activation of the auxin pathway is very localized (Nizampatnam, Schreier et al. 2015,

Wang, Li et al. 2015). miR393 regulates the auxin receptor GmTIR1/AFB3, and its role on nodule development is still unclear. In composite soybean plants where the cassava vein mosaic virus (CsVMV) CVP2 promoter is used to overexpress miR393 in the roots, these auxin hyposensitive roots are not altered in nodule number (Turner, Nizampatnam et al. 2013). However, in transgenic roots where the Cauliflower mosaic virus 35S (CaMV35S) promoter is used to overexpress miR393d, nodule number is decreased (Cai, Wang et al. 2017). This dissimilitude might be due to different expression level strengths and tissue specific variation between the CVP2 and CaMV35S promoters.

In indeterminate nodules, miR390 indirectly targets ARF2, ARF3, and ARF4. Its expression has been observed in vascular bundles and nodule meristem of Medicago and inhibits nodule organogenesis and rhizobial infection. In *M. truncatula*, overexpression of miR160 (Bustos-Sanmamed, Mao et al. 2013), miR166 (Boualem, Laporte et al. 2008), miR171h (Hofferek, Mendrinna et al. 2014) miR169 (Combier, Frugier et al. 2006), and miR164 (D'Haeseleer, Den Herder et al. 2011), which target the ARF 10/16/17, HD-Zip, NSP2, NF-YA1, and NAC1, respectively, reduced nodule number. The repression of positive or negative ARFs by microRNA provides a very contextual and target specific layer of regulation to control auxin level to enable nodule formation.

1.3.5. Auxin transport

Auxin transport is another way to regulate the available auxin pool. Polar auxin transport (PAT) is regulated by auxin influx AUXIN1/LIKE-AUX1 (AUX/LAX) family carriers and auxin efflux PIN-FORMED (PIN) family carriers, reviewed by (Friml 2003). PAT varies between indeterminate and determinate nodule during their respective initiation. During the initiation of indeterminate nodule, acropetal auxin transport inhibition leads to auxin accumulation at the start of nodule initiation in the pericycle, endodermis, and inner cortex cells (Ng and Mathesius 2018). Moreover in Medicago, synthetic auxin transport inhibitors such as 2,3,5-triiodobenzoic acid or 1-N-naphthylphthalamic acid induce pseudo-nodule even in the absence of the *S. meliloti* (Hirsch, Bhuvaneswari et al. 1989). Auxin transport is strongly reduced 24 h after rhizobia infection at the initiation site of indeterminate nodules (Mathesius, Schlaman et al. 1998, Wasson, Pellerone et al. 2006) and Nod factors treatment reduced auxin transport within 4 h, with the strongest reduction from 24 to 48 h (Boot, van Brussel et al. 1999).

PIN genes seems to be involved in the auxin maximum creation during nodule initiation as silencing the expression of MtPINs resulted in fewer nodules (Huo, Schnabel et al. 2006). MtPIN9 is expressed at higher levels in the mature nodule when compared to roots tips and its expression level is altered in the *cytokinin response1* mutant (*cre1*) that have fewer and delayed nodules. In view of the high functional redundancy within PINs, no genetic approach has been able to identify PIN(s) specific to nodule maturation. Nevertheless, MtPIN2/3/4 showed a negative effect on nodulation in *M. truncatula* (Huo, Schnabel et al. 2006). De Billy reported that the auxin influx transporter MtLAX1 and

MtPINs belonging to the auxin exporter gene family are expressed during nodulation (de Billy, Grosjean et al. 2001). MtLAX2 a paralog of the Arabidopsis AUX1 is expressed in the early primordium, in the vascular bundles and in the nodule meristem apex of indeterminate nodules. MtLAX2 promotes nodule elongation, positively regulate nodulation (Roy, Robson et al. 2017) and the *Mtlax2* mutant presents defect of both infection thread formation and nodule development (Roy, Robson et al. 2017). Indeterminate nodule expansion may require auxin transporters to spatially regulate auxin accumulation for proper vascular bundle progression.

During the initiation of determinate nodule, the acropetal auxin transport is increased in *L. japonicus* (Ng and Mathesius 2018) and an auxin response is detected in the outer cortex. (Kohlen et al, 2018). Even though indeterminate and determinate nodules show an elevated auxin response in the cortical cells during the formation of a nodule primordium (van Noorden, Kerim et al. 2007, Takanashi, Sugiyama et al. 2011, Suzaki, Yano et al. 2012, Turner, Nizampatnam et al. 2013) their respective auxin transport control differs. Auxin transport inhibition is responsible of the auxin accumulation at the initiation of indeterminate nodules. Local auxin accumulations are sufficient to trigger nodule initiation in indeterminate nodules. In determinate nodules, the auxin maximum is also necessary but reached via mechanism(s) that is yet to be determined. Other hormones such as cytokinin are also playing a role in auxin and modulation regulation.

1.4. Cytokinin during nodulation

Cytokinin is a class of plant hormones known to regulate cell proliferation and differentiation. Exogenous cytokinin treatment induced pseudonodules in alfalfa (*M. sativa*; (Cooper and Long 1994)), white clover (*Trifolium repens;* (Mathesius, Weinman et al. 2000)), siratro (*M. atropurpureum*; (Relic, Talmont et al. 1993)), *Aeschynomene spp*. (Podlesakova, Fardoux et al. 2013), *L. japonicus* (Heckmann, Sandal et al. 2011), and in the non-legume alder (*Alnus glutinosa*; (RODRIGUEZ-BARRUECO and CASTRO 1973). Note that high cytokinin concentration treatments reduce nodule number, which is most likely due to hormone toxicity (e.g., elevated ethylene production; (Lorteau, Ferguson et al. 2001, Ferguson, Wiebe et al. 2005).

Cytokinin responses have been linked to cortical auxin responses in nodulating legumes but not in non-nodulating species (Gauthier-Coles, White et al. 2018). Trans-zeatin and isopentenyl adenine, the major endogenous cytokinin forms accumulate few minutes after rhizobial inoculation and Nod Factor treatment (van Zeijl, Op den Camp et al. 2015, Reid, Heckmann et al. 2016, Reid, Nadzieja et al. 2017). Cytokinin response using the synthetic TCSn reporter revealed that cytokinin pattern in nodule development is similar in both nodule type. In *L. japonicus*, the cytokinin-induced primordium initiates from the outer cortex (Szczyglowski, Shaw et al. 1998) and the third cortical cell layer (van Spronsen, Grønlund et al. 2001). In Medicago, initial cytokinin induction is reported in the

cortical and pericycle cells, the site of nodule initiation of indeterminate nodule (van Zeijl, Op den Camp et al. 2015).

The cytokinin response then spread to the epidermis in the case of *L. japonicus* (Held, Hou et al. 2014). In Medicago and *L. japonicus*, a cytokinin epidermal response is also observed after rhizobia inoculation (van Zeijl, Op den Camp et al. 2015, Reid, Nadzieja et al. 2017) and the initial cytokinin cortical peak is followed by a second peak in the nodule primordia once it is emerging from the root. In a mature determinate nodule, cytokinin is weakly detected in the nodule parenchyma and vasculature and also present in the infection zone (Fisher, Gaillard et al. 2018). Interestingly, the type A-RR Mt RR4 reporter cytokinin presence in the infection zone of indeterminate nodules (Dolgikh, Kusakin et al. 2020). Note that cytokinin seems to promote meristematic activity in cortical cells of the root during nodulation (Gamas, Brault et al. 2017), which is opposite to its role in root growth. There are multiple ways to regulate the cytokinin action, 1. cytokinin biosynthesis, 2. cytokinin activation and degradation 3. cytokinin signaling.

1.4.1. Cytokinin biosynthesis

Cytokinins are adenine species with an isoprenoid side chains in the N_6 and are synthesized by the ISOPENTENYL TRANSFERASE (IPT) and LONELY GUY (LOG) enzymes, reviewed by (Wybouw and De Rybel 2019). Isopentenyladenine (iP) and trans-zeatin (tZ) are the most important and abundant cytokinin compounds in plants. Cytokinin

biosynthesis is activated during nodulation in various legumes (Mortier, Wasson et al. 2014, Reid, Nadzieja et al. 2017, Dolgikh, Kirienko et al. 2019). Transcriptomic data report that members of gene families involved in cytokinin biosynthesis or activation, isopentenyl transferases (IPT), CYP735A and like LONELY GUYs (LOGs), are upregulated 3 h after Nod Factor treatment in Medicago (van Zeijl, Op den Camp et al. 2015).

IPT2 and KNOX3 a transcription factor that activates IPT3 are expressed in the root epidermis 24 h after Nod Factor external application in Medicago (Jardinaud, Boivin et al. 2016). In *L. japonicus*, the *LjIpt4* mutant plants have reduced nodule number, but overexpression of LjIpt3 or LjLog4 fails to produce pseudonodule (Reid, Nadzieja et al. 2017). Interestingly LjIpt2 and LjLog4 induction occurs independently of LjLhk1 suggesting that they might be involved in the initial cytokinin buildup. Therefore, cytokinins are produced during early infection invent and required for successful nodulation.

1.4.2. Cytokinin activation and degradation

MtLOG1 and MtLOG2 encode for cytokinin riboside 50-monophosphate phosphoribohydrolases that activate cytokinin and are induced during nodulation. Overexpression and silencing of MtLOG1 decrease nodule numbers (Mortier, Wasson et al. 2014) suggesting a fine tuned cytokinin biosynthesis during nodulation in Medicago. Cytokinin can be irreversibly degraded into adenine and 3-methyl-butenal by the Cytokinin

oxidases (CKX). In *L. japonicus*, CKX3 expression is induced by Nod Factors and its symbiont *Mesorhizobium loti* during early nodulation and the *ckx3* mutant has fewer ITs and nodules (Murray, Karas et al. 2007, Reid, Heckmann et al. 2016). Therefore, cytokinin production induced by Nod Factor might trigger cortical nodule organogenesis followed by a feedback via specific cytokinin response regulators in the epidermis to control the infection.

1.4.3. Cytokinin signaling

Cytokinin signaling pathway plays a central role in initiating nodule primordia and is also responsible for meristem activation (Suzaki, Ito et al. 2013). Cytokinin treatment triggers pseudonodule formation in the non-nodulation mutants, *nfr1, nfr5*, *symRK*, *nup133*, *nup85*, *castor*, *pollux*, and *ccamk*, suggesting that cytokinin action is downstream of the Nod factors signal transduction pathway and that cytokinin is necessary and sufficient for the initiation of nodule organogenesis. Activation of cytokinin signaling during nodule development relies on NIN, NSP1, and NSP2 (Heckmann, Sandal et al. 2011).

Cytokinin is perceived by a histidine kinase (HK) phosphorelay system. First, a protein with an extracellular domain perceives the cytokinin. This induces its kinase activity and the protein autophosphorylates. Then, the phosphoryl group is transferred intramolecularly to an aspartate residue. A His-containing phosphotransfer protein receives

the phosphoryl group and transfer it to an aspartate present on a receiver domain of the second component of the system; a response regulator (RR) which is frequently a transcription factor. Type-B RRs are commonly associated with transcriptional activation, and type-A RR with cytokinin signaling inhibition, reviewed by (Hwang, Sheen et al. 2012). Exogenous cytokinin treatment and gain-of-function mutations in the cytokinin receptor LjLhk1 or MtCRE1 induces cytokinin signaling in the root and pseudonodule formation (Tirichine, Sandal et al. 2007, Heckmann, Sandal et al. 2011).

After *M. loti* infection, LHK1 promoter activity has been reported the root cortex first and subsequently in root epidermis (Held, Hou et al. 2014). Consistently, the *L. japonicus* triple mutant *lhk1-1 lhk1a-1 lhk3-1* is not impaired in the infection thread formation, but cortical division is affected (Held, Hou et al. 2014). Hence, the three cytokinin receptors LHK1, LHK1A, and LHK3 don't seem to be involved in epidermal infection but regulate cortical division. In Medicago truncatula the receptor MtCRE1/CHK1 along with MtCHK2, MtCHK3, and MtCHK4 enables initial cortical division (Gonzalez-Rizzo, Crespi et al. 2006, Plet, Wasson et al. 2011, Boivin, Fonouni-Farde et al. 2016).

During nodulation, response regulators are orchestrating cytokinin signaling responses. MtRR4 (type-B RR) is induced in the initial cortical cell division in the primordia and in the nodule meristem (Plet, Wasson et al. 2011). Interestingly, MtRR4 seem to be regulated by the MtKNAT3/4/5-like genes which are homeodomain transcription factors involved in nodule development (Di Giacomo, Laffont et al. 2017).

MtRR1 (type-A RR) is also induced in the initial cortical cell division and can bind to the promotor of NSP2 a transcription factor that trigger nodule organogenesis (Ariel, Brault-Hernandez et al. 2012). MtRR9 expression is upregulated in the epidermis and the root cortex after inoculation with rhizobia or Nod Factor treatment. Moreover, constitutive activation of MtRR9 triggers cortical cell division demonstrating its positive role during nodule primordia formation (Op den Camp, De Mita et al. 2011). Therefore, positive cytokinin signaling is required for the cortical nodule organogenesis initiation but not directly involved in root hair infection.

To summarize, both cytokinin and auxin signaling pathways are involved during nodulation and specific patterns of expression and action are required for proper rhizobia infection and nodule organogenesis.

Auxin is promoting the root hair infection, primordium initiation, is absent/undetectable in the infection zone, present in the vascular bundles of both nodule types and in the meristem of indeterminate nodules. Experimental studies have revealed that auxin biosynthesis is active during the root hair infection of both nodule types and during determinate nodule maturation. In Medicago, GH3 genes are upregulated during the root hair infection and soybean GH3 genes also seem to reduce auxin level in the root epidermis and the nodule primordium. Auxin transport inhibition is responsible of nodule initiation in indeterminate but not determinate nodules. Auxin carriers are active in the early primordium, the vascular bundles and the nodule meristem of indeterminate nodules but haven’t been identified in determinate nodules. In Medicago and soybean, the auxin

signaling pathway is regulated by positive and negative ARFs themselves regulated by microRNAs at different stages and in different tissues types. This enables a very fine and versatile regulation of the pool of auxin and its response and highlights the specificity of auxin action required to produce the different cell types constituting nodules.

Cytokinin treatment induces pseudonodules in determinate and indeterminate nodules. Cytokinin patterns are present in the cortical cells after infection, then in the epidermis, in the emerging primordium and the vasculature of both nodule type. It is also present in the parenchyma of determinate nodule and the infection zone and meristem of indeterminate nodule. Cytokinins are biosynthesized during early infection in Medicago and cytokinin biosynthesis is required for nodulation in *L. japonicus*. Cytokinin activation is tightly regulated in indeterminate nodules and cytokinin degradation is required for determinate nodules. Cytokinin receptors gain-of-function mutants produce pseudonodules and cytokinin signaling pathway is involved in cortical cell division but not root hair infection. Therefore, it appears that cytokinin plays an essential role in nodulation organogenesis of determinate and indeterminate nodules. Interesting patterns of auxin and cytokinin seem to partially overlap and are both involved in nodule induction and organogenesis. The following section will describe how both of these actors are regulating each other during legumes symbiosis with rhizobacteria.

1.5. Auxin/cytokinin ratio during nodule development

1.5.1. Auxin-cytokinin regulation during nodulation

Beyond the role played by auxin and cytokinin individually in controlling cell proliferation and differentiation, reviewed by (Benkova and Hejatko 2009, Suzaki, Ito et al. 2013) considering their ratio is essential to understand their function during nodulation. Indeed, these hormones are known to act antagonistically and/or synergistically to control and regulate several plant developmental processes such as embryogenesis and shoot/root meristem maintenance, reviewed by (Su, Liu et al. 2011).

In nodulation, auxin and cytokinin seem to be involved in the regulation of nodule formation in a rhizobium-independent manner. During the early steps of the infection process, local root epidermis responses are observed for both auxin and cytokinin. After Nod Factor treatment or rhizobium inoculation, the auxin biosynthesis is induced in root hairs and the cytokinin biosynthesis is inhibited in the epidermis in *L. japonicus* (Nadzieja, Kelly et al. 2018). Nadzieja et al., 2018 have proposed that auxin is rapidly accumulated after infection and suppresses cytokinin biosynthesis and signaling, to enable early infection events.

In 2016, Miri et al., were also proposing that the repression of the cytokinin signaling via auxin action was necessary for successful infection events. In fact, type-A RR are induced by Nod Factor treatment and rhizobia inoculation in an auxin-dependent

manner. In return, cytokinin stimulates ethylene production to restrict infection events and nodule development (Penmetsa and Cook 1997, Penmetsa, Uribe et al. 2008).

Cytokinin can also regulate auxin transport via controlling PIN1 distribution and can induce auxin biosynthesis (Pernisová, Klíma et al. 2009, Jones, Gunneras et al. 2010). The Medicago cytokinin receptor CRE1 can influence the auxin level via two ways. By inducing a cytokinin cascade and the activation of ARF16a in the epidermis (Boivin, Kazmierczak et al. 2016), or in modifying the auxin transport via the action of flavonoids (Plet, Wasson et al. 2011, Ng, Hassan et al. 2015).

Auxin and cytokinin responses are observed in the first dividing cortical cells of both determinate and indeterminate nodule (van Noorden, Kerim et al. 2007, Plet, Wasson et al. 2011, Takanashi, Sugiyama et al. 2011) and there are evidences supporting that cytokinin activation is upstream of the auxin response (Plet, Wasson et al. 2011, Suzaki, Yano et al. 2012, Ng, Hassan et al. 2015). For instance, white clover treated with exogenous cytokinin induces auxin responses in the early cell divisions of the inner root cortex (Mathesius, Weinman et al. 2000). Once the nodule is getting more developed, auxin and cytokinin patterns partially overlap. Auxin is absent in the infection zone and present in the vascular bundles in both determinate and indeterminate nodule (Guan, Stacey et al. 2013, Turner, Nizampatnam et al. 2013). Auxin is also present in the meristem of indeterminate nodule, reviewed by (Kohlen, Ng et al. 2018).

Cytokinin has been reported in the nodule meristem and nodule vascular bundle using a type-A RR reporter and throughout the nodule when using a type-B RR reporter in indeterminate nodule (Plet, Wasson et al. 2011, Franssen, Xiao et al. 2015). In determinate nodule, cytokinin transcriptional output reporter has been slightly detected in the parenchyma and the vascular bundles (Held, Hou et al. 2014). Hence, auxin distribution is specifically present in the vascular bundles of determinate and in the meristem and vascular bundles of indeterminate nodule. Concerning cytokinin it is present in the meristem, vascular bundle and infection zone of indeterminate nodules and in the nodule parenchyma, vascular bundles and infection zone of determinate nodules.

To summarize, even though auxin and cytokinin overlap during the infection and early organogenesis stages, it is thought that a high auxin/cytokinin activity is required in the epidermis for successful infection and a low auxin/cytokinin ratio is necessary for effective nodule primordia initiation (Miri, Janakirama et al. 2016). These hypothetical optimal ratios can be regulated by actors like miR160. Indeed, experimental alteration of miR160 expression and activity modifies the sensitivity to auxin over cytokinin or cytokinin over auxin and results in nodulation phenotype.

1.5.2. Auxin/cytokinin measurement

Gene mutation is commonly used to study specifics actors involved in plant development. However, the use of mutant is often problematic in plant signaling pathways

due to extensive redundancy within gene families like in the case of the ARF10/ARF16/ARF17 families (Turner, Nizampatnam et al. 2013). It would necessitate the creation of higher order mutants which can be challenging because of the lack of null mutants and the important number of genes. Indeed, the Arabidopsis triple order mutants *arf10*, *arf16* and *arf17* do not present defects in plant development (Mallory, Bartel et al. 2005, Wang, Wang et al. 2005). Additionally, mutation in signaling components is often associated with pleiotropic effects and early lethality. Therefore, we decided to image fluorescent transcriptional output sensors to estimate which are the relative auxin/cytokinin ratios dictating proper nodule development and to what extend this is controlled by miR160.

This methodology has two main advantages. It enables to perform *in vivo* imaging in a nondestructive way to capture hormone outputs in living tissues. It provides a 3-dimensionnal (3D) quantification of hormone levels and cells response to measure the amount of active forms of hormones and calculate their relative ratios. For cytokinin, we used the specific synthetic sensor, Two Component signaling Sensor new (TCSn) which is to date the most sensible and specific cytokinin sensor that provides a balanced response to the ARABIDOPSIS RESPONSE REGULATOR (ARR) type-B RR family (Zürcher, Tavor-Deslex et al. 2013). It is composed of 24 binding sites arranged in all possible orientations of the consensus sequence of the Myb-like DNA-binding of 11 type-B ARR promoters. Concerning auxin, the synthetic DR5rev promoter reporter have been employed. It comprises the auxin-response element (TGTCTC) repeated 9 times and

placed in inverse orientation to the CaMV minimal 35S promoter (Ulmasov, Murfett et al. 1997). Literature reports that DII:VENUS auxin accumulation sensor has also been used to report auxin amount. DII domain corresponds to the most stable Aux/IAA rested, IAA28 (Brunoud, Wells et al. 2012).

In the absence of auxin, the VENUS signal is expressed and detected. However, when auxin is accumulated, Aux/IAA are degraded by a proteasome mediated by the SCF-TIR1/AFB complex and the VENUS signal is absent. Hence, DII:VENUS can provide a great temporal resolution, nevertheless it has the disadvantage to be an indirect technique (absence of signal means presence of auxin) and is not suitable for ratiometric analysis. DR5rev and TCSn are both present in a single construct to simultaneously quantify auxin and cytokinin outputs. Moreover these reporter are transcriptionally fused to the nuclear-localized enhanced green fluorescent protein (eGFP) and the nuclear-localized tdTomato respectively (DR5rev:eGFP-NLS and TCSn: tdTomato-NLS). Florescence imaging of living sample comes with several challenges.

There is variation due to experimental conditions, aberrations induced by local fluctuations in refractive index and scattering specially in thick legumes roots. Employing this two-reporter construct in addition with relative ratio quantification instead of absolute quantification is expected to moderate these drawbacks and provide a reliable report of the relative auxin and cytokinin ratios. Alternatively, quantification of auxin and cytokinin in Medicago mature nodule has been performed using liquid chromatography–mass spectrometry (LC-MS). In 2019, Demina et al. reported that PAA was the major form of

auxin in nodule and there was no difference between the concentration of active auxin in roots and in nodules, however nodules had more IAA-alanine (Demina, Maity et al. 2019).

Cytokinins were not different from nodules and roots. As both hormones can be quantified, their ratio can be calculated. Nevertheless, LC-MS is tissue destructive and doesn't allow a fine *in vivo* cellular mapping of the hormones and their relative ratio. Using a two-photon induced fluorescence imaging system coupled with the two-reporter construct enabled us to get a 3D resolution of the samples. The images were analyzed via an optimized individual nuclei detection strategy, each hormones output was quantified, and the ratios calculated for every nucleus detected.

1.5.3. miR160 modifies the auxin/cytokinin balance during nodule formation

In 2013, our lab has reported that miR160 is involved in soybean nodule organogenesis in regulating relative auxin/cytokinin ratio via the control of the ARF10/ARF16/ARF17 family (Turner, Nizampatnam et al. 2013, Nizampatnam, Schreier et al. 2015). These ARFs are classified as repressor, in other words they can inhibit the expression of early genes responding to auxin. If miR160 is expressed, it can repress the activity of these ARFs and thus indirectly restores the expression of early genes in response to auxin. Indeed, roots over-expressing miR160 (miR160ox) were hypersensitive to auxin (based on root response to exogenous auxin) and were impaired in nodule primordia

formation. Moreover, they are also hyposensitive to cytokinin, based on the induction of marker genes in response to exogenous cytokinin (Turner, Nizampatnam et al. 2013, Nizampatnam, Schreier et al. 2015).

miR160ox roots were not affected in the number of infection foci while they have a severe deficit of primordium, emerging and mature nodule. Conversely, roots constitutively expressing a short tandem target mimic (STTM160ox) repressing miR160, had reduced sensitivity to auxin and enhanced sensitivity to cytokinin. These roots had more initiated nodules, but their maturation was drastically delayed (Nizampatnam, Schreier et al. 2015). Hence, miR160 seems to be a key regulator that dictates relative auxin/cytokinin ratios.

As nodules are very complex organs resulting from different auxin/cytokinin ratios, tissues specific studies have been done to better characterized miR160 action. miR160 expression is sparsely detected in emerging nodule, but widely detected in mature nodule. Moreover, the auxin pattern is also sparsely present in emerging nodule, however it is restricted to the nodule periphery and absent in the central zone of mature nodule. Hence, it seems that the spatio-temporal expression of miR160 and auxin is essential for proper nodule development.

To assess this, transgenic roots expressing miR160 via the nodule primordium-specific promoter pENOD40 (pENOD40miR160) were generated. pENOD40miR160 showed an equal number of IT reaching the cortex, but fewer emerging and mature nodules

compared to the vector control. These results indicate that miR160 activity in nodule primordium inhibits nodule development. In miR160 silenced roots using pENOD40STTM160, a higher number of initiated nodules was observed (as in STTM160ox), however no delayed in maturation was noticed (contrarily to STTM160ox). Hence, it seems that miR160 acts in the primordium to control nodule formation but regulates nodule maturation through its expression in some other zone. Yet, we still need to determine how miR160 impacts the relative auxin/cytokinin balance in a developmental stage and cell specific manner.

In this dissertation, three different aspects will be presented. The first part will introduce and discuss methodology developed in collaboration with Dr Steve Smith's team from The South Dakota School of Mines & Technology. The relative auxin/cytokinin response ratio (ACRO) approach was created to quantify the relative auxin/cytokinin ratios of individual cells in living tissue. This strategy has been optimized on roots of soybean composite plants. The ratios were measured in different cell types with known relative activities of auxin and cytokinin to assess the reliability of this method. Secondly the ACRO approach was employed to characterize relative auxin/cytokinin ratios at 6 key stages of soybean root nodule development. The relative auxin/cytokinin ratios in roots where miR160 was silenced (STTM160) were also evaluated. Finally, the creation of other plant model species such as *Arabidopsis thaliana* and *Medicago truncatula* constitutively expressing the RAD strategy has been reported. These reporter lines and quantitative imaging methods offer a new approach to study the auxin/cytokinin requirements involved

in the regulation numerous plant process (growth, fructification, pathogenicity, tolerance to stress…) in a variety of organs and/or in the whole plant.

1.6. References

Abdel-Lateif, K., D. Bogusz and V. Hocher (2012). "The role of flavonoids in the establishment of plant roots endosymbioses with arbuscular mycorrhiza fungi, rhizobia and Frankia bacteria." Plant Signal Behav **7**(6): 636-641.

Ariel, F., M. Brault-Hernandez, C. Laffont, E. Huault, M. Brault, J. Plet, M. Moison, S. Blanchet, J. L. Ichante, M. Chabaud, S. Carrere, M. Crespi, R. L. Chan and F. Frugier (2012). "Two direct targets of cytokinin signaling regulate symbiotic nodulation in Medicago truncatula." Plant Cell **24**(9): 3838-3852.

Axtell, M. J. (2013). "Classification and comparison of small RNAs from plants." Annu Rev Plant Biol **64**: 137-159.

Benkova, E. and J. Hejatko (2009). "Hormone interactions at the root apical meristem." Plant Mol Biol **69**(4): 383-396.

Boivin, S., C. Fonouni-Farde and F. Frugier (2016). "How Auxin and Cytokinin Phytohormones Modulate Root Microbe Interactions." Frontiers in plant science **7**: 1240-1240.

Boivin, S., T. Kazmierczak, M. Brault, J. Wen, P. Gamas, K. S. Mysore and F. Frugier (2016). "Different cytokinin histidine kinase receptors regulate nodule initiation

as well as later nodule developmental stages in Medicago truncatula." Plant Cell Environ **39**(10): 2198-2209.

Bond, L. (1948). "Origin and Development Morphology of Root Nodules of Pisum sativum." Botanical Gazette **109**(4): 411-434.

Boot, K. J. M., A. A. N. van Brussel, T. Tak, H. P. Spaink and J. W. Kijne (1999). "Lipochitin Oligosaccharides from Rhizobium leguminosarum bv. viciae Reduce Auxin Transport Capacity in Vicia sativa subsp. nigra Roots." Molecular Plant-Microbe Interactions® **12**(10): 839-844.

Boualem, A., P. Laporte, M. Jovanovic, C. Laffont, J. Plet, J.-P. Combier, A. Niebel, M. Crespi and F. Frugier (2008). "MicroRNA166 controls root and nodule development in Medicago truncatula." The Plant Journal **54**(5): 876-887.

Breakspear, A., C. Liu, S. Roy, N. Stacey, C. Rogers, M. Trick, G. Morieri, K. S. Mysore, J. Wen, G. E. D. Oldroyd, J. A. Downie and J. D. Murray (2014). "The root hair "infectome" of Medicago truncatula uncovers changes in cell cycle genes and reveals a requirement for Auxin signaling in rhizobial infection." The Plant cell **26**(12): 4680-4701.

Brunoud, G., D. M. Wells, M. Oliva, A. Larrieu, V. Mirabet, A. H. Burrow, T. Beeckman, S. Kepinski, J. Traas, M. J. Bennett and T. Vernoux (2012). "A novel sensor to map auxin response and distribution at high spatio-temporal resolution." Nature **482**(7383): 103-106.

Bustos-Sanmamed, P., G. Mao, Y. Deng, M. Elouet, G. A. Khan, J. Bazin, M. Turner, S. Subramanian, O. Yu, M. Crespi and C. Lelandais-Brière (2013). "Overexpression of miR160 affects root growth and nitrogen-fixing nodule number in Medicago truncatula." Functional Plant Biology **40**(12): 1208-1220.

Cai, Z., Y. Wang, L. Zhu, Y. Tian, L. Chen, Z. Sun, I. Ullah and X. Li (2017). "GmTIR1/GmAFB3-based auxin perception regulated by miR393 modulates soybean nodulation." New Phytologist **215**(2): 672-686.

Capoen, W., J. Den Herder, S. Rombauts, J. De Gussem, A. De Keyser, M. Holsters and S. Goormachtig (2007). "Comparative transcriptome analysis reveals common and specific tags for root hair and crack-entry invasion in Sesbania rostrata." Plant Physiol **144**(4): 1878-1889.

Combier, J.-P., F. Frugier, F. de Billy, A. Boualem, F. El-Yahyaoui, S. Moreau, T. Vernié, T. Ott, P. Gamas, M. Crespi and A. Niebel (2006). "MtHAP2-1 is a key transcriptional regulator of symbiotic nodule development regulated by microRNA169 in Medicago truncatula." Genes & development **20**(22): 3084-3088.

Cooper, J. B. and S. R. Long (1994). "Morphogenetic Rescue of Rhizobium meliloti Nodulation Mutants by trans-Zeatin Secretion." The Plant cell **6**(2): 215-225.

D'Haeseleer, K., G. Den Herder, C. Laffont, J. Plet, V. Mortier, C. Lelandais-Briere, S. De Bodt, A. De Keyser, M. Crespi, M. Holsters, F. Frugier and S. Goormachtig

(2011). "Transcriptional and post-transcriptional regulation of a NAC1 transcription factor in Medicago truncatula roots." New Phytol **191**(3): 647-661.

Damodaran, S., C. S. Westfall, B. A. Kisely, J. M. Jez and S. Subramanian (2017). "Nodule-Enriched GRETCHEN HAGEN 3 Enzymes Have Distinct Substrate Specificities and Are Important for Proper Soybean Nodule Development." Int J Mol Sci **18**(12).

de Billy, F., C. Grosjean, S. May, M. Bennett and J. V. Cullimore (2001). "Expression studies on AUX1-like genes in Medicago truncatula suggest that auxin is required at two steps in early nodule development." Mol Plant Microbe Interact **14**(3): 267-277.

Demina, I. V., P. J. Maity, A. Nagchowdhury, J. L. P. Ng, E. van der Graaff, K. N. Demchenko, T. Roitsch, U. Mathesius and K. Pawlowski (2019). "Accumulation of and Response to Auxins in Roots and Nodules of the Actinorhizal Plant Datisca glomerata Compared to the Model Legume Medicago truncatula." Frontiers in Plant Science **10**(1085).

Di Giacomo, E., C. Laffont, F. Sciarra, M. A. Iannelli, F. Frugier and G. Frugis (2017). "KNAT3/4/5-like class 2 KNOX transcription factors are involved in Medicago truncatula symbiotic nodule organ development." New Phytol **213**(2): 822-837.

Dolgikh, A. V., A. N. Kirienko, I. A. Tikhonovich, E. Foo and E. A. Dolgikh (2019). "The DELLA Proteins Influence the Expression of Cytokinin Biosynthesis and Response Genes During Nodulation." Frontiers in plant science **10**: 432-432.

Dolgikh, E. A., P. G. Kusakin, A. B. Kitaeva, A. V. Tsyganova, A. N. Kirienko, I. V. Leppyanen, A. V. Dolgikh, E. L. Ilina, K. N. Demchenko, I. A. Tikhonovich and V. E. Tsyganov (2020). "Mutational analysis indicates that abnormalities in rhizobial infection and subsequent plant cell and bacteroid differentiation in pea (Pisum sativum) nodules coincide with abnormal cytokinin responses and localization." Ann Bot.

Ferguson, B. J., A. Indrasumunar, S. Hayashi, M. H. Lin, Y. H. Lin, D. E. Reid and P. M. Gresshoff (2010). "Molecular analysis of legume nodule development and autoregulation." J Integr Plant Biol **52**(1): 61-76.

Ferguson, B. J., E. M. Wiebe, R. J. Neil Emery and F. C. Guinel (2005). "Cytokinin accumulation and an altered ethylene response mediate the pleiotropic phenotype of the pea nodulation mutant R50 (sym16)." Canadian Journal of Botany **83**(8): 989-1000.

Fisher, J., P. Gaillard, C. R. Fellbaum, S. Subramanian and S. Smith (2018). "Quantitative 3D imaging of cell level auxin and cytokinin response ratios in soybean roots and nodules." Plant Cell Environ **41**(9): 2080-2092.

Franssen, H. J., T. T. Xiao, O. Kulikova, X. Wan, T. Bisseling, B. Scheres and R. Heidstra (2015). "Root developmental programs shape the Medicago truncatula nodule meristem." Development **142**(17): 2941-2950.

Friml, J. (2003). "Auxin transport - shaping the plant." Curr Opin Plant Biol **6**(1): 7-12.

Fukuhara, H., Y. Minakawa, S. Akao and K. Minamisawa (1994). "The Involvement of Indole-3-Acetic Acid Produced by Bradyrhizobium elkanii in Nodule Formation." Plant and Cell Physiology **35**(8): 1261-1265.

Gage, D. J. (2004). "Infection and invasion of roots by symbiotic, nitrogen-fixing rhizobia during nodulation of temperate legumes." Microbiol Mol Biol Rev **68**(2): 280-300.

Gamas, P., M. Brault, M. F. Jardinaud and F. Frugier (2017). "Cytokinins in Symbiotic Nodulation: When, Where, What For?" Trends Plant Sci **22**(9): 792-802.

Gauthier-Coles, C., R. G. White and U. Mathesius (2018). "Nodulating Legumes Are Distinguished by a Sensitivity to Cytokinin in the Root Cortex Leading to Pseudonodule Development." Front Plant Sci **9**: 1901.

Gonzalez-Rizzo, S., M. Crespi and F. Frugier (2006). "The Medicago truncatula CRE1 Cytokinin Receptor Regulates Lateral Root Development and Early Symbiotic Interaction with Sinorhizobium meliloti." The Plant Cell **18**(10): 2680-2693.

Guan, D., N. Stacey, C. Liu, J. Wen, K. S. Mysore, I. Torres-Jerez, T. Vernié, M. Tadege, C. Zhou, Z.-y. Wang, M. K. Udvardi, G. E. D. Oldroyd and J. D. Murray (2013). "Rhizobial infection is associated with the development of peripheral vasculature in nodules of Medicago truncatula." Plant physiology **162**(1): 107-115.

Heckmann, A. B., N. Sandal, A. S. Bek, L. H. Madsen, A. Jurkiewicz, M. W. Nielsen, L. Tirichine and J. Stougaard (2011). "Cytokinin induction of root nodule primordia

in Lotus japonicus is regulated by a mechanism operating in the root cortex." Mol Plant Microbe Interact **24**(11): 1385-1395.

Held, M., H. Hou, M. Miri, C. Huynh, L. Ross, M. S. Hossain, S. Sato, S. Tabata, J. Perry, T. L. Wang and K. Szczyglowski (2014). "Lotus japonicus Cytokinin Receptors Work Partially Redundantly to Mediate Nodule Formation." The Plant Cell **26**(2): 678-694.

Herrbach, V., X. Chirinos, D. Rengel, K. Agbevenou, R. Vincent, S. Pateyron, S. Huguet, S. Balzergue, A. Pasha, N. Provart, C. Gough and S. Bensmihen (2017). "Nod factors potentiate auxin signaling for transcriptional regulation and lateral root formation in Medicago truncatula." Journal of experimental botany **68**(3): 569-583.

Hirsch, A. M., T. V. Bhuvaneswari, J. G. Torrey and T. Bisseling (1989). "Early nodulin genes are induced in alfalfa root outgrowths elicited by auxin transport inhibitors." Proceedings of the National Academy of Sciences of the United States of America **86**(4): 1244-1248.

Hofferek, V., A. Mendrinna, N. Gaude, F. Krajinski and E. A. Devers (2014). "MiR171h restricts root symbioses and shows like its target NSP2 a complex transcriptional regulation in Medicago truncatula." BMC Plant Biology **14**(1): 199.

Huo, X., E. Schnabel, K. Hughes and J. Frugoli (2006). "RNAi Phenotypes and the Localization of a Protein::GUS Fusion Imply a Role for Medicago truncatula PIN Genes in Nodulation." Journal of Plant Growth Regulation **25**(2): 156-165.

Hwang, I., J. Sheen and B. Muller (2012). "Cytokinin signaling networks." Annu Rev Plant Biol **63**: 353-380.

Jardinaud, M. F., S. Boivin, N. Rodde, O. Catrice, A. Kisiala, A. Lepage, S. Moreau, B. Roux, L. Cottret, E. Sallet, M. Brault, R. J. Emery, J. Gouzy, F. Frugier and P. Gamas (2016). "A Laser Dissection-RNAseq Analysis Highlights the Activation of Cytokinin Pathways by Nod Factors in the Medicago truncatula Root Epidermis." Plant Physiol **171**(3): 2256-2276.

Jones, B., S. A. Gunneras, S. V. Petersson, P. Tarkowski, N. Graham, S. May, K. Dolezal, G. Sandberg and K. Ljung (2010). "Cytokinin regulation of auxin synthesis in Arabidopsis involves a homeostatic feedback loop regulated via auxin and cytokinin signal transduction." Plant Cell **22**(9): 2956-2969.

Kohlen, W., J. L. P. Ng, E. E. Deinum and U. Mathesius (2017). "Auxin transport, metabolism, and signalling during nodule initiation: indeterminate and determinate nodules." Journal of Experimental Botany **69**(2): 229-244.

Kohlen, W., J. L. P. Ng, E. E. Deinum and U. Mathesius (2018). "Auxin transport, metabolism, and signalling during nodule initiation: indeterminate and determinate nodules." J Exp Bot **69**(2): 229-244.

Kouchi, H., H. Imaizumi-Anraku, M. Hayashi, T. Hakoyama, T. Nakagawa, Y. Umehara, N. Suganuma and M. Kawaguchi (2010). "How many peas in a pod? Legume genes responsible for mutualistic symbioses underground." Plant Cell Physiol **51**(9): 1381-1397.

Lerouge, P., P. Roche, C. Faucher, F. Maillet, G. Truchet, J. C. Prome and J. Denarie (1990). "Symbiotic host-specificity of Rhizobium meliloti is determined by a sulphated and acylated glucosamine oligosaccharide signal." Nature **344**(6268): 781-784.

Lorteau, M. A., B. J. Ferguson and F. C. Guinel (2001). "Effects of cytokinin on ethylene production and nodulation in pea (Pisum sativum) cv. Sparkle." Physiol Plant **112**(3): 421-428.

Mallory, A. C., D. P. Bartel and B. Bartel (2005). "MicroRNA-directed regulation of Arabidopsis AUXIN RESPONSE FACTOR17 is essential for proper development and modulates expression of early auxin response genes." The Plant cell **17**(5): 1360-1375.

Marin, E., V. Jouannet, A. Herz, A. S. Lokerse, D. Weijers, H. Vaucheret, L. Nussaume, M. D. Crespi and A. Maizel (2010). "miR390, Arabidopsis TAS3 tasiRNAs, and their AUXIN RESPONSE FACTOR targets define an autoregulatory network quantitatively regulating lateral root growth." The Plant cell **22**(4): 1104-1117.

Mashiguchi, K., K. Tanaka, T. Sakai, S. Sugawara, H. Kawaide, M. Natsume, A. Hanada, T. Yaeno, K. Shirasu, H. Yao, P. McSteen, Y. Zhao, K.-i. Hayashi, Y. Kamiya and H. Kasahara (2011). "The main auxin biosynthesis pathway in Arabidopsis." Proceedings of the National Academy of Sciences of the United States of America **108**(45): 18512-18517.

Mathesius, U., H. R. Schlaman, H. P. Spaink, C. Of Sautter, B. G. Rolfe and M. A. Djordjevic (1998). "Auxin transport inhibition precedes root nodule formation in white clover roots and is regulated by flavonoids and derivatives of chitin oligosaccharides." Plant J **14**(1): 23-34.

Mathesius, U., J. J. Weinman, B. G. Rolfe and M. A. Djordjevic (2000). "Rhizobia can induce nodules in white clover by "hijacking" mature cortical cells activated during lateral root development." Mol Plant Microbe Interact **13**(2): 170-182.

Miri, M., P. Janakirama, M. Held, L. Ross and K. Szczyglowski (2016). "Into the Root: How Cytokinin Controls Rhizobial Infection." Trends Plant Sci **21**(3): 178-186.

Mortier, V., A. Wasson, P. Jaworek, A. De Keyser, M. Decroos, M. Holsters, P. Tarkowski, U. Mathesius and S. Goormachtig (2014). "Role of LONELY GUY genes in indeterminate nodulation on Medicago truncatula." New Phytol **202**(2): 582-593.

Muller, D. and O. Leyser (2011). "Auxin, cytokinin and the control of shoot branching." Ann Bot **107**(7): 1203-1212.

Murray, J. D., B. J. Karas, S. Sato, S. Tabata, L. Amyot and K. Szczyglowski (2007). "A Cytokinin Perception Mutant Colonized by Rhizobium in the Absence of Nodule Organogenesis." Science **315**(5808): 101-104.

Nadzieja, M., S. Kelly, J. Stougaard and D. Reid (2018). "Epidermal auxin biosynthesis facilitates rhizobial infection in Lotus japonicus." Plant J **95**(1): 101-111.

Newcomb, W. (1976). "A correlated light and electron microscopic study of symbiotic growth and differentiation in Pisum sativum root nodules." Canadian Journal of Botany **54**(18): 2163-2186.

Ng, J. L., S. Hassan, T. T. Truong, C. H. Hocart, C. Laffont, F. Frugier and U. Mathesius (2015). "Flavonoids and Auxin Transport Inhibitors Rescue Symbiotic Nodulation in the Medicago truncatula Cytokinin Perception Mutant cre1." Plant Cell **27**(8): 2210-2226.

Ng, J. L. P. and U. Mathesius (2018). "Acropetal Auxin Transport Inhibition Is Involved in Indeterminate But Not Determinate Nodule Formation." Frontiers in plant science **9**: 169-169.

Nizampatnam, N. R., S. J. Schreier, S. Damodaran, S. Adhikari and S. Subramanian (2015). "microRNA160 dictates stage-specific auxin and cytokinin sensitivities and directs soybean nodule development." Plant J **84**(1): 140-153.

Oldroyd, G. E., J. D. Murray, P. S. Poole and J. A. Downie (2011). "The rules of engagement in the legume-rhizobial symbiosis." Annu Rev Genet **45**: 119-144.

Op den Camp, R. H., S. De Mita, A. Lillo, Q. Cao, E. Limpens, T. Bisseling and R. Geurts (2011). "A phylogenetic strategy based on a legume-specific whole genome duplication yields symbiotic cytokinin type-A response regulators." Plant Physiol **157**(4): 2013-2022.

Penmetsa, R. V. and D. R. Cook (1997). "A Legume Ethylene-Insensitive Mutant Hyperinfected by Its Rhizobial Symbiont." Science **275**(5299): 527-530.

Penmetsa, R. V., P. Uribe, J. Anderson, J. Lichtenzveig, J. C. Gish, Y. W. Nam, E. Engstrom, K. Xu, G. Sckisel, M. Pereira, J. M. Baek, M. Lopez-Meyer, S. R. Long, M. J. Harrison, K. B. Singh, G. B. Kiss and D. R. Cook (2008). "The Medicago truncatula ortholog of Arabidopsis EIN2, sickle, is a negative regulator of symbiotic and pathogenic microbial associations." Plant J **55**(4): 580-595.

Pernisová, M., P. Klíma, J. Horák, M. Válková, J. Malbeck, P. Souček, P. Reichman, K. Hoyerová, J. Dubová, J. Friml, Za, E. žímalová and J. Hejátko (2009). "Cytokinins modulate auxin-induced organogenesis in plants via regulation of the auxin efflux." Proceedings of the National Academy of Sciences **106**(9): 3609-3614.

Plet, J., A. Wasson, F. Ariel, C. Le Signor, D. Baker, U. Mathesius, M. Crespi and F. Frugier (2011). "MtCRE1-dependent cytokinin signaling integrates bacterial and plant cues to coordinate symbiotic nodule organogenesis in Medicago truncatula." Plant J **65**(4): 622-633.

Podlesakova, K., J. Fardoux, D. Patrel, K. Bonaldi, O. Novak, M. Strnad, E. Giraud, L. Spichal and N. Nouwen (2013). "Rhizobial synthesized cytokinins contribute to but are not essential for the symbiotic interaction between photosynthetic Bradyrhizobia and Aeschynomene legumes." Mol Plant Microbe Interact **26**(10): 1232-1238.

Reid, D., M. Nadzieja, O. Novák, A. B. Heckmann, N. Sandal and J. Stougaard (2017). "Cytokinin Biosynthesis Promotes Cortical Cell Responses during Nodule Development." Plant Physiology **175**(1): 361-375.

Reid, D. E., A. B. Heckmann, O. Novák, S. Kelly and J. Stougaard (2016). "CYTOKININ OXIDASE/DEHYDROGENASE3 Maintains Cytokinin Homeostasis during Root and Nodule Development in Lotus japonicus." Plant Physiology **170**(2): 1060-1074.

Relic, B., F. Talmont, J. Kopcinska, W. Golinowski, J. C. Prome and W. J. Broughton (1993). "Biological activity of Rhizobium sp. NGR234 Nod-factors on Macroptilium atropurpureum." Mol Plant Microbe Interact **6**(6): 764-774.

RODRIGUEZ-BARRUECO, C. and F. B. CASTRO (1973). "Cytokinin-induced Pseudonodules on Alnus glutinosa." Physiologia Plantarum $V 29(2).

Roy, S., F. Robson, J. Lilley, C.-W. Liu, X. Cheng, J. Wen, S. Walker, J. Sun, D. Cousins, C. Bone, M. J. Bennett, J. A. Downie, R. Swarup, G. Oldroyd and J. D. Murray (2017). "MtLAX2, a Functional Homologue of the Arabidopsis Auxin Influx Transporter AUX1, Is Required for Nodule Organogenesis." Plant Physiology **174**(1): 326-338.

Santi, C., D. Bogusz and C. Franche (2013). "Biological nitrogen fixation in non-legume plants." Ann Bot **111**(5): 743-767.

Shen, C., R. Yue, T. Sun, L. Zhang, L. Xu, S. Tie, H. Wang and Y. Yang (2015). "Genome-wide identification and expression analysis of auxin response factor gene family in Medicago truncatula." Front Plant Sci **6**: 73.

Staswick, P. E., B. Serban, M. Rowe, I. Tiryaki, M. T. Maldonado, M. C. Maldonado and W. Suza (2005). "Characterization of an Arabidopsis enzyme family that conjugates amino acids to indole-3-acetic acid." Plant Cell **17**(2): 616-627.

Su, Y. H., Y. B. Liu and X. S. Zhang (2011). "Auxin-cytokinin interaction regulates meristem development." Mol Plant **4**(4): 616-625.

Suzaki, T., M. Ito and M. Kawaguchi (2013). "Genetic basis of cytokinin and auxin functions during root nodule development." Front Plant Sci **4**: 42.

Suzaki, T., K. Yano, M. Ito, Y. Umehara, N. Suganuma and M. Kawaguchi (2012). "Positive and negative regulation of cortical cell division during root nodule development in Lotus japonicus is accompanied by auxin response." Development **139**(21): 3997-4006.

Szczyglowski, K., R. S. Shaw, J. Wopereis, S. Copeland, D. Hamburger, B. Kasiborski, F. B. Dazzo and F. J. de Bruijn (1998). "Nodule Organogenesis and Symbiotic Mutants of the Model Legume Lotus japonicus." Molecular Plant-Microbe Interactions® **11**(7): 684-697.

Takanashi, K., A. Sugiyama and K. Yazaki (2011). "Involvement of auxin distribution in root nodule development of Lotus japonicus." Planta **234**(1): 73-81.

Taylor-Teeples, M., A. Lanctot and J. L. Nemhauser (2016). "As above, so below: Auxin's role in lateral organ development." Dev Biol **419**(1): 156-164.

Tirichine, L., N. Sandal, L. H. Madsen, S. Radutoiu, A. S. Albrektsen, S. Sato, E. Asamizu, S. Tabata and J. Stougaard (2007). "A gain-of-function mutation in a cytokinin receptor triggers spontaneous root nodule organogenesis." Science **315**(5808): 104-107.

Torres, D., I. Benavidez, F. Donadio, E. Mongiardini, S. Rosas, S. Spaepen, J. Vanderleyden, A. Pencik, O. Novak, M. Strnad, J. Frebortova and F. Cassan (2018). "New insights into auxin metabolism in Bradyrhizobium japonicum." Res Microbiol **169**(6): 313-323.

Towe, K. M. (2002). "Evolution of Nitrogen Fixation." Science **295**(5556): 798-799.

Turner, M., N. R. Nizampatnam, M. Baron, S. Coppin, S. Damodaran, S. Adhikari, S. P. Arunachalam, O. Yu and S. Subramanian (2013). "Ectopic expression of miR160 results in auxin hypersensitivity, cytokinin hyposensitivity, and inhibition of symbiotic nodule development in soybean." Plant Physiol **162**(4): 2042-2055.

Ulmasov, T., J. Murfett, G. Hagen and T. J. Guilfoyle (1997). "Aux/IAA proteins repress expression of reporter genes containing natural and highly active synthetic auxin response elements." The Plant cell **9**(11): 1963-1971.

van Noorden, G. E., T. Kerim, N. Goffard, R. Wiblin, F. I. Pellerone, B. G. Rolfe and U. Mathesius (2007). "Overlap of proteome changes in Medicago truncatula in response to auxin and Sinorhizobium meliloti." Plant Physiol **144**(2): 1115-1131.

van Spronsen, P. C., M. Grønlund, C. P. Bras, H. P. Spaink and J. W. Kijne (2001). "Cell Biological Changes of Outer Cortical Root Cells in Early Determinate Nodulation." Molecular Plant-Microbe Interactions® **14**(7): 839-847.

van Zeijl, A., R. H. Op den Camp, E. E. Deinum, T. Charnikhova, H. Franssen, H. J. Op den Camp, H. Bouwmeester, W. Kohlen, T. Bisseling and R. Geurts (2015). "Rhizobium Lipo-chitooligosaccharide Signaling Triggers Accumulation of Cytokinins in Medicago truncatula Roots." Mol Plant **8**(8): 1213-1226.

Wang, J.-W., L.-J. Wang, Y.-B. Mao, W.-J. Cai, H.-W. Xue and X.-Y. Chen (2005). "Control of root cap formation by MicroRNA-targeted auxin response factors in Arabidopsis." The Plant cell **17**(8): 2204-2216.

Wang, Y., K. Li, L. Chen, Y. Zou, H. Liu, Y. Tian, D. Li, R. Wang, F. Zhao, B. J. Ferguson, P. M. Gresshoff and X. Li (2015). "MicroRNA167-Directed Regulation of the Auxin Response Factors GmARF8a and GmARF8b Is Required for Soybean Nodulation and Lateral Root Development." Plant physiology **168**(3): 984-999.

Wang, Y., W. Yang, Y. Zuo, L. Zhu, A. H. Hastwell, L. Chen, Y. Tian, C. Su, B. J. Ferguson and X. Li (2019). "GmYUC2a mediates auxin biosynthesis during root development and nodulation in soybean." Journal of experimental botany **70**(12): 3165-3176.

Wasson, A. P., F. I. Pellerone and U. Mathesius (2006). "Silencing the flavonoid pathway in Medicago truncatula inhibits root nodule formation and prevents auxin transport regulation by rhizobia." The Plant cell **18**(7): 1617-1629.

Wybouw, B. and B. De Rybel (2019). "Cytokinin - A Developing Story." Trends Plant Sci **24**(2): 177-185.

Zürcher, E., D. Tavor-Deslex, D. Lituiev, K. Enkerli, P. T. Tarr and B. Müller (2013). "A robust and sensitive synthetic sensor to monitor the transcriptional output of the cytokinin signaling network in planta." Plant physiology **161**(3): 1066-1075.

CHAPTER II

2. Quantitative 3d imaging of cell level auxin and cytokinin response ratios in soybean roots (status: published[a])

Jon Fisher[1], Paul Gaillard[2], Carl R. Fellbaum[2], Senthil Subramanian[2, 3,*], Steve Smith[1,*]

1. Nanoscience and Nanoengineering, South Dakota School of Mines and Technology, Rapid City, SD 57701
2. Department of Agronomy, Horticulture, and Plant Science, South Dakota State University, Brookings, South Dakota, 57007
3. Department of Biology & Microbiology, South Dakota State University, Brookings, South Dakota, 57007

Correspondence: Senthil.Subramanian@sdstate.edu or Steve.Smith@sdsmt.edu

---

[a] Fisher, J, Gaillard, P, Fellbaum, CR, Subramanian, S, Smith, S. Quantitative 3D imaging of cell level auxin and cytokinin response ratios in soybean roots and nodules. *Plant Cell Environ*. 2018; 41: 2080– 2092. https://doi.org/10.1111/pce.13169

2.1. Abstract

Legume-Rhizobium symbiosis results in root nodules where rhizobia fix atmospheric nitrogen into plant usable forms in exchange for plant-derived carbohydrates. The development of these specialized root organs involves a set of carefully orchestrated plant hormone signaling. In particular, a spatio-temporal balance between auxin and cytokinin appears to be crucial for proper nodule development. We put together a construct that carried nuclear localized fluorescence sensors for auxin and cytokinin and used two photon induced fluorescence microscopy for concurrent quantitative 3-dimensional imaging to determine cellular level auxin and cytokinin outputs and ratios in root and nodule tissues of soybean. The use of nuclear localization signals on the markers, and nuclei segmentation during image processing enabled accurate monitoring of outputs in 3D image volumes. The ratiometric method used here largely compensates for variations in individual outputs due to sample turbidity and scattering, an inherent issue when imaging thick root and nodule samples typical of many legumes. Overlays of determined auxin/CK ratios on specific root zones and cell types accurately reflected those predicted based on previously reported outputs for each hormone individually. Importantly, distinct auxin/CK ratios corresponded to distinct nodule cell types indicating a key role for these hormones in nodule cell type identity.

Keywords: symbiosis, development, hormones, auxin, cytokinin, nodule, soybean, two photon induced fluorescence (TPIF), local maxima detection method (LMDM)

2.2. Introduction

Leguminous plants have evolved to symbiotically interact with diazotropic soil bacteria, collectively named rhizobia, and produce symbiotic nodules. There are two major classes of legume nodules: (i) determinate nodules that do not have a persistent nodule meristem and are spherical in shape, typically produced by tropical legumes such as soybean and *Lotus japonicus;* and (ii) indeterminate nodules that have a persistent meristem and oblong shape, typically produced by temperate legumes such as white clover and *Medicago truncatula* (reviewed by (Sprent 2007)). The development of these specialized root organs involves a set of carefully orchestrated plant developmental pathways. A number of different plant hormones have been implicated in nodule development (reviewed by (Ferguson & Mathesius 2014)). Of particular interest are the key plant hormones auxin and cytokinin (Suzaki *et al.* 2013).

Cytokinin (CK) activity is necessary and sufficient for the initiation of nodule development. Loss of function mutations in CK signaling components causes impairments in nodule primordia initiation (e.g. (Murray *et al.* 2007; Plet *et al.* 2011; Held *et al.* 2014). On the other hand, constitutive activation of a CK receptor results in spontaneous nodules even in the absence of rhizobia (Tirichine *et al.* 2007). CK acts upstream of several key transcription factors crucial for nodule initiation specifically in the root cortex (Madsen *et al.* 2010). In addition, CK is also active in the root epidermis and root hair where it appears to play a negative role to inhibit subsequent rhizobial

infection (Op den Camp *et al.* 2011; Miri *et al.* 2016). Therefore, CK plays both positive and negative roles in a tight interplay with key transcriptional regulators (reviewed in (Gamas *et al.* 2017)).

Auxin accumulation and/or perception also appears to be crucial for both determinate and indeterminate nodule initiation (Wasson 2006; Kohlen *et al.* 2017; Cai *et al.* 2017). However, enhanced response to auxin inhibits nodule formation (Bustos-Sanmamed *et al.* 2013; Turner *et al.* 2013; Wang *et al.* 2015). It is likely that a narrow window of auxin activity promotes proper nodule development (Mao *et al.* 2013).

In addition to their independent roles on nodule development, key interactions between auxin and CK also shape proper nodule development. *M. truncatula cre1* mutants deficient in CK perception, auxin transport regulation, and nodule initiation can be rescued through the exogenous addition of flavonoid compounds that inhibit auxin transport suggesting that a crucial role for CK during initiation of indeterminate nodule primordia is to direct the accumulation of auxin in specific root cortex cells (Plet *et al.* 2011) (Ng *et al.* 2015).

Spontaneous nodules that result from constitutive activation of a CK receptor in *L. japonicus* also display auxin responsive gene expression suggesting that CK might activate auxin accumulation for determinate nodule initiation as well (Suzaki *et al.* 2012). However, deregulated auxin activity appears to inhibit post-initiation development of nodules. For example, exogenous auxin or enhanced sensitivity to auxin inhibited nodule

formation in *M. truncatula* (van Noorden *et al.* 2006) (Breakspear *et al.* 2014; Hobecker *et al.* 2017), and conversely resistance to auxin resulted in enhanced nodule development in this species (Kuppusamy *et al.* 2009). In soybean, enhanced sensitivity to auxin resulted in reduced nodule formation (Wang *et al.* 2015), and was associated with reduced sensitivity to CK (Turner *et al.* 2013).

Exogenous CK restored nodule numbers in these roots, suggesting that the underlying reason for reduced nodulation in auxin hypersensitive roots is reduced CK activity (Nizampatnam *et al.* 2015). These observations suggested that an appropriate balance between auxin and CK might be crucial for proper nodule development similar to other plant developmental processes such as formation of the embryonic root pole, maintenance of root meristem size, xylem differentiation, lateral root formation, shoot apical meristem activity, and shoot axillary bud development (reviewed in (Vanstraelen & Benková 2012; Schaller *et al.* 2015)).

Although the auxin-CK ratio is likely to be an important determinant of legume nodule development, the mechanism has yet to be defined. Recent studies are unraveling molecular mechanisms by which auxin and CK interact at the levels of biosynthesis, inactivation/degradation, transport, and signaling in plants [reviewed in (Vanstraelen & Benková 2012; Schaller *et al.* 2015)]. One of the first steps in elucidating mechanisms by which auxin and CK interact to dictate proper nodule development is to map and quantify the cellular outputs of these hormones.

While many methods exist to measure auxin and CK distributions in root systems, fluorescence imaging allows for non-invasive observation of hormone outputs (a combination of both hormone levels and a cell's response). While both perception and transcriptional output sensors are available for auxin (Ulmasov *et al.* 1997; Liao *et al.* 2015), only transcriptional output sensors have been developed for CK (D'Agostino *et al.* 2000; Müller & Sheen 2008; Zürcher *et al.* 2013). We reasoned that using transcriptional output sensors for both hormones would allow the best possible comparison of relative cellular outputs of these hormones in specific cell types during nodule development.

In legumes, transcriptional output sensors based on the auxin-responsive GH3 promoter and the synthetic DR5 promoter reporter have been used to successfully identify domains of auxin output during nodule development (Suzaki *et al.* 2012; Turner *et al.* 2013; Breakspear *et al.* 2014; Ng *et al.* 2015). Auxin output was detected in the root hairs and infection zone, nodule initial cells, early nodule primordium, nodule meristem, and in the nodule vasculature. While the GH3 promoter appears to closely reflect auxin outputs, it is likely to be under regulation by other cues. Therefore, we decided to use the DR5 promoter that specifically responds to auxin. Similarly, transcriptional output sensors based on the Arabidopsis ARR5 promoter, and the synthetic TCS and TCSn promoters have been used to map domains of CK output during nodule development (Lohar *et al.* 2004; Held *et al.* 2014; Franssen *et al.* 2015; Gamas *et al.* 2017; Reid *et al.* 2017).

CK output has been detected in nodule initial cells, the entire nodule primordium, root epidermis and root hairs, and in most cells of mature nodules. We chose the TCSn promoter which is the most sensitive and also specific to CK. Previous studies on legumes used these sensors for qualitative spatio-temporal mapping of auxin or CK outputs. The use of fluorescent proteins that localize to the nucleus as output markers would enable accurate quantification, as outputs from nuclear localized signals are unlikely to be affected by cell size and vacuolization. For example, quantification of auxin perception in specific root cell files using the R2D2 sensor in Arabidopsis root tips revealed that CK maintains the position of the transition zone by controlling both polar auxin transport and local auxin degradation (Di Mambro *et al.* 2017).

To enable simultaneous quantitative imaging of auxin and CK outputs, we generated a single construct that carried transcriptional output sensors for both hormones. The construct contained transcriptional fusions of nuclear-localized green fluorescent protein (GFP) to the auxin-responsive DR5 promoter, and nuclear-localized tdTomato, to the CK-responsive TCSn promoter (DR5:GFP-NLS and TCSn:tdTomato-NLS). Given that the distribution of auxin and CK outputs along the main axis of the root and during lateral root formation have been separately demonstrated in the literature, we used these tissues to validate the construct and quantification methods. For example, CK response is high in the columella, somewhat diminished in the quiescent center (QC), and strong in the vasculature of the elongation zone (Zürcher *et al.* 2013; Antoniadi *et al.* 2015). Auxin

response on the other hand, is high in the QC and initial columella cells (Petersson *et al.* 2009; Suzaki *et al.* 2012; Turner *et al.* 2013).

Each of these qualitative measures, while informative, fail to reveal the relative outputs of these two key regulatory hormones as a function of the root architecture. In addition, imaging is sensitive to varying experimental conditions, including aberrations caused by local fluctuations in refractive index and scattering particularly in species with thicker roots such as soybean and other legumes. Using the two-color construct reported here, in combination with quantitative analysis, and the use of relative ratios rather than absolute outputs, is expected to minimize these influences and be a more faithful reporter of relative hormone outputs. We combined 3-D imaging using multiphoton microscopy with image analysis tools to detect individual nuclei, quantify hormone outputs, and calculate relative ratios of auxin and CK outputs in each nucleus. We applied the methods to premature nodule tissues of soybean to determine relative auxin/CK ratios in different nodule zones/ cell types.

2.3. Materials and Methods

2.3.1. DNA vector and composite plant transformation

A plant binary vector containing DR5:GFP-NLS and TCSn:tdT-NLS transcriptional fusions where the auxin-responsive promoter DR5 (Ulmasov *et al.* 1997)

drove the expression of GFP and CK-responsive promoter TCSn (Zürcher *et al.* 2013) drove the expression of tdTomato, both florophores with a NLS, was generated as follows. The DR5:GFP-NLS sequence was reported by (Suzaki *et al.* 2012), and was kindly provided by Dr. Takuya Suzaki, National Institute for Basic Biology, Okazaki, Japan. The TCSn:tdTomato-NLS composed of the TCSn promoter sequence (Zürcher *et al.* 2013) kindly provided by Dr. Bruno Mueller, University of Zurich, Switzerland, tdTomato coding sequence, and the NLS sequence from the construct above. The sequences were synthesized by Genscript, and cloned in to pCAM backbone obtained from pCAM-GFP-GW (Subramanian lab, unpublished). The NLS sequence was added in frame to the C-terminus end of the fluorophores to concentrate them in the nucleus for enhanced sensitivity, and accurate quantification irrespective of cell size or vacuolization status.

Soybean (*Glycine max* 'William 82') transgenic composite plants were generated using *Agrobacterium rhizogenes*-mediated transformation as described by (Collier *et al.* 2005). Three weeks post *A. rhizogenes* treatment, composite plants were screened under a dissection microscope to identify and tag transgenic roots of interest based on tdT epifluorescence at the root tip. Composite plants were transferred to a 4" pot filled with sterilized 3:1 vermiculite: perlite mix, and watered with nitrogen free plant nutrient solution (N^- PNS). Five days-post transfer, the plants were inoculated with a suspension of *Bradyrhizobium japonicum USDA110* cells re-suspended in N^- PNS to $OD_{600\ nm}$ of 0.08. About 25 mL of this suspension was added uniformly to each pot. Roots were

harvested at 7 to 30 days post rhizobium inoculation for imaging of premature nodules (Figure S4a). For mock-inoculated plants, the same quantity of N^- PNS was applied, and used for imaging of root tips and lateral root primordia.

2.3.2. TPIF Imaging of GFP, tdTomato, and FM4-64

All images were obtained using an Olympus FV1000MPE multi-photon scanning laser microscope. An InSight® DS+ laser from Spectra Physics was mode-locked with an average power of 1.71W at 950nm, which is where GFP and tdTomato have similar two-photon absorption cross-sections (spectra.arizone.edu). Excitation power used varied between 5%, 8%, and 16% in successive images to measure unsaturated epidermal fluorescence at lower powers and to measure deep tissue sections at higher powers. Two PMTs collected fluorescence from this excitation at 500-540nm for green, and 580-640nm for red, digitized at 12-bit resolution. Because GFP has a long emission tail, an average of 9.6% of the GFP signal is detected in the red channel which was subtracted out during post-processing. Additionally, a Mai Tai laser was mode-locked with an average power of 0.85W at 750nm to image two photon induced autofluorescence of the cell walls and root epidermis. Autofluorescence was excited at 8% power and filtered by a 400-450nm bandpass filter.

Samples were mounted in dH_2O between a glass slide and coverslip, then imaged using a XLPL25XWMP 25X 1.05NA water immersion objective from Olympus. Images

were obtained at 512x512 resolution in the XY dimensions with a varying number of Z-slices depending on the sample. Each voxel is 1x1x1μm^3 which was chosen to balance acquisition speed and resolution. Optical images showed signal up to an average of 150μm depth, which generally is larger than the root apex radius. The deeper the penetration, the lower the resolution, likely related to the aberrations in the beam caused by variable refractive index and scattering due to the inhomogeneity in tissue type and shape with depth.

After imaging, root tip and root segments with LRP were stained for 30 minutes using FM4-64 dye, which binds to the cell membranes (Bolte *et al.* 2004). Additional images were obtained at 950nm and 1-2% excitation power to observe root cell morphology. Lateral and distal sectional slices after staining showed nearly uniform penetration of FM4-64 stains throughout the root sample. Premature nodule sections did not stain well with FM4-64 precluding the identification of nodule zones. We used autofluorescence and nuclear density in grayscale versions of hormone output images to distinguish different nodule zones (See "*Region of Interest (ROI) Sectioning*" subsection below).

2.3.3. Particle Segmentation to detect nuclei

Collected images were analyzed by a modified 3D particle segmentation routine referred to here as the local maxima detection method (LMDM), originally developed by

Weeks (Crocker & Weeks) and later adapted to MATLAB by Kilfoil (Kilfoil; Gao & Kilfoil 2009). The basic functions of the routine operate as follows. First, local maxima are detected throughout the image. Next, a pre-defined volume mask is created about the maxima. All nearby shells are then rejected. Finally, the shell is relocated to the center of mass of the found particle. All signal within this shell is summed as the particle intensity. Particle sums below a defined signal threshold are filtered from the final result. Analysis of root images presented here using this method showed nearly zero false positives and an approximately 85% detection rate compared to manual inspection. See *Results* section for details on optimization of these parameters for detecting nuclei.

Nuclei will only fluoresce when the cell contains auxin, CK, or both. This can result in a different number of observed nuclei in the red and green channels. Thus, to co-localize root nuclei using the above routine, both red and green channels were added together before segmentation. The resulting particle centroids and volume masks were applied to sum the red and green channels separately.

2.3.4. Region of Interest (ROI) Sectioning

After nuclei segmentation, tissue domains of interest within each image were identified and digitally sectioned. A generalized sectioning can be performed by creating regions of interest (ROIs) in the data using simple 3D masks, typically a cuboid or a cylinder (See cylindrical sectioning algorithm in supplemental materials). For root tip and

LRP images, the regions were identified using FM4-64 stained images which display root cell wall morphology, thereby identifying the specific root architecture, and the ROIs were transferred to corresponding GFP/tdTomato images to evaluate auxin-CK outputs. For premature nodule images, FM4-64 staining was not as efficient in distinguishing individual cells. Therefore, the distinction between infection zone and its surrounding parenchyma was determined based on the autofluorescence of a layer of cells bordering the infection zone. The vascular bundles were characterized by the presence of a cluster of nuclei within the parenchyma. The outer boundary of the parenchyma region was determined based on sclerenchyma and epidermal cell autofluorescence (Figure 2.4.5-2 a, Figure 2.4.5-3b). We were able to manually confirm the boundaries of infection zone, nodule parenchyma, and vascular bundles (where visible) switching between fluorescence and white light through the eye piece.

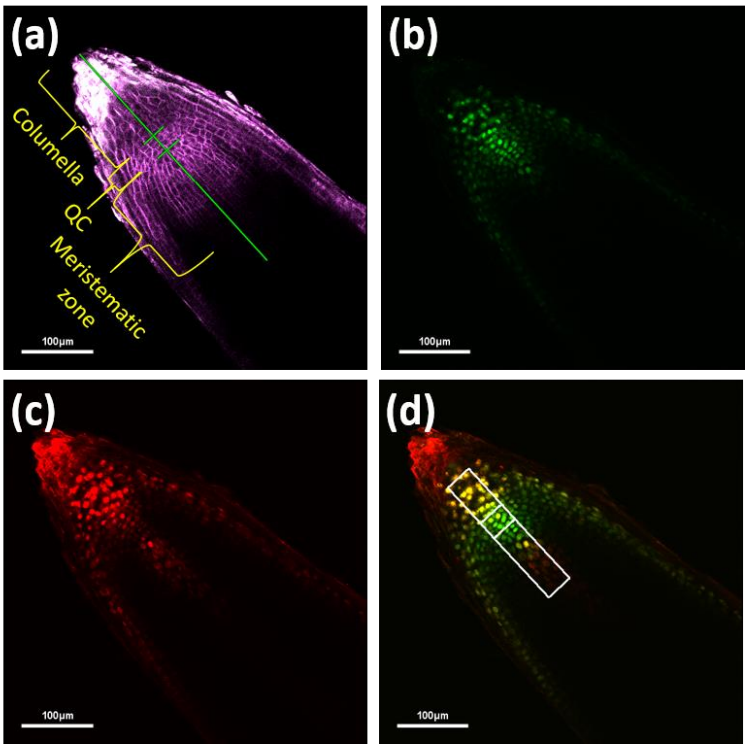

Figure 2.3.4-1: Auxin and CK outputs along the longitudinal axis of a soybean root tip. *A median optical section along the longitudinal axis of a soybean composite plant primary root tip expressing DR5:GFP-NLS and TCSn:tdTomato-NLS where output collected using the (a) FM4-64 channel, (b) green channel indicating auxin output, (c) red channel indicating CK output, and (d) a composite of red and green are shown. The green line in (a) indicates the main axis along which hormones outputs were quantified. Segments in (a) and (d) indicate the root cap columella, QC, and proximal meristem starting from the root tip. The image shown is representative of 14 out of 15 primary roots evaluated.*

2.4. Results

2.4.1. Auxin and cytokinin outputs in soybean composite plant roots closely reflect that observed in other plant species

Reporter constructs based on DR5 and TCSn promoters were previously used to localize auxin and CK outputs at cellular resolution (e.g. (Friml *et al.* 2003) (Zürcher *et al.* 2013). To validate the use of these markers in composite soybean plant roots, the expression patterns of DR5:GFP-NLS and TCSn:tdTomato-NLS were evaluated by two-color TPIF imaging. DR5:GFP-NLS was clearly visible in root cap columella cells, QC, and dividing meristematic cells (Figure 2.4-1a and 2.4-1b). A lower, albeit clearly detectable, expression level was observed in other cells of the root cap. TCSn:tdTomato-NLS was also clearly observed in the columella cells, but was much lower in the QC and meristematic cells (Figure 2.4-1a and 2.4-1c). The expression was prominent in the outer layer of the root cap compared to other root cap cells. The observed expression pattern of the reporters was in agreement with those observed in other plant species stably transformed with these markers, indicating that composite soybean plants expressing these markers are a suitable experimental system to study hormone output in roots and nodules.

2.4.2. Optimized Parameters for detecting nuclei

Determination of cell level auxin and CK outputs requires high-throughput automated detection of nuclei. We employed the local maxima detection method (LMDM) developed by Weeks (Crocker & Weeks), a highly sensitive algorithm by design. In addition, due to variations in size of the nuclei and their close proximity to each other in the root meristem and nodule primordium tissues, LMDM is likely to be better at identifying individual nuclei compared to other methods relying on signal boundary such as watershed segmentation (Roerdink & Meijster 2000). However, LMDM requires optimization for each specific application. Optimization was conducted through processing 40x40x40μm^3 volumes from different regions in the root tip and manually validating the results through visual inspection. Three general parameters required adjustment: (i) particle mask diameter to account for nuclei of different sizes, (ii) volume count threshold to reduce the number of false positives, and (iii) separation distance to confidently detect individual nuclei in regions of high cell density.

The most efficient particle mask diameter was the smallest possible diameter, which collects the most nuclei. Nuclei are approximately spherical with ≈5μm diameters near the QC and ≈7μm in the meristematic elongation zone. Imaged nuclei were slightly elongated in the z-axis due to the point spread function of the microscope. All collected images were obtained at 1x1x1μm^3 resolution. Thus, 5x5x7 voxel diameters were chosen to capture the full volume of the smallest nuclei.

Volume count thresholds are needed to reduce the number of false positives detected in the image. Many false positives can be detected near arbitrarily bright voxels which register as a local maximum. Volume thresholding eliminates these false positives. Using a 5x5x7 nuclei volume mask, each volume mask has a total of 123 voxels. The average background per pixel within collected images was 40 ± 10 counts. Thus, the background level in a single mask could reach 4920±1230 counts. However, image intensities were offset by 40 counts before LMDM processing, leading to at most 1230 counts from noise. The thresholding limit was set to 10,000 counts to be well above this floor but still able to detect dim nuclei. Since the maximum counts per voxel is 4096 for 12-bit resolution, only exceptionally bright anomalous regions could register as false positives at this limit. The final limiting parameter is particle separation distance. For close-packed regions, this parameter is recommended by Weeks to be 1/2 particle diameter. Using this setting no evident false positives were detected by visual inspection in the subsections evaluated.

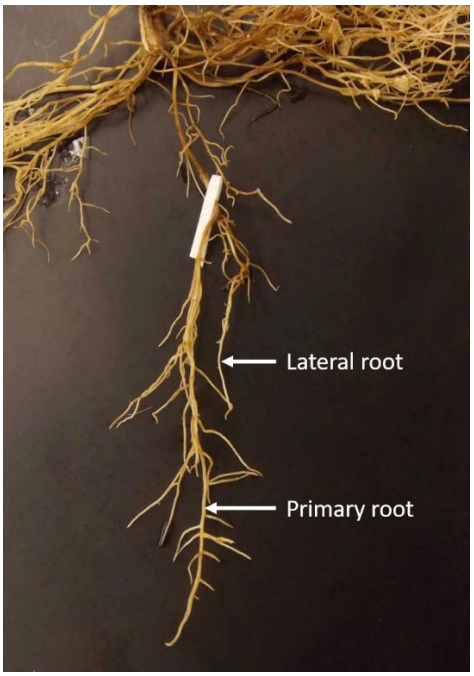

Figure 2.4.2-1: Picture showing an example of a primary and lateral root (labeled) in a composite soybean plant. *Transgenic roots were identified based on TCSn:tdTomato-NLS fluorescence at the root tip using a dissection microscope and labeled using a Tough tag.*

Root tips are one of the most studied plant organs for auxin and CK outputs. Multiple signaling modules that confer key cell identities in the root tip are also known. As the first step towards establishing parameters for imaging and quantification of auxin and CK output, we imaged primary and lateral root tips using TPIF microscopy and analyzed auxin and CK outputs in the central core. However, as the original primary roots are cut during the composite plant transformation process, all composite plant roots are essentially secondary roots. We refer to the roots originating directly from the cut end of

the stem as primary roots, and those emerging from these roots as lateral roots (Figure 2.4.3-4).

2.4.3. Auxin and Cytokinin Output and ratios along different cell types of the central root core

Our goal was to identify key cell types and associated auxin-CK outputs and ratios. FM4-64 (Vida & Emr 1995) staining was used to identify cell morphology and thus conventional cell types, and the hormone response markers were used to determine hormone outputs. An example cross-sectional image of a primary root tip can be seen in Figure 2.3.4-1. Regions of interest (ROIs) for detection of nuclei and quantification of hormone outputs were identified along the central root apex axis as follows. A cylindrical section was created about a vector that began in the root apex and ended in the root meristem; the selection of these points was aided by FM4-64 staining (Figure 2.3.4-1a). Three cylindrical subsections along the root main axis which identified the root cap columella, the QC, and the dividing cells of the meristem were created based on cell morphology (Figure 2.3.4-1a).

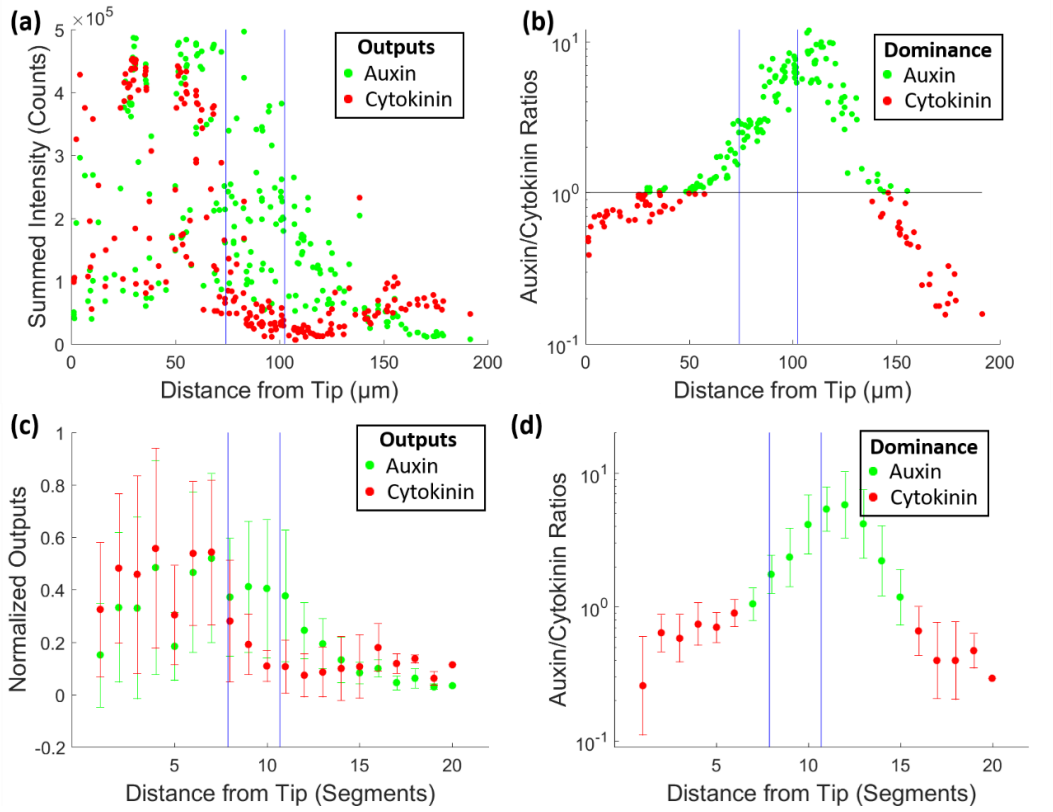

Figure 2.4.3-1: Quantification of auxin and CK output and relative ratios along the central root axis. *(a) Auxin and CK output and (b) relative ratio in each nucleus plotted as a function of distance from the tip of the primary root shown in Figure 2.3.4-1. Each dot represents a nucleus. Vertical blue lines indicate the boundaries of root cap columella, QC, and proximal meristem. (c) Average auxin and CK outputs and (d) ratios obtained from three independent transgenic roots (n=3). See Figure 2.4.3-2 for raw data. Auxin and CK outputs and relative auxin/CK ratios in nuclei from 20 normalized segments (≈18μm each) in each root along the root axis were determined and averaged. Segments along the root axis for each root were normalized by scaling the QCs to the same size.*

The cylindrical ROI mask had an average radius of 15µm per root sample, as determined by the meristem radius. Sloughed off root cap cells still attached to the root tip (observed mostly in primary roots) fluoresced in the red channel (Figure 2.3.4-1a and 2.3.4-1c). These regions were ignored during analysis. The ROIs were transferred over to the hormone output images by measuring the distance from the tip to the QC boundaries in the FM4-64 images and transferring this to the fluorescent hormone image (Figure 2.3.4-1d). Nuclei in the images were segmented into ellipsoidal volumes with 5µm x 5µm x7µm diameters and a minimum threshold of 10,000 counts.

All segmented nuclei within the masks were characterized as a function of distance from the root apex along the drawn vector. Figure 2.4.3-1 shows both fluorescence outputs and relative ratios of auxin and CK for the root image shown in Figure 2.3.4-1 as a function of distance along the root tip. Each green/red dot in Figure 2.4.3-1a represents a single nucleus denoting auxin/CK output respectively. In Figure 2.4.3-1b, each dot represents a single nucleus denoting the ratio of auxin/CK. The dots in Figure 2.4.3-1b are color coded with green/red to indicate if that particular nucleus is auxin (ratios above 1.0) or CK dominant (ratios below 1.0). Thus, our construct, imaging and quantification methods enable us to determine relative auxin-CK outputs and ratios at cellular resolution through concurrent expression and visualization of nuclear-localized markers for auxin and CK. To evaluate consistency among different roots, a total of 317 nuclei were assayed from the central cores of primary root tips from three independent transgenic roots. Hormone outputs were normalized by scaling to that of the nucleus with

maximum auxin output in each root. The average values and standard deviation of hormone outputs and auxin/CK ratios for these roots can be observed in Figure 2.4.3-1c and 2.4.3-1d respectively.

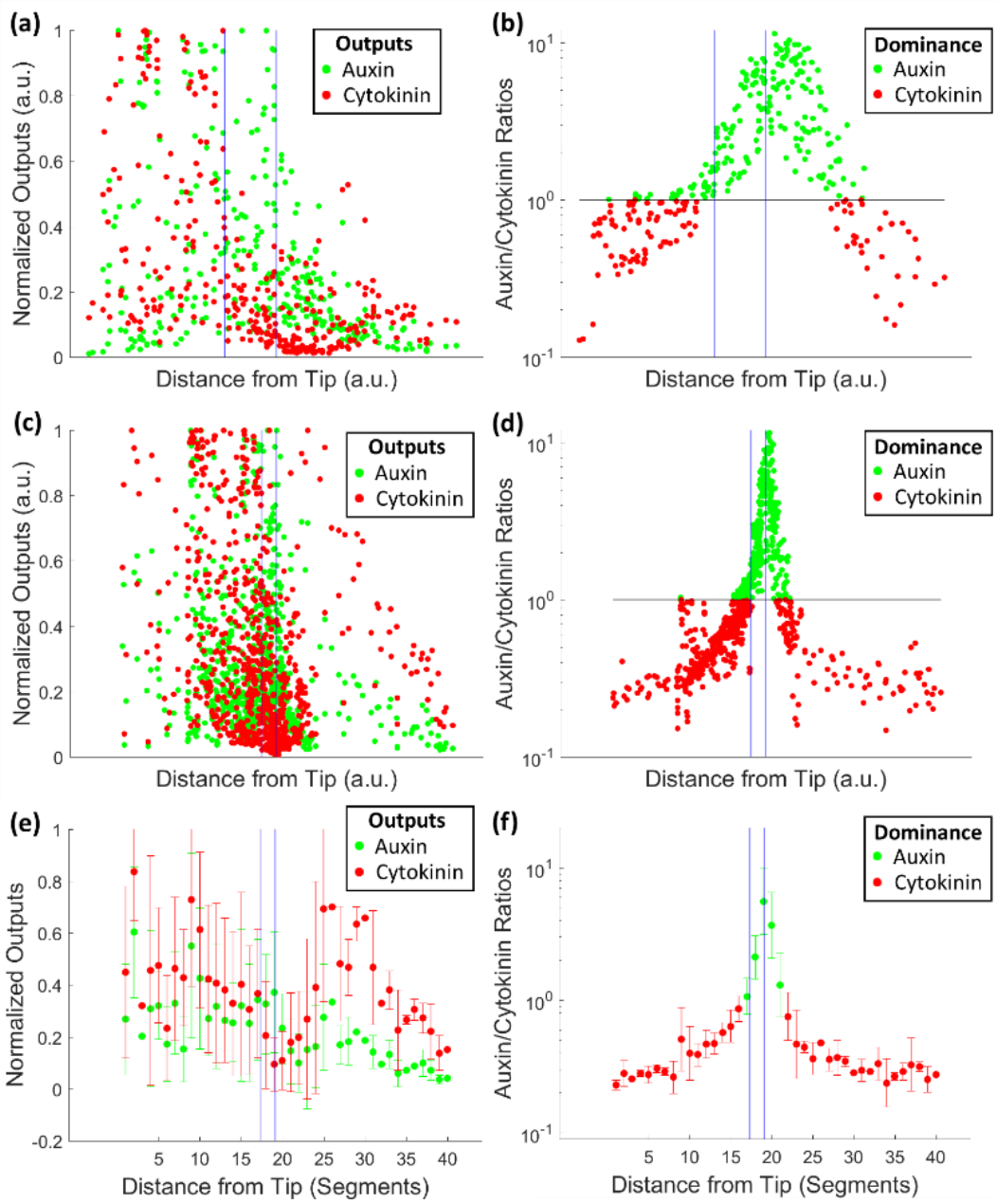

Figure 2.4.3-2: Auxin and CK output and relative ratios along the central root axis for primary root tips. *(a) Auxin and CK output and (b) relative ratio in each nucleus plotted as a function of distance for the three roots overlay normalized by the QC boundaries as determined by FM4-64 staining. These figures correspond to the 3 primary-root averages in Figure 2.4.3-2c and 2.4.3-2d. (c) Auxin and CK output and (d) relative ratio in each nucleus for 9 primary-root overlay wherein the QC is approximated by the rising edge of the auxin dominant peak. Corresponding 40 segment averages and standard deviations of these overlays (≈28μm each) are shown for both (e) outputs and (f) ratios.*

Raw data is presented in Figure 2.4.3-2a and 2.4.3-2b. Absolute outputs showed a decay in both channels relating to the increasing penetration depth in the sample and other extrinsic factors, however, the relative ratios of the two fluorophores should be insensitive to these variations. Both auxin/CK outputs (Figure 2.4.3-2c) and relative ratios (Figure 2.4.3-2d) showed substantial differences in different cell types. The highest auxin CK ratio was observed in the dividing cells of the proximal meristem, closest to the QC (Figure 2.4.3-2d; segments 11-12). In the shootward direction, the ratio quickly drops, heavily favoring CK, in cells of the proximal meristem (segments 13-20). The ratio also drops, albeit at a slower rate, towards the root cap along the QC region (segments 10-7), reaching a near uniform relative ratio of auxin to CK along the middle region of the columella (segments 2-6).

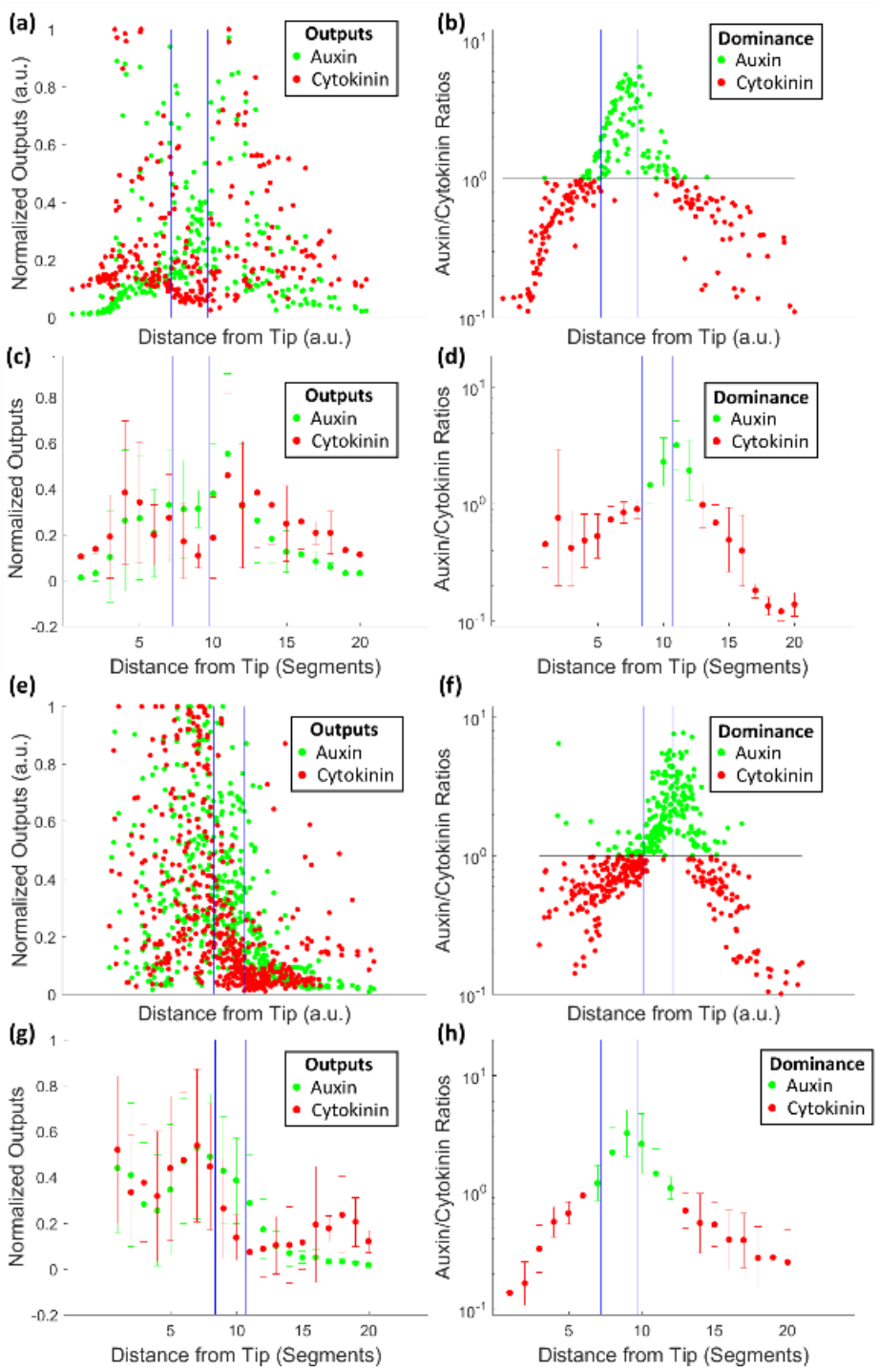
(a)
Outputs
Auxin
Cytokinin
Normalized Outputs (a.u.)
Distance from Tip (a.u.)
(b)
Dominance
Auxin
Cytokinin
Auxin/Cytokinin Ratios
Distance from Tip (a.u.)
(c)
Outputs
Auxin
Cytokinin
Normalized Outputs
Distance from Tip (Segments)
(d)
Dominance
Auxin
Cytokinin
Auxin/Cytokinin Ratios
Distance from Tip (Segments)
(e)
Outputs
Auxin
Cytokinin
Normalized Outputs (a.u.)
Distance from Tip (a.u.)
(f)
Dominance
Auxin
Cytokinin
Auxin/Cytokinin Ratios
Distance from Tip (a.u.)
(g)
Outputs
Auxin
Cytokinin
Normalized Outputs
Distance from Tip (Segments)
(h)
Dominance
Auxin
Cytokinin
Auxin/Cytokinin Ratios
Distance from Tip (Segments)

Figure 2.4.3-3: Auxin and CK output and relative ratios along the central root axis for lateral root tips. *(a) Auxin and CK output and (b) relative ratio in each nucleus plotted as a function of distance for the 3-root overlay normalized by the QC boundaries as determined by FM4-64 staining. Corresponding averages and standard deviations for the 3 lateral-root overlay are plotted in 20 segments (≈20μm each) for both (c) outputs and (d) ratios. Additionally, an 11 lateral-root overlay of lateral roots was produced by approximating the QC boundaries by the rising edge of the auxin dominant peak, showing both (e) Auxin and CK output and (f) relative ratio in each nucleus. Corresponding averages and standard deviations for the 11-root overlay are plotted in 20 segments (≈22μm each) for both (g) outputs and (h) ratios*

To evaluate if an independent assessment of auxin/CK ratios can be used to determine root architecture independent of FM4-64 staining, auxin-CK outputs and ratios obtained from an additional 6 primary roots (Figure 2.4.3-3c to 2.4.3-3f) were overlaid with distance normalized to the "predicted" QC of each root. The QC was predicted based on the extent of the auxin dominant region as observed in Figure 2.4.3-1d. Thus, a total of 9 primary roots were assessed for their average auxin/CK ratio values. The quantitative patterns of auxin/CK ratios along the root axis were consistent among the group of primary root tips (Figure 2.4.3-3f).

Analysis of 191 nuclei from lateral roots of three independent transgenic roots stained with FM4-64 (Figure 2.4.3-3a to 2.4.3-3d) displayed similar distribution of auxin and CK outputs and ratios as observed for primary roots. An additional 8 lateral roots

where auxin and CK outputs and ratios were evaluated independent of FM4-64 staining also displayed similar patterns (Figure 2.4.3-3e to 2.4.3-3h). It should be noted that the peak auxin/CK ratio in primary roots was 7.5±3.4:1 and that of lateral roots was 3.4±1.1:1. Our results demonstrate that concurrent imaging of auxin and cytokinin outputs and determination of their ratios at cellular resolution using the construct and analysis methods used were able to accurately correlate the root architecture zones/cell types to relevant auxin/CK ratios.

2.4.4. Lateral root primordia show a transition to cytokinin dominance post-breach of epidermis

The quantitative hormone output imaging method was applied on lateral root primordia (LRP) to obtain a better understanding of spatio-temporal changes in auxin-CK levels during the development of this organ in soybean. In particular, two types of LRP were investigated, Stage V and Stage VI, which signify before and after breaching the epidermis, respectively, following Herrbach, et al. (Herrbach *et al.* 2014). These stages were chosen as the major transition from auxin-rich to auxin-CK patterns occurs during LR emergence in Arabidopsis (Bielach *et al.* 2012; Chang *et al.* 2013; Zürcher *et al.* 2013). Primordia stages were identified based on morphology observed in FM4-64 stained images. Because of their early formation orientation, the QC was barely visible based on morphology. ROIs in these LRPs were marked as cylinders along the root center axis. Since the QC could not be determined in younger LRPs (Stage V), it

becomes untenable to create multi-root overlays as there is no obvious commonality, either morphologically or in hormone outputs, to normalize the results.

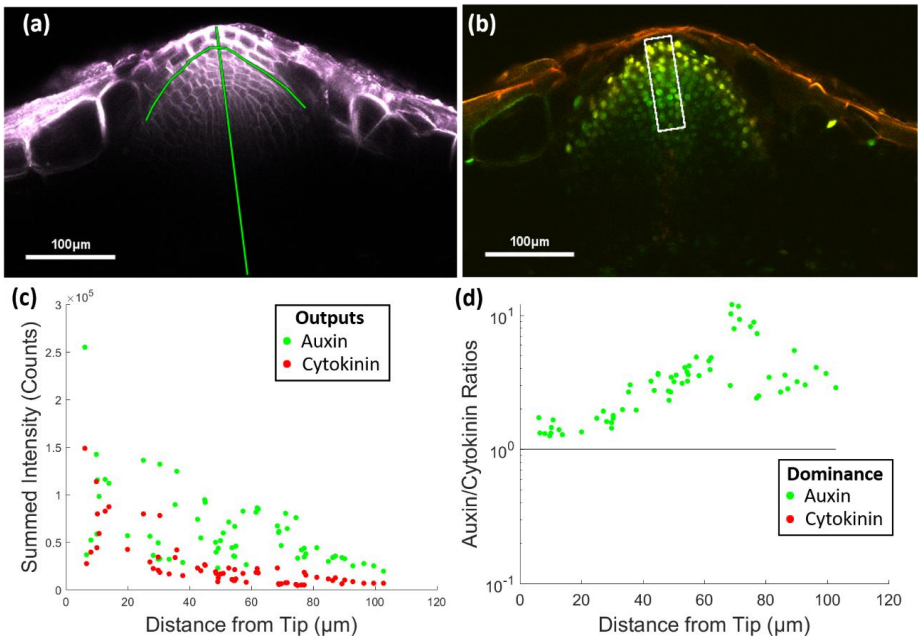

Figure 2.4.4-1: Representative images and hormone outputs from a Stage V lateral root primordium. *(a & b) Median optical sections along the longitudinal axis of the lateral root primordium expressing DR5:GFP-NLS and TCSn:tdTomato-NLS. Output collected using the (a) FM4-64 channel, and (b) a composite of red and green are shown. The straight green line in (a) indicates the main axis along which hormones outputs were quantified. The curved greenline marks the outer boundary of LRP. The ROI box in (b) indicates the region analyzed for hormone outputs. (c) Auxin and CK outputs and (d) relative ratios in each nucleus plotted as a function of distance from the tip of the primary root shown in (a). Each dot represents a nucleus. The image shown is representative of 7 out of 8 LRPs evaluated.*

Therefore, representative examples of each type are shown. Four out of five LRPs imaged showed similar spatial patterns of hormone outputs and ratios. Figure 2.4.4-1a and 2.4.4-1b show cross-sectional TPIF images of a Stage V lateral root with many small cell layers. No clear distinction between columella and the QC can be observed at this stage based on cell morphology (Figure 2.4.4-1a). Fluorescence images show mainly auxin dominance in the Stage V (Figure 2.4.4-1b). Quantification of hormone outputs (Figure 2.4.4-1c) clearly indicate high auxin and basal levels of CK along the LRP axis. Relative auxin/CK ratios (Figure 2.4.4-1d) indicate near equal ratios close to the tip and a higher auxin peak at the base. CK is involved in early stages of breaching the root cap, but never has greater relative output than auxin.

Post-breach, Stage VI samples can also be determined with FM4-64 staining based on the discontinuous primary root epidermal layer (Figure 2.4.4-2a). A noticeable CK dominance can be observed in these images, in particular in the root cap (Figure 2.4.4-2b). Stage VI samples show substantial shift from auxin dominance to the familiar CK-Aux-CK patterning present in primary and lateral root tips (Figure 2.4.4-2c and 2.4.4-2d). Four out of five LRPs imaged showed similar patterns of hormone outputs and ratios. Because the Stage VI organ is small, the shift between auxin and CK dominance is more abrupt than in fully developed root tips (Figure 2.4.3-2).

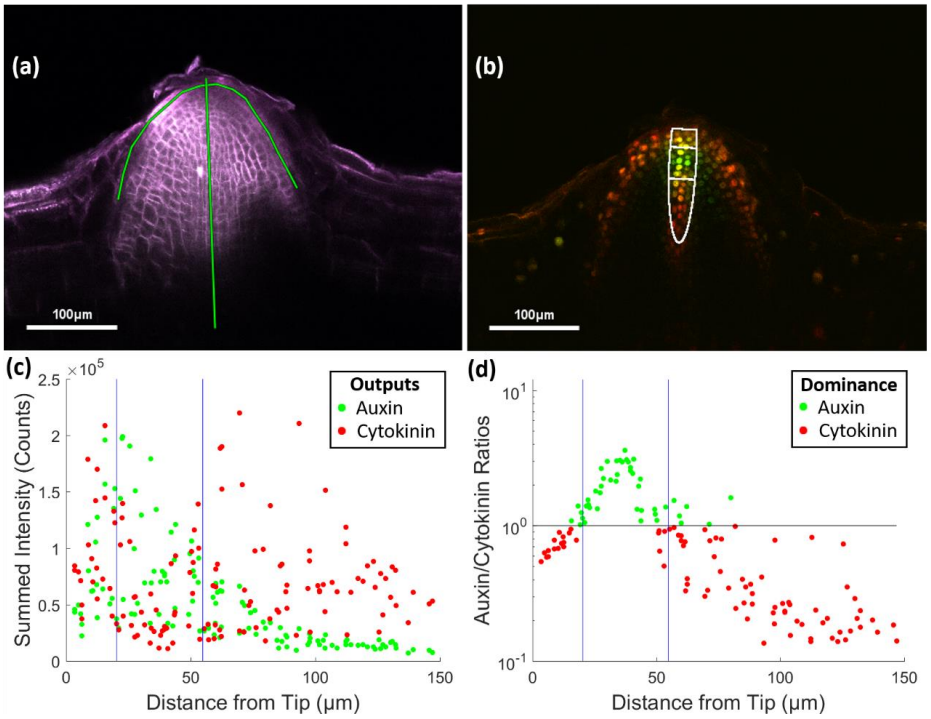

Figure 2.4.4-2: Representative images and hormone outputs from a Stage VI lateral root primordium. *(a & b) Median optical sections along the longitudinal axis of the lateral root primordium expressing DR5:GFP-NLS and TCSn:tdTomato-NLS. Output collected using the (a) FM4-64 channel, and (b) a composite of red and green are shown. The straight green line in (a) indicates the main axis along which hormones outputs were quantified. The curved greenline marks the outer boundary of LRP.. The ROI box in (b) indicates the region analyzed for hormone outputs. (c) Auxin and CK outputs and (d) relative ratios in each nucleus plotted as a function of distance from the tip of the primary root shown in (a). Each dot represents a nucleus. Blue lines indicate shift between auxin and CK dominance corresponding to segments in (b). The image shown is representative of 9 out of 10 LRPs evaluated.*

Several distinctions between Stage V and Stage VI primordia can be drawn from these examples. First, auxin dominates the primordia tissue during Stage V as previously reported, and CK dominates during Stage VI except for a small region along the core where the QC is likely to be located. This shift is associated with the transition from dividing cells in Stage V to cellular elongation and cell type differentiation in Stage VI. Remarkably, Stage VI auxin/CK peak values ranged from 2.0-2.5 which were close to the 3.5 average of fully emerged mature lateral roots.

2.4.5. Pre-mature determinate nodules show distinct cell type-associated auxin-cytokinin ratios

The quantitative hormone output imaging method was adapted and applied to nodule tissues where little is known about the relative auxin and CK outputs. Premature determinate nodules of soybean were selected for initial analysis as they have visibly distinct nodulation zones and cell types. These were identified by their rounded shape, ≈500µm diameter, an incomplete emergence from the root and perpendicular angle compared to the root from which they initiated (Figure 2.4.5-1a). The highly spherical nature of nodules made optical sectioning through the tissue difficult, as there is a wide dynamic range in fluorescence between regions on the periphery and the center, related to the varying imaging depth. To produce a more uniform image intensity with depth, nodules were hand-sectioned to 40-80µm flat segments by a razor blade and imaged as described for the root samples.

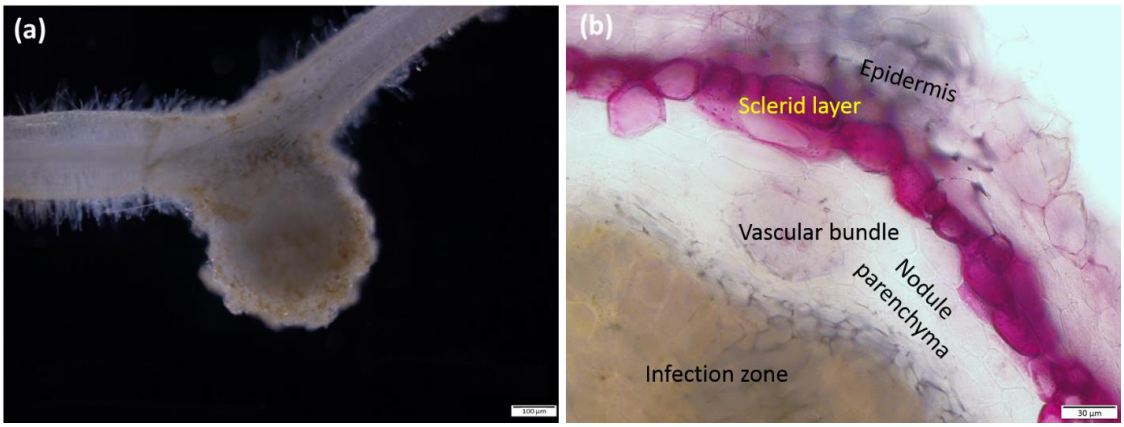

Figure 2.4.5-1: Representative image of a Soybean Premature nodule. *Premature nodule corresponds to the developmental category between the nodule primordia and the fully functional mature nodule. This developmental category is characterized by an incomplete emergence from the root. An angle of 90^{o} (±15) between the nodule epidermis and the adjacent root epidermis permits to determine the Premature nodule identity. Scale bar at: 200µm. (b) A portion of a cross section of a mature nodule stained with phloroglucinol showing morphological features of the infection zone, nodule parenchyma, and vascular bundle. A layer of smaller cells with thicker walls that displayed autofluorescence separated the infection zone and parenchyma. Vascular bundles appeared as near circular bodies with a relatively higher cell density located within the parenchyma.*

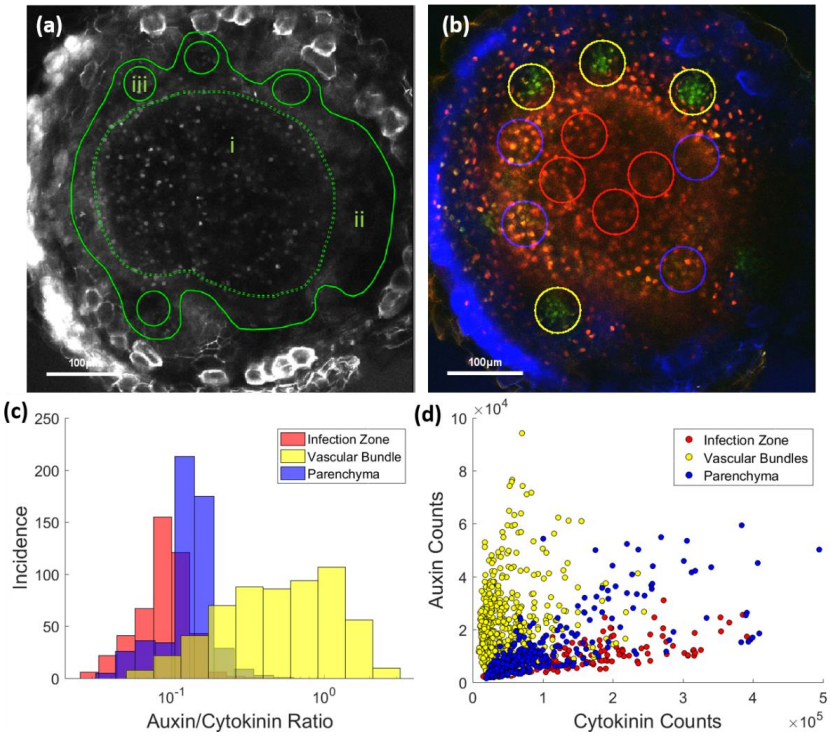

Figure 2.4.5-2: Auxin/CK ratios in different nodule zones. *(a) Manually identified (i) central infection zone, (ii) parenchyma along the outer edge, and (iii) the vascular bundles, in cross sections of premature soybean nodules. (b) Select cylindrical ROI sub-sections for quantification of auxin and CK outputs and ratios in each nodule zone. Red, blue, and yellow circles indicate randomly selected sub-section ROIs of infection zone, parenchyma, and vascular bundle respectively. The image has been contrast stretched in the green and blue channels for easy visualization of all signals and appears mainly red in the unadjusted image. (c) Histograms of auxin/CK ratios and (d) scatter plot of auxin and CK outputs from selected ROIs in pre-mature nodule sections. Each histogram has a 10-bar width on a log10 scale auxin-CK ratio. Data in (c) and (d) are derived from a total of 1577 nuclei from four separate nodules (n=4) on independent transgenic roots.*

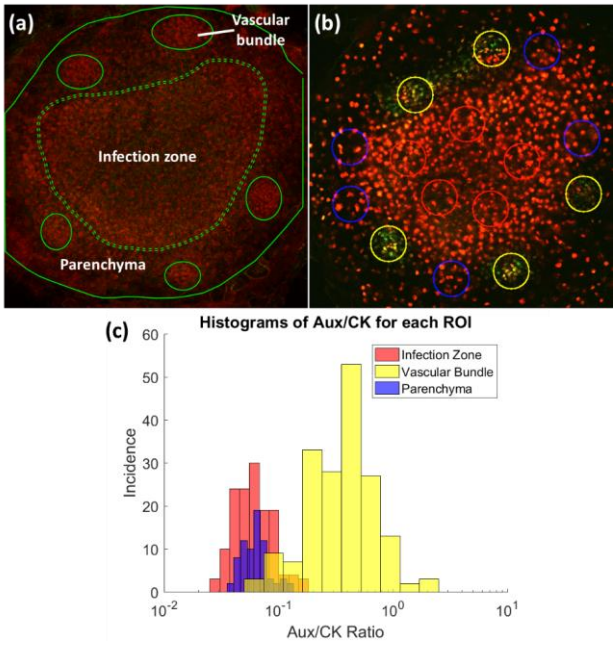

Figure 2.4.5-3: Auxin/CK ratios in different nodule zones identified with propidium iodide. *(a) Propidium Iodide stained pre-mature nodule section with green lines marking boundaries of nodule zones of interest - the central infection zone, vascular bundles, and the parenchyma. (b) Select cylindrical ROI sub-sections for quantification of auxin and CK outputs and ratios in each nodule zone. Red, blue, and yellow circles indicate randomly selected sub-section ROIs of infection zone, parenchyma, and vascular bundle respectively. The image has been contrast stretched in the green and blue channels for easy visualization of all signals and appears mainly red in the unadjusted image. The image is contrast stretched in the green channel to distinguish auxin prominent regions. Blue autofluorescence was not obtained and is not shown. (c). Histograms of auxin/CK ratios for all nuclei within each cylindrical section from part (b).*

Some red autofluorescence signals, which appear as blurred noise, were observed within the infection zone, which can result in false positives during nuclei detection. Therefore, this signal was filtered using the rolling ball background subtraction filter in ImageJ with a 25-pixel radius, which was chosen to 5X the average nucleus diameter. This filter operates by subtracting the average counts of all pixels in a given radius from the central pixel. Filters were used only to find particle centroids but not to calculate summed data. Most of the false positives were removed through filtering, verified by manual inspection.

To determine auxin/CK ratios in specific nodule zones, (i) the infection zone, (ii) the parenchyma, and (iii) the vascular bundles were identified using local cellular densities or previously known distinguishing features in grayscale images of the 2-color pre-mature nodule sections (Figure 2.4.5-2a; Figure 2.4.5-1; See *Methods* subsection). We resorted to the use of grayscale images for identification of zones as FM4-64 did not efficiently stain nodule tissues. From these identified zones, cylindrical subsection ROIs (60µm diameter, 15µm height) were digitally constructed (Figure 2.4.5-2b). All nuclei within each cylinder were identified and their auxin and CK outputs quantified and associated with the corresponding nodule zone.

Compiled auxin-CK data from premature nodules of 4 independent transgenic nodules are shown in Figure 2.4.5-2c and 2.4.5-2d. The data corresponds to 582 vascular bundle nuclei, 464 infection zone nuclei, and 530 parenchyma nuclei. The distributions of relative auxin/CK ratios for vascular bundles, infection zone, and parenchyma were

centered at 0.79, 0.10, and 0.14 respectively (Figure 2.4.5-2c). A pronounced increase in auxin output can be seen in vascular bundle ROIs, but CK is still dominant in these tissues as indicated by ratios of less than 1. The lower tail of this ROI distribution, below 0.1 auxin/CK ratio, is likely from the inexact selection of ROIs, as the cylindrical sections may include nuclei not part of the vascular bundle. Both the infection zone and parenchyma have auxin/CK ratios centered near 0.1, which may be influenced by the noise floor, suggesting that little to no auxin output is present in these zones.

A scatterplot of auxin output to CK output showed two distinct populations of nuclei associated with vascular bundles and the infection zone (Figure 2.4.5-2d). However, the parenchyma nuclei appear to have two sub-populations, one with slightly increased auxin content. These peaks suggest that distinct nodule zones and potentially individual cell types might have distinct on auxin/CK ratios. We also evaluated the use of propidium iodide (1.5mM for 1 min) to stain nodule sections to identify the different zones. Auxin/CK ratios of ROIs from nodule zones identified using this method were in agreement with those identified using the grayscale images (Figure 2.4.5-3). However, the use of grayscale images is preferred due to non-uniform staining of nodule tissues by propidium iodide in our experience.

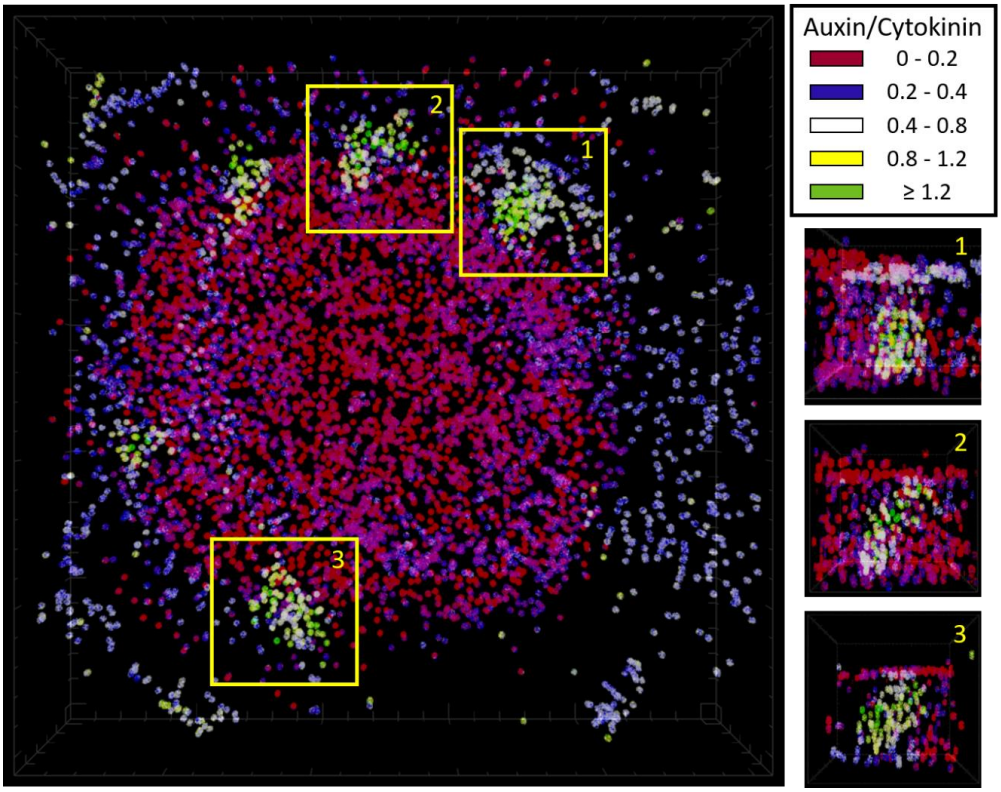

Figure 2.4.5-4: 3D maximum intensity projection of auxin/CK ratios in a pre-mature nodule section. *Ratios of auxin/CK represented through a five-color non-linear pallet for the pre-mature nodule section in Figure 2.1.5-2. Insets show lateral subsections of select vascular bundles.*

Results shown in Figure 2.4.5-2 indicated that distinct nodule zones and cell types could be identified solely based on their distinct auxin/CK ratios. Therefore, in a second approach, images were rendered based on the ratio of auxin/CK, represented through a five-color pallet and evaluated for agreement with manually identified nodule zones. Figure 2.4.5-4 shows a 3D rendering of all detected nuclei from the nodule image shown in Figure 2.4.5-2, their color indicating auxin/CK ratio, using a nonlinear five-color

pallet. Vascular bundles are distinct using this color scheme and show very high auxin/CK output ratios near their center (green, 1.0-3.0 auxin/CK), and relatively higher auxin in other vascular cell types (yellow and white).

This is very clear from lateral sections of select vascular bundles (Figure insets). The majority of the infection zone cells are CK dominant (red, 0-0.2 auxin/CK). Interestingly, while nodule parenchyma cells were also CK dominant, this zone was distinguished by an abundance of cells with relatively weaker CK dominance (blue, 0.2-0.4 auxin/CK) than the infection zone cells. These results indicate that distinct cell types in nodules indeed have distinct auxin/CK ratios despite an overall CK dominance. It is exciting to note that auxin/CK ratios can be used to directly identify key cell types in nodules.

2.5. Discussion

2.5.1. Quantitative imaging of fluorescent markers to determine spatio-temporal hormone outputs

While many studies have demonstrated qualitative outputs of auxin and CK in different plant tissues individually, concurrent localization and quantification of relative ratios at cellular resolution has not been reported. TPIF imaging of fluorescent markers for auxin and CK outputs not only enabled quantitative monitoring of their outputs, but

also the relative ratios of these phytohormones at single cell resolution. It should, however, be noted that the measured outputs depend on the target tissue depth in the sample and the signal intensity diminishes with increased depth due to increased scattering and absorption.

This problem could be partially mitigated by measuring the distance to the surface of the root in the image, and rescaling the signal, though there is a great deal of uncertainty in the exact correction and therefore was not attempted in this study. We used the relative ratios of the hormone outputs, which should be immune to these variations, assayed on an individual nucleus basis to overcome this limitation. Another approach could be to use constitutively expressed, nuclear-localized fluorophores to normalize signal outputs.

Accurate detection of individual nuclei is crucial for proper spatio-temporal quantification of the nuclear localized fluorescent output markers. The LMDM has a number of advantages to other segmentation routines such as a watershed or variable intensity method for detection of nuclei. First, while a predefined volume mask does not collect the exact nuclei shape, it will prevent false identification of super-particle segments in a close-packed sample, which would distort the average and sum outputs of the signal. Thus, this method can be effective for monitoring localized hormone outputs in relatively close-packed particle distributions such as the root meristem. Second, this method is relatively independent of intensity, which allows for identifying particles throughout a deep tissue sample where intensity varies considerably. Finally, by using an

intensity threshold, the only observable false positives created by the routine result from AF in the root samples, a problem any segmentation routine would struggle to resolve.

Because particle volumes are fixed, segmentation is restricted to only similarly shaped particles and useful for experiments which prioritize output and location. Considering the near uniformity of nuclei sizes in root samples, this did not present a significant concern in this study. Most importantly, the fixed volume mask size used in this study effectively treats summed intensity outputs as a concentration density, thus, critical information is not lost by failing to sum the whole nucleus.

2.5.2. Auxin/CK ratios in soybean root and nodule tissues

The construct and the methods described here allowed us to quantify and determine relative outputs of auxin and CK for specific cell types or regions of interest. In the root cap columella cells, we observed near-uniform auxin CK ratios, but there was a trend of high CK towards the tip and high auxin towards the base within the columella cells (Antoniadi *et al.* 2015). Modeling of auxin concentrations and experimental evaluation using a DR5-GFP reporter line suggest that indeed such a gradient of auxin is present along the columella cells resulting from auxin transporter activity (Grieneisen *et al.* 2007). Both cell type-specific measurements and immunolocalization showed high CK levels in the distal root cap columella cells, in agreement with our observations.

There was a sharp increase in auxin/CK ratio in the QC, as predicted. In many independent studies, QC and stem cells indeed show very high levels of auxin response and little if any CK response. There was a sharp decline in the auxin-CK ratio in cells of the proximal meristem. This is consistent with differentiation of protoxylem and formation of distinct cell identities in this region. A mutually inhibitory feedback loop between auxin and CK in this region was shown to set distinct boundaries (Bishopp *et al.* 2011). The protoxylem cells (fewer in number at this stage) show high auxin response whereas the procambial cells (the majority of the vascular core) show high CK response. Consistent with these observations we observed auxin/CK ratios that were very low in this region.

Cell type-specific measurements of both auxin (IAA) and CKs in Arabidopsis root tips are largely consistent with hormone response marker outputs observed in specific cell types (Petersson *et al.* 2009; Antoniadi *et al.* 2015). However, key differences exist between hormone levels and hormone response in some cell types. For example, even though the levels of auxin were relatively low in the root cap columella cells, high auxin response has been observed in these cells based on auxin perception/response reporters. It is likely that this is due to modulation of sensitivity. Similarly, high levels of CK are reported in the columella cells, lateral root cap, and QC cells. However, CK response is highest in the columella cells and very low in QC cells.

Indeed, modulation of hormone sensitivity in a zone-specific manner in the root tip has been well documented. In addition, CK also regulates auxin levels in the lateral

root cap cells through modulation of auxin transport, in particular the auxin influx carrier AUX1 (Street *et al.* 2016). Expression patterns of the CK biosynthesis gene *IPT5* and immunolocalization of CKs indicated that the columella cells are the primary sites of CK biosynthesis in the root tip (Miyawaki *et al.* 2004; Aloni *et al.* 2005; Chang *et al.* 2015). Therefore, quantifying cellular hormone outputs, likely the ultimate determinant of the hormone's impact on cellular outcome, can integrate both hormone levels and sensitivity. Fluorescence imaging of hormone output markers, combined with post-experiment quantitative analysis, enables 3- and 4- dimensional non-invasive quantification that can be used to reconstruct spatio-temporal changes in hormone action during organogenesis and development.

Cytokinins also regulate lateral root formation through the effect on auxin. While ectopic CK biosynthesis in xylem-pole pericycle cells can inhibit LR formation, young LRPs (stages I to IV) are not sensitive to CK-induced inhibition (Laplaze *et al.* 2007). Little or no CK output is present in LRPs until LR emergence (Bielach *et al.* 2012; Chang *et al.* 2013; Zürcher *et al.* 2013). At advanced stages, CK activity was re-established resulting in CK output patterns seen in the primary root (Nishimura *et al.* 2004; Stolz *et al.* 2011). This suggests that CK signaling is turned on during the emergence phase of the LR (between stages V and VI). Our results in soybean were in agreement with these observations in Arabidopsis, suggesting the existence of similar mechanisms and underscoring the ability of the reporters in composite soybean plant roots to quantify auxin and CK responses.

In addition, auxin accumulation at the tip of the growing LRP appears to be crucial for proper lateral root emergence. Such auxin accumulation enhances the expression of auxin influx transporter LAX3 in the cortex and epidermis cells directly above the LRP (Bielach *et al.* 2012; Vilches-Barro & Maizel 2014); in turn, auxin accumulation in these cells upregulates the expression of the cell wall remodeling enzymes starting softening of these cells to enable LR emergence. Using a combination of mathematical modeling and experimental evaluation, it was shown that sequential activation of PIN3 followed by LAX3 in cells abutting the LRP enables auxin to move towards the outer tissues from the LRP, leading to softening. In agreement with this result, we observed predominant auxin activity until stage V, and a shift towards CK and establishment of the familiar CK-aux-CK pattern observed in mature root tips. It appears from our results that emergence might trigger CK synthesis in the lateral root cap and columella cells resulting in establishment of an auxin transport stream establishing distinct cell types and root zones in the root tip.

We also determined relative auxin-CK outputs and ratios in distinct zones of premature soybean nodules. As expected, the majority of nodule tissues had enriched CK response. However, we identified four distinct cell populations with distinct auxin-CK ratios. Two with relatively high auxin-CK ratios were associated with vascular bundles. A cluster of cells near the center of the bundles had the highest auxin-CK ratio (typically from 1.0-3.0). In agreement, we and others have reported readily detectable auxin reporter expression associated with vascular bundles (Takanashi *et al.* 2011; Suzaki *et al.*

2012; Turner *et al.* 2013). In fact, nodule vascular development was impaired in *L. japonicus* plants treated with auxin transport inhibitor, and soybean composite plants with reduced auxin sensitivity (arising from suppression of microRNA160 level (Nizampatnam *et al.* 2015)) suggesting that high auxin-CK ratio might be crucial for proper nodule vascular development.

By assaying relative ratios, we were able to identify two distinct sub populations of cells within the vascular bundle. We presume that the central cells with high auxin-CK ratio correspond to the xylem elements (Bishopp *et al.* 2011). Evaluation of auxin-CK outputs and ratios and vascular development in nodules where auxin levels/response is chemically/genetically altered would help correlate specific auxin-CK ratios to vascular differentiation. The majority of the nodule cells associated with the infection zone were CK enriched with little to no auxin response detectable. Another group of cells with auxin-CK ratios from 0.2-0.4 appeared to be preferentially located in proximity to the periphery of the infection zone. While it remains to be seen how these cells are distinct from other cells in the infection zone, their auxin-CK ratios are similar to those of the nodule parenchyma cells. These results indicate that subtle changes in auxin-CK ratiometric outputs might dictate nodule cell type identity.

Given the high tissue penetration of TPIF imaging, germinal processes such as lateral root primordia formation can be observed effectively. However, the 150µm depth penetration we observed in soybean tissues limits observation of deep tissue processes. For example, for imaging of premature nodules, we had to resort to hand-sectioning prior

to imaging. Nevertheless, combined with methods being developed for tissue clearing (Warner *et al.* 2014), non-invasive imaging of large organs such a 1mm sized mature soybean nodule might be possible using this method.

In conclusion, the construct put together in this study enabled concurrent imaging and quantification of cell-level auxin and CK outputs in soybean roots and nodules. The use of nuclear localization signals on the markers and in turn LMDM for nuclei segmentation enabled accurate monitoring of outputs through 3D image volumes. Overlays of determined auxin/CK ratios on specific root zones and cell types accurately reflected those predicted based on previously reported outputs for each hormone individually. The ratiometric method used here is shown to largely compensate for variations in individual outputs due to sample turbidity and scattering, an inherent issue when imaging thick root and nodule samples typical of many legume species. Importantly, distinct auxin/CK ratios corresponded to distinct nodule cell types indicating a key role for these hormones in nodule cell type identity. Future applications of the method for time-course imaging of auxin/CK outputs and ratios along the course of nodule development are expected to provide key insights on hormonal control of cell differentiation during nodule development.

2.6. Acknowledgements:

This research was supported by funds from the National Science Foundation through EPSCoR Cooperative Agreement #IIA-1355423 and DMR-BMAT #1206908, SD Agricultural Experiment Station (H351-09 and H543-15), South Dakota State University, and the State of South Dakota. We thank Dr. Takuya Suzaki, National Institute for Basic Biology, Okazaki, Japan for the DR5:GFP-NLS cassette, Dr. Bruno Mueller, University of Zurich, Switzerland for the TCSn synthetic promoter, and Suresh Damodaran for obtaining the image shown in Figure S4b. The use of instruments available at South Dakota State University's Functional Genomics Core Facility supported in part by the National Science Foundation/EPSCoR Grant No. 0091948 and by the State of South Dakota, are gratefully acknowledged. The authors have no conflict of interest to declare.

2.7. References

Aloni R., Langhans M., Aloni E., Dreieicher E. & Ullrich C.I. (2005) Root-synthesized cytokinin in Arabidopsis is distributed in the shoot by the transpiration stream. *Journal of Experimental Botany* **56**, 1535–1544.

Antoniadi I., Plačková L., Simonovik B., Doležal K., Turnbull C., Ljung K. & Novák O. (2015) Cell-Type-Specific Cytokinin Distribution within the Arabidopsis Primary Root Apex. *The Plant Cell* **27**, 1955–67.

Bielach A., Podlešáková K., Marhavý P., Duclercq J., Cuesta C., Müller B., … Benková

E. (2012) Spatiotemporal Regulation of Lateral Root Organogenesis in *Arabidopsis* by Cytokinin. *The Plant Cell* **24**, 3967–3981.

Bishopp A., Lehesranta S., Vate A., Help H., El-showk S. & Scheres B. (2011) Phloem-Transported Cytokinin Regulates Polar Auxin Transport and Maintains Vascular Pattern in the Root Meristem. *Current Biology* **21**, 927–932.

Bolte S., Talbot C., Boutte Y., Catrice O., Read N.D. & Satiat-Jeunemaitre B. (2004) FM-dyes as experimental probes for dissecting vesicle trafficking in living plant cells. *Journal of Microscopy* **214**, 159–173.

Breakspear A., Liu C., Roy S., Stacey N., Rogers C., Trick M., … Murray J.D. (2014) The Root Hair "Infectome" of Medicago truncatula Uncovers Changes in Cell Cycle Genes and Reveals a Requirement for Auxin Signaling in Rhizobial Infection. *The Plant Cell* **26**, 4680–4701.

Bustos-Sanmamed P., Mao G., Deng Y., Elouet M., Khan G.A., Bazin J., … Lelandais-Brière C. (2013) Overexpression of miR160 affects root growth and nitrogen-fixing nodule number in *Medicago truncatula*. *Functional Plant Biology* **40**, 1208–1220.

Cai Z., Wang Y., Zhu L., Tian Y., Chen L., Sun Z., … Li X. (2017) GmTIR1/GmAFB3-based auxin perception regulated by miR393 modulates soybean nodulation. *New Phytologist* **215**, 672–686.

Chang L., Ramireddy E. & Schmülling T. (2013) Lateral root formation and growth of Arabidopsis is redundantly regulated by cytokinin metabolism and signalling genes.

Journal of Experimental Botany **64**, 5021–5032.

Chang L., Ramireddy E. & Schmülling T. (2015) Cytokinin as a positional cue regulating lateral root spacing in Arabidopsis . *Journal of Experimental Botany* **66**, 4759–4768.

Collier R., Fuchs B., Walter N., Kevin Lutke W. & Taylor C.G. (2005) Ex vitro composite plants: an inexpensive, rapid method for root biology. *The Plant Journal* **43**, 449–457.

Crocker J.C. & Weeks E.R. Tracking in 3D.

D'Agostino I.B., Deruere J. & Kieber J.J. (2000) Characterization of the response of the arabidopsis response regulator gene family to cytokinin. *Plant Physiology* **124**, 1706–1717.

Ferguson B.J. & Mathesius U. (2014) Phytohormone Regulation of Legume-Rhizobia Interactions. *Journal of Chemical Ecology* **40**, 770–790.

Franssen H.J., Xiao T.T., Kulikova O., Wan X., Bisseling T., Scheres B. & Heidstra R. (2015) Root developmental programs shape the Medicago truncatula nodule meristem. *Development* **142**, 2941–2950.

Friml J., Vieten A., Sauer M., Weijers D., Schwarz H., Hamann T., … Jürgens G. (2003) Efflux-dependent auxin gradients establish the apical–basal axis of Arabidopsis. *Nature* **426**, 147–153.

Gamas P., Brault M., Jardinaud M.F. & Frugier F. (2017) Cytokinins in Symbiotic

Nodulation: When, Where, What For? *Trends in Plant Science* **22**, 792–802.

Gao Y. & Kilfoil M.L. (2009) Accurate detection and complete tracking of large populations of features in three dimensions. *Optics express* **17**, 4685–4704.

Grieneisen V.A., Xu J., Marée A.F.M., Hogeweg P. & Scheres B. (2007) Auxin transport is sufficient to generate a maximum and gradient guiding root growth. *Nature* **449**, 1008.

Held M., Hou H., Miri M., Huynh C., Ross L., Hossain M.S., … Szczyglowski K. (2014) Lotus japonicus Cytokinin Receptors Work Partially Redundantly to Mediate Nodule Formation. *The Plant Cell* **26**, 678–694.

Herrbach V., Remblière C., Gough C. & Bensmihen S. (2014) Lateral root formation and patterning in Medicago truncatula. *Journal of Plant Physiology* **171**, 301–310.

Hobecker K.V., Reynoso M.A., Bustos-Sanmamed P., Wen J., Mysore K.S., Crespi M., … Zanetti M.E. (2017) The MicroRNA390/TAS3 Pathway Mediates Symbiotic Nodulation and Lateral Root Growth. *Plant Physiology* **174**, 2469 LP-2486.

Kilfoil M.L. Mechanics of the Cell.

Kohlen W., Ng J.L.P., Deinum E.E. & Mathesius U. (2017) Auxin transport, metabolism, and signalling during nodule initiation: indeterminate and determinate nodules. *Journal of Experimental Botany*.

Kuppusamy K.T., Ivashuta S., Bucciarelli B., Vance C.P., Gantt J.S. & VandenBosch

K.A. (2009) Knockdown of CELL DIVISION CYCLE16 Reveals an Inverse Relationship between Lateral Root and Nodule Numbers and a Link to Auxin in Medicago truncatula. *PLANT PHYSIOLOGY* **151**, 1155–1166.

Laplaze L., Benkova E., Casimiro I., Maes L., Vanneste S., Swarup R., … Bennett M. (2007) Cytokinins Act Directly on Lateral Root Founder Cells to Inhibit Root Initiation. *the Plant Cell Online* **19**, 3889–3900.

Liao C.Y., Smet W., Brunoud G., Yoshida S., Vernoux T. & Weijers D. (2015) Reporters for sensitive and quantitative measurement of auxin response. *Nature Methods* **12**, 207–210.

Lohar D.P., Schaff J.E., Laskey J.G., Kieber J.J., Bilyeu K.D. & Bird D.M.K. (2004) Cytokinins play opposite roles in lateral root formation, and nematode and Rhizobial symbioses. *Plant Journal* **38**, 203–214.

Madsen L.H., Tirichine L., Jurkiewicz A., Sullivan J.T., Heckmann A.B., Bek A.S., … Stougaard J. (2010) The molecular network governing nodule organogenesis and infection in the model legume Lotus japonicus. *Nature Communications* **1**.

Di Mambro R., De Ruvo M., Pacifici E., Salvi E., Sozzani R., Benfey P.N., … Sabatini S. (2017) Auxin minimum triggers the developmental switch from cell division to cell differentiation in the *Arabidopsis* root. *Proceedings of the National Academy of Sciences* **114**, E7641–E7649.

Mao G., Turner M., Yu O. & Subramanian S. (2013) miR393 and miR164 influence

indeterminate but not determinate nodule development. *Plant signaling & behavior* **8**.

Miri M., Janakirama P., Held M., Ross L. & Szczyglowski K. (2016) Into the Root: How Cytokinin Controls Rhizobial Infection. *Trends in Plant Science* **21**, 178–186.

Miyawaki K., Matsumoto-Kitano M. & Kakimoto T. (2004) Expression of cytokinin biosynthetic isopentenyltransferase genes in Arabidopsis: tissue specificity and regulation by auxin, cytokinin, and nitrate. *The Plant Journal* **37**, 128–138.

Müller B. & Sheen J. (2008) Cytokinin and auxin interplay in root stem-cell specification during early embryogenesis. *Nature* **453**, 1094–1097.

Murray J.D., Karas B.J., Sato S., Tabata S., Amyot L. & Szczyglowski K. (2007) A Cytokinin Perception Mutant Colonized by Rhizobium in the Absence of Nodule Organogenesis. *Science* **315**, 101 LP-104.

Ng J.L.P., Hassan S., Truong T.T., Hocart C.H., Laffont C., Frugier F. & Mathesius U. (2015) Flavonoids and Auxin Transport Inhibitors Rescue Symbiotic Nodulation in the Medicago truncatula Cytokinin Perception Mutant cre1. *The Plant Cell* **27**, 2210–2226.

Nishimura C., Ohashi Y., Sato S., Kato T., Tabata S. & Ueguchi C. (2004) Histidine Kinase Homologs That Act as Cytokinin Receptors Possess Overlapping Functions in the Regulation of Shoot and Root Growth in Arabidopsis. *The Plant Cell* **16**, 1365–1377.

Nizampatnam N.R., Schreier S.J., Damodaran S., Adhikari S. & Subramanian S. (2015) MicroRNA160 dictates stage-specific auxin and cytokinin sensitivities and directs soybean nodule development. *Plant Journal* **84**, 140–153.

van Noorden G.E., Ross J.J., Reid J.B., Barry G.R. & Ulrike M. (2006) Defective Long-Distance Auxin Transport Regulation in the Medicago truncatula super numeric nodules Mutant. *Plant Physiology* **140**, 1494–1506.

Op den Camp R.H.M., De Mita S., Lillo A., Cao Q., Limpens E., Bisseling T. & Geurts R. (2011) A Phylogenetic Strategy Based on a Legume-Specific Whole Genome Duplication Yields Symbiotic Cytokinin Type-A Response Regulators. *Plant Physiology* **157**, 2013–2022.

Petersson S. V, Johansson A.I., Kowalczyk M., Makoveychuk A., Wang J.Y., Moritz T., … Ljung K. (2009) An auxin gradient and maximum in the Arabidopsis root apex shown by high-resolution cell-specific analysis of IAA distribution and synthesis. *Plant Cell* **21**, 1659–1668.

Plet J., Wasson A., Ariel F., Le Signor C., Baker D., Mathesius U., … Frugier F. (2011) MtCRE1-dependent cytokinin signaling integrates bacterial and plant cues to coordinate symbiotic nodule organogenesis in Medicago truncatula. *The Plant Journal* **65**, 622–633.

Reid D., Nadzieja M., Novák O., Heckmann A.B., Sandal N. & Stougaard J. (2017) Cytokinin Biosynthesis Promotes Cortical Cell Responses during Nodule

Development. *Plant Physiology* **175**, 361 LP-375.

Roerdink J. & Meijster a (2000) The Watershed Transform: Definitions, Algorithms and Parallelization Strategies. *Fundamenta Informaticae* **41**, 187–228.

Schaller G.E., Bishopp A. & Kieber J.J. (2015) The Yin-Yang of Hormones: Cytokinin and Auxin Interactions in Plant Development. *The Plant Cell Online* **27**, 44–63.

Sprent J.I. (2007) Evolving ideas of legume evolution and diversity: A taxonomic perspective on the occurrence of nodulation: Tansley review. *New Phytologist* **174**, 11–25.

Stolz A., Riefler M., Lomin S.N., Achazi K., Romanov G.A. & Schmülling T. (2011) The specificity of cytokinin signalling in Arabidopsis thaliana is mediated by differing ligand affinities and expression profiles of the receptors. *Plant Journal* **67**, 157–168.

Street I.H., Mathews D.E., Yamburkenko M. V., Sorooshzadeh A., John R.T., Swarup R., … Schaller G.E. (2016) Cytokinin acts through the auxin influx carrier AUX1 to regulate cell elongation in the root. *Development* **143**, 3982–3993.

Suzaki T., Ito M. & Kawaguchi M. (2013) Genetic basis of cytokinin and auxin functions during root nodule development . *Frontiers in Plant Science* **4**, 42.

Suzaki T., Yano K., Ito M., Umehara Y., Suganuma N. & Kawaguchi M. (2012) Positive and negative regulation of cortical cell division during root nodule development in Lotus japonicus is accompanied by auxin response. *Development*.

Takanashi K., Sugiyama A. & Yazaki K. (2011) Involvement of auxin distribution in root nodule development of Lotus japonicus. *Planta* **234**, 73–81.

Tirichine L., Sandal N., Madsen L.H., Radutoiu S., Albrektsen A.S., Sato S., … Stougaard J. (2007) A Gain-of-Function Mutation in a Cytokinin Receptor Triggers Spontaneous Root Nodule Organogenesis. *Science* **315**, 104–107.

Turner M., Nizampatnam N.R., Baron M., Coppin S., Damodaran S., Adhikari S., … Subramanian S. (2013) Ectopic expression of miR160 results in auxin hypersensitivity, cytokinin hyposensitivity, and inhibition of symbiotic nodule development in soybean. *Plant Physiology* **162**, 2042–55.

Ulmasov T., Murfett J., Hagen G. & Guilfoyle T.J. (1997) Aux/lAA Proteins Repress Expression of Reporter Genes Containing Natural and Highly Active Synthetic Auxin Response Elements. *The Plant Cell* **9**, 1963–1971.

Vanstraelen M. & Benková E. (2012) Hormonal Interactions in the Regulation of Plant Development. *Annual Review of Cell and Developmental Biology* **28**, 463–487.

Vida T.A. & Emr S.D. (1995) A new vital stain for visualizing vacuolar membrane dynamics and endocytosis in yeast. *Journal of Cell Biology* **128**, 779–792.

Vilches-Barro A. & Maizel A. (2014) Talking through walls: Mechanisms of lateral root emergence in Arabidopsis thaliana. *Current Opinion in Plant Biology* **23**, 31–38.

Wang Y., Li K., Chen L., Zou Y., Liu H., Tian Y., … Li X. (2015) MicroRNA167-

Directed Regulation of the Auxin Response Factors and Is Required for Soybean Nodulation and Lateral Root Development. *Plant Physiology* **168**, 984 LP-999.

Warner C. a., Biedrzycki M.L., Jacobs S.S., Wisser R.J., Caplan J.L. & Sherrier D.J. (2014) An Optical Clearing Technique for Plant Tissues Allowing Deep Imaging and Compatible with Fluorescence Microscopy. *Plant Physiology* **166**, 1684 LP-1687.

Wasson A.P. (2006) Silencing the Flavonoid Pathway in Medicago truncatula Inhibits Root Nodule Formation and Prevents Auxin Transport Regulation by Rhizobia. *the Plant Cell* **18**, 1617–1629.

Zürcher E., Tavor-Deslex D., Lituiev D., Enkerli K., Tarr P.T. & Müller B. (2013) A robust and sensitive synthetic sensor to monitor the transcriptional output of the cytokinin signaling network in planta. *Plant physiology* **161**, 1066–75.

2.8. Supplementary information

2.8.1. Cylindrical Sectioning Algorithm

The following describes the math to create a cylinder in 3D space. These cylinders were used to segment regions of interest (ROIs) in the digital images for characterization of hormone outputs.

The distance of a point, p, to an infinite line collinear to a vector defined by $p_1 - p_2$, is:

$$d = \frac{|(p-p_1)\times(p-p_2)|}{|p_1-p_2|} \quad (1)$$

This can be extended to an infinite cylinder by squaring the results. Thus, the equation of an infinite cylinder along arbitrary axis is:

$$r^2 = \frac{|(p-p_1)\times(p-p_2)|^2}{|p_1-p_2|^2} = c(p) \quad (2)$$

where r is the radius of the cylinder. To create a finite cylinder between p_1 and p_2, infinite planes at each point normal to the vector $p_1 - p_2$ can be considered. Point p can be determined to be on one side of the plane by taking the dot product of the vector $p_1 - p_2$ with the vector created by p to the given point by the equations:

$$a = (p_1 - p_2) \cdot (p - p_2) \quad (3)$$

$$b = (p_1 - p_2) \cdot (p - p_1) \quad (4)$$

Thus, p can be considered within a cylinder with height and orientation determined by vector $p_1 - p_2$ and a radius r if the following conditions are met:

$$c(p) \leq r \ \& \ a \leq 0 \leq b \quad (5)$$

CHAPTER III

3. Auxin and cytokinin response ratios in soybean nodule primordium at different developmental stages. (status: manuscript in preparation[b])

3.1. Abstract

Stage-specific auxin/CK balance dictates proper nodule development. Alteration in these ratios can inhibit, promote or delay nodule formation. We used two photon-induced fluorescence microscopy for quantitative 3-dimensional imaging of fluorescent markers to characterize cellular level auxin and cytokinin outputs and ratios during nodule development in soybean. The six different nodule developmental stages presented unique patterns of auxin/cytokinin ratios suggesting a tight cell type-level hormonal regulation during nodule organogenesis. Based on these patterns we hypothesize that auxin bursts promote pattern initiation and cytokinin bursts promote differentiation. Soybean roots with reduced levels of microRNA160 that produce more nodules with

---

[b] Gaillard P, Nurmalasari NPD, Smith S, Subramanian S (2020) Auxin and cytokinin response ratios in soybean nodule primordium at different developmental stages (tentative).

delayed maturity were examined to determine changes in cell type-level auxin/cytokinin ratios. Based on the results, we hypothesize that lower auxin/cytokinin ratio in nodule initials allow development of more primordia but delay their maturation.

3.2. Introduction

Phytohormones regulate nearly all aspects of plant growth and development (Su, Liu et al. 2011). Among these, auxin and cytokinin (CK) play a crucial role in controlling cell proliferation and differentiation (Benkova and Hejatko 2009, Suzaki, Ito et al. 2013) and therefore are crucial for genesis of organs. These hormones act antagonistically or synergistically to regulate several plant developmental processes such as embryogenesis and shoot/root meristem maintenance (Su, Liu et al. 2011). Moreover, auxin and cytokinin control *de novo* initiation and development of organs such as lateral root, axillary bud and nodule.

Comprehensive studies report that cell type specificity and auxin/CK balance are the major factors dictating the proper development of these organs. In lateral roots, auxin promotes cell division and initiates central lateral root founder cell priming, while cytokinin inhibits this priming and triggers cell differentiation in the periphery of the organ (De Smet, Tetsumura et al. 2007, Laplaze, Benkova et al. 2007). In axillary buds, cytokinin promotes cell division in the center of the bud, while auxin is located in the outside to inhibit outgrowth (Riou-Khamlichi, Huntley et al. 1999, Muller and Leyser

2011). Even though Suzaki has suggested that an auxin/CK balance might be involved in nodule formation, little is known about the auxin/CK dynamics and its organization during nodule initiation and development (Suzaki, Ito et al. 2013).

Root nodules are organs dedicated to symbiotic N_2 fixation. They host diazotrophic bacteria that provide nitrogen in exchange for carbohydrates supplied by the plant (Oldroyd 2013). The symbiotic interaction starts with rhizobia attachment and root hair curling. Rhizobia progress into the root hair via an infection thread and are delivered to newly produced primordium in the root cortex. As the cortical cells differentiate, the nodule matures, and rhizobia are differentiated into bacteroids to efficiently fix N_2 and supply the plant. Nodules can be divided into two main categories based on their site of primordium initiation and meristem persistence: (i) determinate nodules that initiate in the outer cortex and have a transient meristem resulting in a spherical nodule (such as soybean and *Lotus japonicus* nodule); and (ii) indeterminate nodules that initiate in the inner cortex and have a persistent meristem, engendering an oblong nodule shape (such as barrel clover's nodule) (Ferguson, Indrasumunar et al. 2010).

In a determinate nodule, auxin seems to be involved during the early steps of nodule initiation but is not observed during maturation except in the nodule vasculature and parenchyma (Takanashi, Sugiyama et al. 2011). An indeterminate nodule has a similar auxin profile, but auxin is continuously present in the meristematic zone at the apex of the nodule. Additionally, exogenous polar auxin transport inhibitors are sufficient to induced pseudo-nodule formation in plant producing indeterminate (Hirsch,

Bhuvaneswari et al. 1989), but not in plants producing determinate nodules. In both nodule types, CK signaling pathway plays a central role in initiating primordia and is responsible of the meristem activation (Suzaki, Ito et al. 2013). Application of exogenous CK induces nodule primordia-like structures in the absence of rhizobium in determinate and indeterminate nodule types (Joshi, Caetano-Anollés et al. 1991, Heckmann, Sandal et al. 2011). Therefore, auxin and CK seem to be involved in the regulation of nodule formation in a rhizobium independent manner (Bensmihen 2015).

During the early steps of the infection process, local root epidermis responses are observed for both auxin and CK. The cytokinin receptor, Cytokinin Response1 (CRE1) induces the cytokinin signaling cascade and the transcription factor (TF) Auxin Response Factor 16a (ARF16a) activates the auxin response in the epidermis (Boivin, Kazmierczak et al. 2016). The response to auxin is mediated by three groups of proteins: AUXIN RESPONSE FACTORs (ARFs), AUXIN/INDOLE-3- ACETIC ACID (Aux/IAA) and TRANSPORT INHIBITOR RESISTANT 1/AUXIN SIGNALING F-BOX (TIR1/AFB). ARFs are transcriptional activators or repressors that can respectively induce or inhibit the expression of early expressed genes in response to auxin (Teale, Paponov et al. 2006). The Aux/IAA family includes repressors proteins that inhibit ARF activity through dimerization and repress the expression of auxin-response genes. The Aux/IAA proteins can be degraded by the auxin receptor F-box protein proteins such as TRANSPORTER INHIBITOR RESPONSE1 (TIR1) to regulate plant development. However, the activity of repressor ARFs does not appear to be controlled by this mechanism. Some microRNAs

(miRNAs) have been described to regulate specifics ARF gene family and can potentially impact the auxin/CK ratio (Marin, Jouannet et al. 2010, Wang, Li et al. 2015).

miRNAs are 21 to 22 nucleotides long sequences that regulate transcripts by facilitating degradation of mRNAs or inhibiting their translation in a sequence-specific manner (Axtell 2013). They are involved in root, shoot and leaf development. Indeed, it has been demonstrated that miR160 can regulate the level of the ARF10/ARF16/ARF17 family in Arabidopsis (Mallory, Bartel et al. 2005). In 2013, our team revealed that miR160 inhibits the auxin repressor ARF10/ARF16/ARF17 family in soybean. This activity affects soybean nodule development by dictating developmental stage-specific auxin/CK balance. Roots over-expressing miR160 (miR160ox) are hypersensitive to auxin and hyposensitive to cytokinin and have a nodule primordium deficit (Turner, Nizampatnam et al. 2013). On the contrary, roots constitutively expressing a short tandem target mimic (STTM160ox) repressing miR160 are hypersensitive to cytokinin and hyposensitive to auxin and have more initiated nodules, but their maturation is delayed (Nizampatnam, Schreier et al. 2015).

Hence, miR160 is a key regulator of nodule development that seems to dictate the auxin/CK ratio. Nodules are complex organs composed of different cell types having specific auxin/CK requirements. However, the different auxin/CK ratios involved in nodule development have never been described. Moreover, the actor(s) targeted by miR160 to regulate these ratios is/are unknown. Therefore, we decided to characterize

nodules auxin/CK ratios at the cellular level in roots with typical and altered miR160 levels and to investigate miR160's target(s).

The auxin/CK ratios were examined as mentioned in Fisher et al 2018 using auxin and cytokinin transcriptional output sensors. In this study, we evaluated the auxin/CK ratios in six different nodule developmental stages. They presented unique patterns suggesting a tight cell type-level hormonal regulation during nodule organogenesis. Based on these patterns we hypothesize that auxin bursts promote primordium initiation and cytokinin bursts promote differentiation.

Additionally, STTM160 soybean roots were examined to determine changes in cell type-level of the auxin/CK ratios. Based on the results, we hypothesize that lower auxin/CK ratio in nodule initials allow development of more primordia but delay their maturation. These findings provide key insights on hormonal control of cell differentiation during nodule development, nodule cell identity and nodule maturation. Outcomes from these studies include genetic markers that correspond to distinct auxin/CK ratios in nodule tissues which can be used to breed soybeans with higher number of nodules that mature slowly providing a continuous supply of nitrogen.

3.3. Material and methods

3.3.1. Plasmid construct

The AuxCysensor vector carries an auxin transcriptional sensor (DR5rev:eGFP2-NLS) and a cytokinin transcriptional sensor (TCSn:tdTomato-NLS) as described in Fisher et al. 2018. AuxCysensor STTM160 carries a sequence complementary to miR160 (STTM160) expressed by a constitutive pine SuperUbiquitin promoter and was generated via LR recombination between the binary destination vector AuxCysensor and the entry vector pCR8GW:STTM160 (Parizotto, Dunoyer et al. 2004, Nizampatnam, Schreier et al. 2015) . mTagBFP2 was PCR amplified from pBAD-mTagBFP2 (Addgene) and cloned into pmH40ENTR4-mTagBFP2-NLS-miR160sensor. pmH40ENTR4-mTagBFP2-NLS-NOmiR160sensor was restriction digested by NcoI and XbaI to remove the miR160 sensor and ligated to generate pmH40ENTR4-mTagBFP2-NLS-NOmiR160sensor. AuxCyBFP2-NLS-miR160sensor and AuxCyBFP2-NLS-NOmiR160sensor were created by LR recombination between the AuxCysensor and pmH40ENTR4-mTagBFP2-NLS-miR160sensor or pmH40ENTR4-mTagBFP2-NLS-NOmiR160sensor respectively. A mCer3-NLS-miR160sensor 1046 base pairs gblocks gene fragments (Integrated DNA Technology) was cloned into pCR8/GW/TOPO (Thermofisher) to generate pCr8mCer3-NLS-miR160sensor. pCR8mCer3-NLS-miR160sensor was digested by PacI and XbaI to remove the miR160 sensor and generate pCR8mCer3-NLS-NOmiR160sensor. AuxCymCer3-NLS-miR160sensor and AuxCymCer3-NLS-NOmiR160sensor were created by LR recombination between the AuxCysensor and pCR8mCer3-NLS-miR160sensor or pCR8mCer3-NLS-NOmiR160sensor respectively.

3.3.2. Plant transformation and rhizobia treatments

Vectors were electroporated into *Agrobacterium rhizogenes* K599 cells and Soybean William 82 transgenic composite plants were generated as described by Collier in 2005 (Collier, Fuchs et al. 2005). Roots were screened 4 weeks after plant transformation, placed into pots (3:1 vermiculite: perlite mix) watered with nitrogen free plant nutrient solution (N− PNS) and inoculated with *Bradyrhizobium diazoefficiens* USDA 110 (previously named *Bradyrhizobium japonicum* USDA 110) or *Bradyrhizobium diazoefficiens* USDA 110 expressing the nptII:GUS construct (a kind gift from Gary Stacey, Divisions of Plant Sciences and Biochemistry, University of Missouri, Columbia, MO, USA) as mentioned in (Fisher, Gaillard et al. 2018).

3.3.3. Imaging of nodule primordia and premature nodule with the AuxCysensor strategy

Intact AuxCysensor and AuxCysensor STTM160 primordia were observed at 3 days post inoculation (dpi) (stage 1), 4dpi (stage2), 5dpi (stage3) and 7dpi (stage4). Premature nodule (PMN) were harvested at 10dpi. PMNs fresh tissues were hand-sectioned with a razor blade to generate section between 250 and 500µm prior imaging. Samples were observed with an Olympus FV1000MPE multiphoton scanning laser microscope to produce 3D image volumes as previously described (Fisher, Gaillard et al.

2018). Laser intensity was gradually and manually increased as the scanning was effectuated from the surface to the center of the sample.

3.3.4. Imaging of nodule primordia colonized by Bradyhizobium diazoefficiens USDA 110 GUS

Wild type roots inoculated with *Bradyrhizobium diazoefficiens* USDA 110 GUS were harvested at 7dpi, vacuumed infiltrated for 6 hours with GUS buffer and x-Gluc and placed at 37°C for 24 hours in the dark. Then they were fixed for 2 days with 4% glutaraldehyde 4°C and cleared with 10% Clorox during 1 hour before imaging. Images were acquired with an AX70 upright microscope, DP70 digital camera and CellSens software (Version 2.1, Olympus, Shinjuku, Tokyo, Japan) with a resolution of 4080 × 3072 pixels.

3.3.5. Nodule primordium counting

Twenty-one AuxCysensor and AuxCysensor STTM160 roots inoculated with *Bradyrhizobium diazoefficiens* USDA 110 were harvested at 15 and 22dpi. Their number of emerging and mature nodule were compared using zero inflated Poisson distribution package available in R.

3.3.6. Image post-processing

Images were analyzed using 3D particle segmentation or local maxima detection method (LMDM) in MATLAB as described previously (Fisher et al., 2018). Briefly, constant background level was subtracted from the images and nuclei were detected based on the LMDM with three adjustable parameters: voxel size, an intensity threshold, and a minimum separation distance. The parameters were varied to obtain the closest match to the average nucleus size and brightness, with minimal overlap between neighboring nuclei. Our methods was adapted from the LMDM originally developed by Weeks and adapted by Kilfoil (Gao and Kilfoil 2009). The code works by identifying local intensity maxima in the image and a predefined volume mask. Each maximum is fit to an ellipsoidal mask and the centroid X, Y, Z is determined. The summed intensity for each ellipsoid is compared to a threshold value empirically set to minimize false positives. Our adaptation of local LMDM is contained in the file *LocalMax3DRG.m* used for all analyses. The code adds the green/auxin channel to the red/cytokinin channel and uses the sum to find local maxima using code in *feature3dMB.m* where LMDM is applied to detect the nuclei. After all nuclei are found and their XYZ positions obtained, these positions are used to obtain the nuclei intensity in the green and red channels.

Auxin to cytokinin ratio was analyzed based on specific regions of interest (ROIs), such as “cell division”, “cortical cells”, etc. For root nodule development we applied a rectangular box and / or cylindrical ROIs. p_1, p_2, p_3 are coordinates at the corner of the base of the box while p_4 was coordinate at the corner of top box which is colinear with p_1. The rectangular box sides were determined by a vector: $\overrightarrow{v_1} = p_2 - p_1$, $\overrightarrow{v_2} = p_3 -$

$p_1 \, and \, \overrightarrow{v_3} = p_4 - p_1$ where $\overrightarrow{v_1}$, $\overrightarrow{v_2}$, $\overrightarrow{v_3}$ are all orthogonal. A point p is within this box if it satisfies the inequalities below:

$$0 \leq (p - p_1) \cdot (p_2 - p_1) \leq (p_2 - p_1) \cdot (p_2 - p_1)$$

$$0 \leq (p - p_1) \cdot \ (p_3 - p_1) \leq (p_3 - p_1) \cdot (p_3 - p_1)$$

$$0 \leq (p - p_1) \cdot (p_4 - p_1) \leq (p_4 - p_1) \cdot (p_4 - p_1)$$

While cylindrical ROI was drawn starting with an infinite cylinder in 3D space which was colinear with an input vector. Then the cylinder was capped by two planes on both endpoints of an input vector. Mathematically for a given vector $\vec{v} = p_2 - p_1$ where p_1 and p_2 were points in 3D coordinates system distance of any arbitrary point p to a line colinear with $\bar{v}$ is

$$d = \frac{|(\vec{p} - \overrightarrow{p_1}) \times (\vec{p} - \overrightarrow{p_2})|}{|\overrightarrow{p_1} - \overrightarrow{p_2}|}$$

$$r^2 = \frac{|(\vec{p} - \overrightarrow{p_1}) \times (\vec{p} - \overrightarrow{p_2})|^2}{|\overrightarrow{p_1} - \overrightarrow{p_2}|^2}$$

Where r is the radius of the cylinder in the equation above and can be described in the Cartesian coordinate as below:

$$r^2 = \frac{((y - y_1)(z - z_2) - (z - z_1)(y - y_2))^2}{(x_2 - x_1)^2 + (y_2 - y_1)^2 + (z_2 - z_1)^2}$$

$$+ \frac{((z - z_1)(x - x_2) - (x - x_1)(z - z_2))^2}{(x_2 - x_1)^2 + (y_2 - y_1)^2 + (z_2 - z_1)^2}$$

$$+ \frac{((x - x_1)(y - y_2) - (y - y_1)(x - x_2))^2}{(x_2 - x_1)^2 + (y_2 - y_1)^2 + (z_2 - z_1)^2}$$

Equation above is used to draw indefinite cylinder in 3D, in this case any point p is within this cylinder if $r \geq d$ A cylinder of a finite length determined by $\vec{v}$ has two planes normal to $\vec{v}$ at $p_1$and p_2. A point can be determined from the dot products of $\vec{v}$ and the vectors from points p_1 and p_2 $to\ point\ p$ as defined by

$$a = (p_2 - p_1) \cdot (p - p_1)$$

$$b = (p_2 - p_1) \cdot (p - p_2)$$

At any point p is between these two planes and within the cylinder if the following relationships are true:

$$a \geq 0 \geq b$$

$$r \geq d$$

For cylindrical ROI, auxin to cytokinin ratio was measured radially (a disk ROI).

For analysis, we choose a mask with voxel size 7x7x9 based on the smallest diameter of the nuclei, with minimum separation equal to diameter/2 for dense particles to avoid nuclei loss. The total number of voxels was 253 for a volume mask of 7x7x9, for images with a background noise of 100, the total intensity is 25,300. Because auxin and cytokinin channel were added for the detection a 50,000-intensity threshold was chosen per nuclei as a start. The intensity threshold was adjusted and validated for each image by overlapping raw images with nuclei detected by LMDM. Images were manually inspected in a 3D manner by Arivis Vision4D.

For soybean stage 1-1 cell file and stage1-2 cell files, the ROI's were three rectangular boxes with height/Z slices of 10µm, 30µm and 60 µm corresponding to "cell division", "cortical cells", and "root cells" ROI. The nuclei in cortical cells were acquired by subtracting the nuclei in the middle box with the smallest box while root cell ROIs are obtained by subtracting all nuclei detected in the biggest ROI with the second biggest (middle) rectangular box. For Soybean at stage 2, the ROIs were a combination of rectangular boxes and cylinders, the height/Z slices are 20µm, 30µm and 60µm for nodule primordium, cortical cell, and root cells. The ROIs for soybean root nodule stage 3 and 4 are cylindrical with height/Z equal to 20 µm. ROIs were divided into three different zones by drawing cylinders with zone 1 being a third of the radius of zone 3, and zone 2 radius being two-thirds of the radius of zone 3. The ROI for soybean premature nodules was categories into 3 areas: an infection zone at the center, parenchyma at the periphery, and vascular bundles at the periphery. Cylinders ware drawn with a height of 15µm and radius varies depending on the area that is being examined.

Auxin/cytokinin ratio was mapped and compared statistically at different stages of nodule development. In this analysis, violin plots were generated using GraphPad Prism version 8 which shows the frequency distribution of data and plot lines at the median and quartiles. (Unpaired t) test and one-way ANNOVA (Tukey test) were used to measure statistical analysis of two groups and more than two groups of data respectively. P-value higher than 0.05 means the value is not significant (ns), P value less than or equal to ≤ 0.05,

≤0.01, ≤0.001 and ≤0.0001 mean significant difference which correspond to *, **, ***, and **** respectively.

The number and the surface area of vascular bundle in AuxCysensor and AuxCysensor STTM160 from 4 independent PMNs nodule was calculated using ImageJ and compared with Student's t-test. The presence and surface of the vascular bundle was determined by: 1- absence of autofluorescence, contrary to the surrounding parenchyma and neighboring infection zone, the vascular bundle doesn't auto-fluoresce when excited in the 400–450 nm bandpass filter. 2- nuclei size and arrangement, in vascular bundles, nuclei have a reduced size, are clustered and oriented toward each other contrary to the nuclei present in other tissues types.

3.3.7. Gene Expression Assays

To test whether the STTM160 insert present in the AuxCysensor STTM160 roots was reducing the level of miR160, quantitative PCRs were performed as described in Turner et al., 2013. Gene expression levels were normalized to those of GmmiR1515 (Turner, Nizampatnam et al. 2013) and compared using the $2^{-\Delta\Delta CT}$ method (Livak and Schmittgen 2001).

3.4. Results

3.4.1. Auxin-cytokinin relative output ratios spatio-temporal dynamic

3.4.1.1. Auxin-cytokinin relative output ratio is high in nodule initials, low in young primordia and displays a radial pattern in maturing primordia

We quantified nodule primordium auxin-cytokinin relative output (ACRO) ratios at 6 different stages of soybean nodule development. Stage 1-1 corresponds to primordium initiation where the first anticlinal cell divisions occur and was frequently found at 3 days-post-inoculation (dpi) (Figure 3.4.1.1a). Stage 1-2 is comprised of primordia with anticlinal and periclinal cell divisions and was also present at 3dpi (Figure 3.4.1.1b). In stage 2 nodule primordia appear spherical and were frequently observed at 4dpi (Figure 3.4.1.1c). For stages 1 and 2, three regions of interest (ROIs) were selected for quantification of ACRO ratios: 1) The dividing cells of the nodule primordium, 2) Two layers of cortical cells surrounding the nodule primordium, and 3) The rest of the root cells in the field of view. We quantified the ACRO ratios of each ROI in nodule primordia derived from 5-6 independent transgenic roots for each stage. In addition, we

also visualized the ACRO ratios using a 4-color map scale to determine local specificities and variations in an unbiased manner at cellular resolution (Fisher, Gaillard et al. 2018).

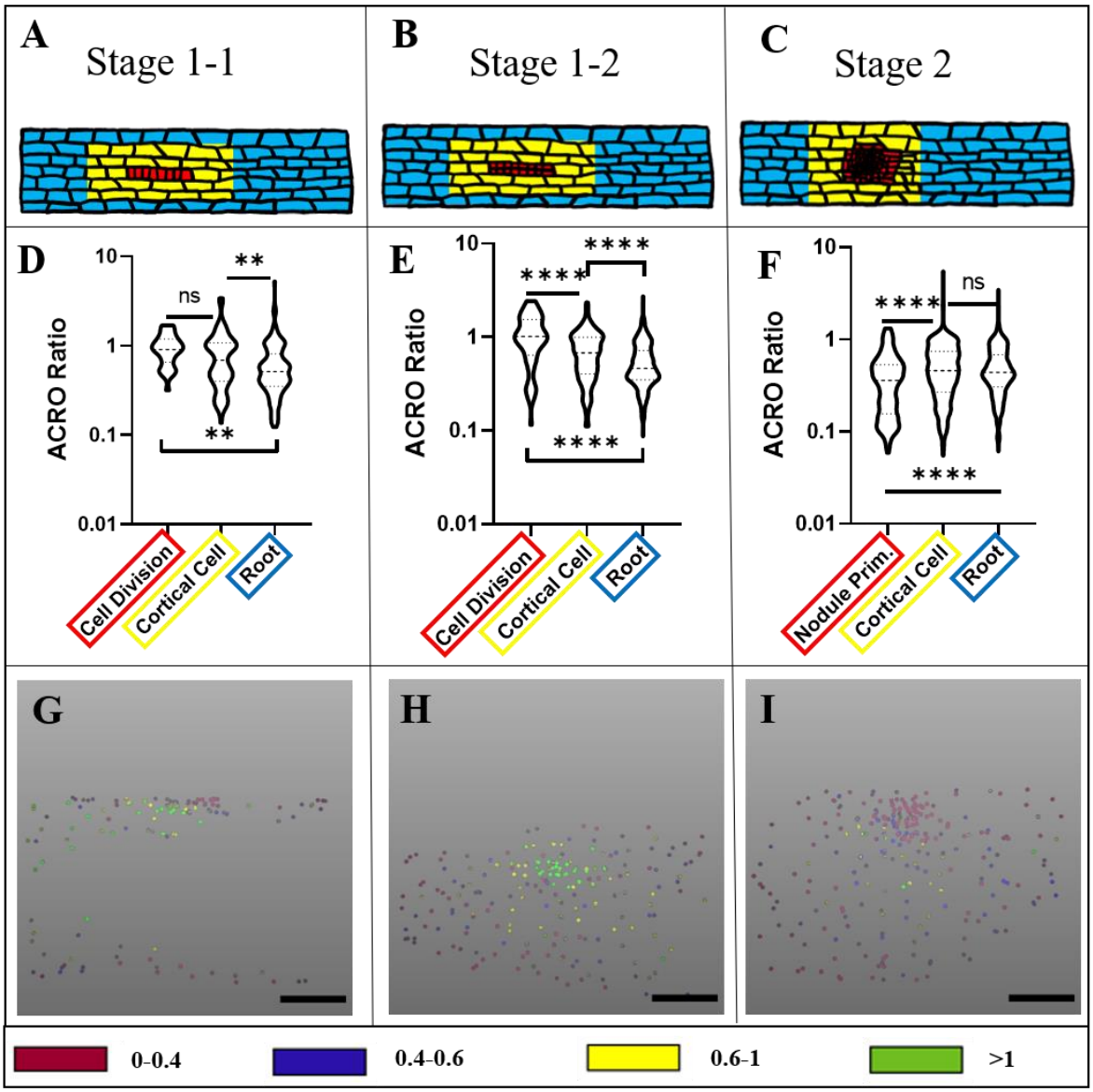

Figure 3.4.1-1: Auxin-cytokinin relative output (ACRO) ratios during soybean nodule primordium initiation. *Nodule development is represented at the stage 1-1 (A), 1-2 (B) and 2 (C). Diagrams of roots represent the ROIs used for the analysis. The red rectangles at stage 1-1 and 1-2 and the red circle at stage 2 represent dividing cells and nodule primordia respectively. Yellow and blue rectangles at stage 1-1, 1-2 and 2 correspond to cortical and root cells respectively. Violin plots lines at the median and quartile and shows distribution of the values of the average ACRO ratios for each ROI and compared to each other at stage 1-1 (D), 1-2 (E) and 2 (F). Root single nucleus ACRO ratios are represented using a 4-color map scale. Red color corresponds to ACRO from 0 to 0.4, blue from 0.4 to 0.6, yellow from 0.6 to 1 and green 1 and higher. Scale bar=100µm. Statistical analysis using one way-ANOVA with multiple comparison using Tukey test with confidence level 0.05. P value of * is <0.05, ** is <= 0.01, *** is <= 0.001 and **** is <= 0.0001, ns means non-significant.*

At stage 1.1, the average ACRO ratio of the dividing cells (0.96±0.06) and the surrounding cortex cells (0.83±0.06) were significantly higher than the root cells (0.64±0.02; Figure 3.4.1.1d). At stage 1.2, the average ACRO ratio was significantly higher in the dividing cells (1.07±0.07) than in the surrounding cortex cells (0.712±0.03) which themselves had a significantly higher ACRO ratio than that of the root cells (0.56±0.01; Figure 3.4.1.1e). Moreover, the 4-color ACRO map scale represented the

dividing cells with an ACRO ratio higher than one (green color) and the ACRO ratios are lowering (from 1 to 0) as the cells are distant from the dividing cells (Figure 3.4.1.1g and 3.4.1.1h). This observation suggested that nodule initial cell division might require a high auxin-CK ratio.

At stage 2, the average ACRO ratio in the nodule primordium cells was (0.40±0.01) which was significantly lower compared to those in the surrounding cortex (0.53±0.02) and root cells (0.52±0.01; Figure 3.4.1.1f). The ACRO ratio color mapping indicated a low ACRO ratio (between 0 and 0.4) in the primordium cells (cluster of red nuclei), while the surrounding cells have primarily a higher ACRO ratio associated with yellow colored nuclei (between 0.6 and 1) and the roots have ACRO ratios between 0 and 0.6 represented by blue and red nuclei (Figure 3.4.1.1i).

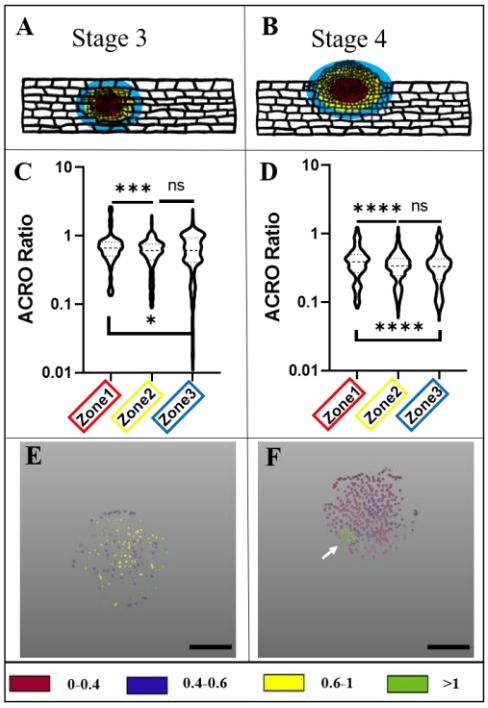

Figure 3.4.1-2: ACRO ratios during soybean nodule primordium development. *Nodule development is represented at the stage 3 (A) and 4 (B). Diagrams of roots represent the ROIs used for the analysis. Nodule primordia at stage 3 and 4 have three ROIs, there is a red inner circle (Zone 1), a yellow middle ring (Zone 2) and a blue outer ring (Zone 3). Average ACRO ratios were quantified for each ROI and compared to each other at stage 3 (C) and 4(D). C and D were represented via violin plots where lines at the median and quartile showed distribution of the values. Single nucleus ACRO ratios of zones 1, 2 and 3 were represented using a 4-color map scale at stage 3 (E) and 4 (F). Red color corresponds to ACRO from 0 to 0.4, blue from 0.4 to 0.6, yellow from 0.6 to 1 and green 1 and higher. White arrow indicates putative vascular bundle. Scale bar=100µm. Statistical analysis using one way-ANOVA with multiple comparison using Tukey test with confidence level 0.05. P value of * is <0.05, ** is <= 0.01, *** is <= 0.001 and **** is <= 0.0001, ns means non-significant.*

Nodule primordium stage 3 corresponds to an enlarge primordium that has not emerged out from the root and was present at 5dpi (Figure 3.4.1-2a). Stage 4 represents nodule primordium emerging from the root and was present at 7dpi (Figure 3.4.1-2b). Three ROIs marked by equidistant concentric circles going from the center to the periphery of the nodule primordia were selected in stages 3 and 4 for ACRO ratios quantification. At stage 3, the average ACRO ratio in the central zone of the primordium (0.72±0.03) was significantly higher compared to the middle zone (0.60±0.01) which was not significantly different from that of the outer zone (0.64±0.02; Figure 3.4.1-2c). These

traits were confirmed by the 4-color map scale as most of the nuclei in the central zone are represented by a yellow color, while the middle and peripheric regions contain yellow blue and red nuclei (Figure 3.4.1-2e). At stage 4, it seems that a higher relative ACRO ratio in the center of the primordium compared to the periphery might be required for nodule growth (Figure 3.4.1-2d). The average ACRO ratio pattern from zone to zones is similar to the stage 3 (Figure 3.4.1-2f). Interestingly, local auxin accumulation can specifically be observed at the primordia periphery (Figure 3.4.1-2f).

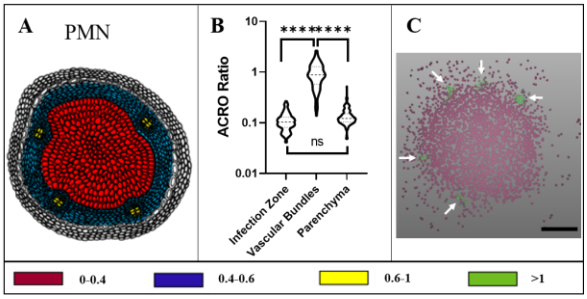

Figure 3.4.1-3: ACRO ratios in PMN. *(A): diagram of PMN section with its ROIs. Red corresponds to the infection zone, yellow to vascular bundles and blue to parenchymatic cells. (B): Violin plots lines at the median and quartile and shows distribution of the values of the average ACRO ratios for each ROI and compared to each other. (C) 4-color map scale representing the different ACRO ratio per nuclei in a PMN section. Red color corresponds to ACRO from 0 to 0.4, blue from 0.4 to 0.6, yellow from 0.6 to 1 and green 1 and higher. White arrow indicates putative vascular bundle. Scale bar=100µm. Statistical analysis using similar method to Figure 3.4.1 2.*

The pre-mature nodules (PMNs) composed of three distinct ROIs, the infection zone at the center, the surrounding parenchyma and the vascular bundles were frequently present at 10dpi (Figure 3.4.1-3a). We reanalyzed PMNs ACRO ratios from Fisher et al., 2018 with similar results, but used violin plots to better represent the ACROs distribution. The average ACRO ratio of PMNs in the infection zone (0.11±0.00) is significantly lower compared to the parenchymatic tissue (0.14±0.00), itself significantly lower than the vascular bundles (0.95±0.05; Figure 3.4.1-3b). Green nuclei in a position associated with the vascular bundles stand out from the parenchymal nuclei colored in blue and red, while the nuclei in the infection are predominantly red, illustrating a tissue specific ACRO ratio (Figure 3.4.1-3c). Based on both representations it was clear that distinct nodule zones (represented by the ROIs) has distinct ACRO ratios. It is likely that the changes in ACRO ratios dictate the development of these nodule zones.

3.4.1.2. The average ACRO ratios present during nodule primordium development follow an oscillation pattern

We compared ACRO ratios of the same cell types and/or nodule zones at different developmental stages. The average ACRO ratios of dividing cells in stages 1-1 (0.96±0.06) and 1-2 (1.07±0.07) were similar, but the ACRO ratio of the corresponding zone in stage 2 was significantly lower (0.40±0.01; Figure 3.4.1-4a). The average ACRO ratios in cortical cells and root cells of the stages 1-1, 1-2, and 2 decrease gradually and significantly as nodule development progresses (from 0.83±0.06 and 0.64±0.02 to

0.72±0.03 and 0.56±0.01 to 0.53±0.02 and 0.52±0.01 respectively; Figure 3.4.1-4b and 3.4.1-4c). The inner circle (Zone 1), the middle ring (Zone 2) and the outer ring (Zone 3) of stage 3 nodule primordia (0.72±0.03; 0.60±0.01 and 0.64±0.02 respectively; Figure 3.4.1-4d, 3.4.1-4e and 3.4.1-4f) had significantly higher average ACRO ratios than the corresponding zones in stage 4 (0.41±0.01; 0.35±0.01 and 0.35±0.01respectively; Figure 3.4.1-4d, 3.4.1-4e and 3.4.1-4f). The PMNs being a category by its own, they were not compared to the other nodule primordia stages.

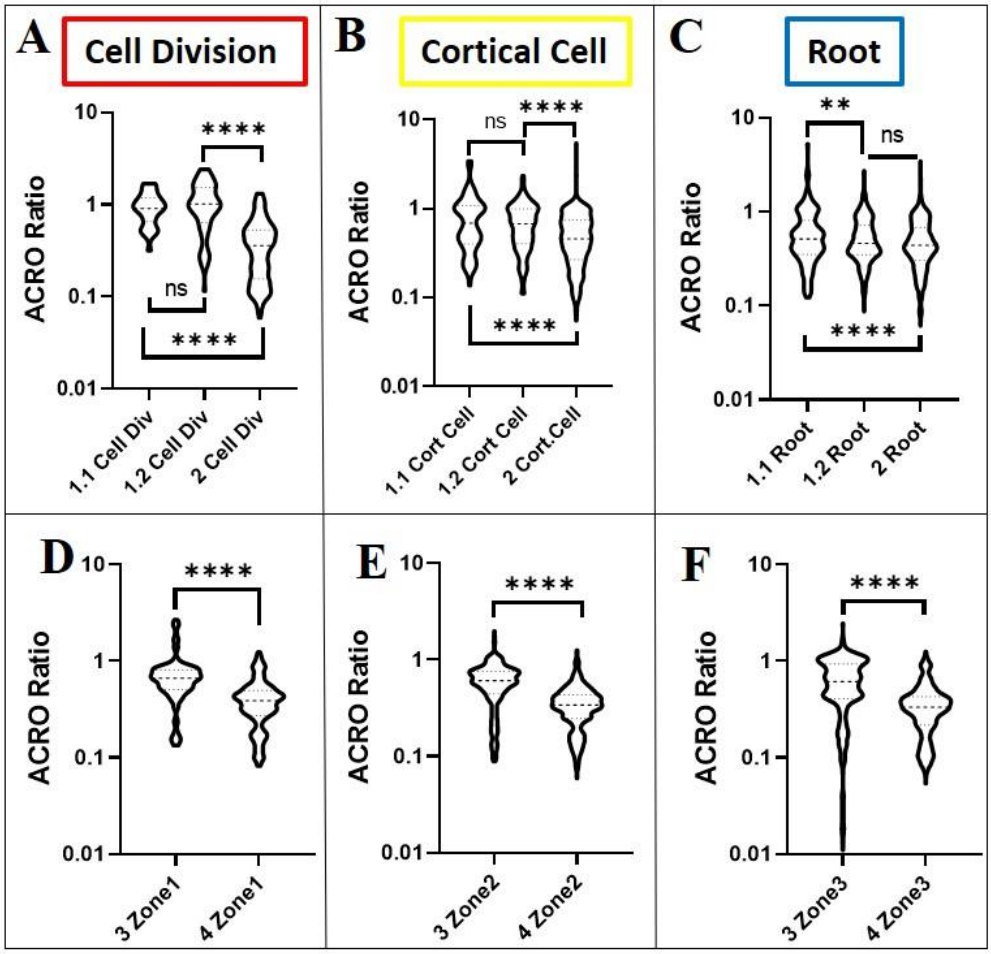

Figure 3.4.1-4: Comparison of zone specific ACRO ratios from stages 1 to 4. *Average ACRO ratios at stage 1-1, 1-2 and 2 in the diving cells (A), cortical cells (B) and root cells (C). Average ACRO ratios at stage 3 and 4 in Zone 1 (D), Zone 2 (E) and Zone 3 (F). A to F were represented via violin plots where lines at the median and quartile showed distribution of the values. Statistical analysis using one way-ANOVA with multiple comparison using Tukey test with confidence level 0.05. P value of * is <0.05, ** is <= 0.01, *** is <= 0.001 and **** is <= 0.0001, ns means non-significant.*

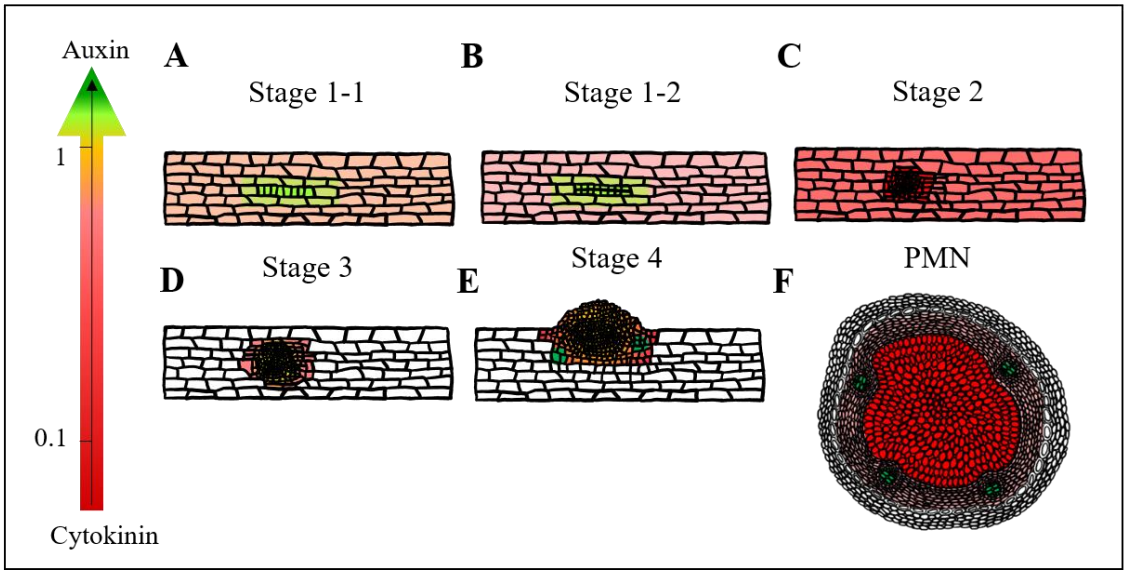

Figure 3.4.1-5: Schematic representation of the ACRO ratios during nodule development. *Average ACRO ratios presented at stage 1-1 (A), 1-2 (B), 2 (C), 3 (D), 4 (E) and PMN (F). Average ACRO ratios are represented by a color scale going from dark red associated with a low ACRO ratio to dark green associated with a high ACRO ratio.*

If we follow ACRO ratios over nodule initiation and development, an oscillation pattern appears. First, a high average ACRO ratio in the dividing cells is associated with nodule primordium initiation (Figure 3.4.1.1d, 3.4.1.1e, 3.4.1-4a, 3.4.1-5a and 3.4.1-5b). Then, the early primordium at stage 2 is associated with a low average ACRO ratio (Figure 3.4.1.1f, 3.4.1-4a and 3.4.1-5c). Finally, a high average ACRO ratio is present in the stage 3 primordium and significantly reduces at stage 4 (Figure 3.4.1-2c, 3.4.1-2d, 3.4.1-4d, 3.4.1-4e, 4f, 3.4.1-5d and 3.4.1-5e). Given that primordium formation and development is the result of successful rhizobia infection and cell division, we decided to evaluate the average ACRO ratio present in the infected and colonized cells.

3.4.2. Low ACRO ratio in stage 2 coincides with colonization by rhizobia

We imaged different nodule developmental stages infected by *B. diazoefficiens* constitutively expressing the nptII:GUS reporter construct to determine if the infection and colonization processes are associated with specific ACRO ratios dynamics. At stages 1.1 and 1.2, the infection process has started, and GUS activity from *B. diazoefficiens* was present in the epidermal cells, the root hairs and in the dividing cortical cells (Figure 3.4.2-1a and 3.4.2-1b). Even though we demonstrated a disparity of the average ACRO ratios between diving cells and the rest of the root, colonization by *B. diazoefficiens* seemed homogenous between the different cell types based on GUS staining.

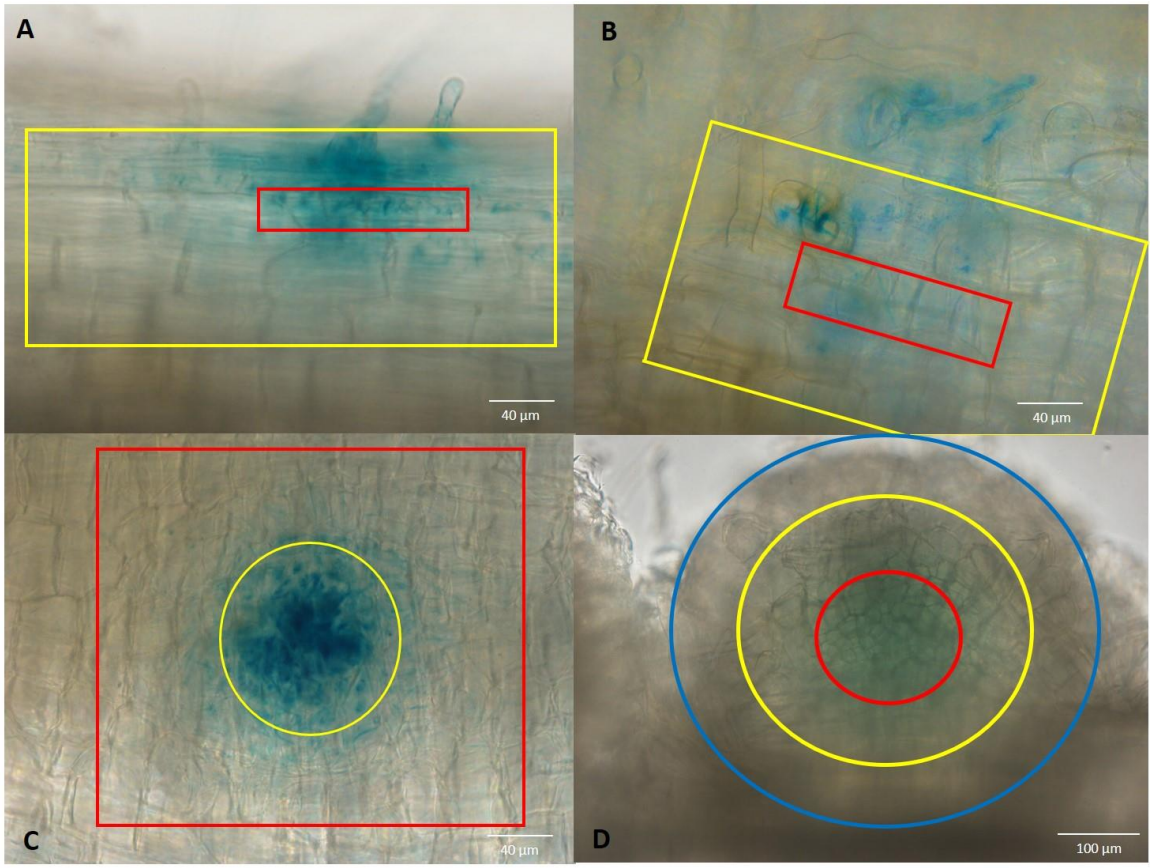

Figure 3.4.2-1: *B. diazoefficiens* nptII:GUS infection and colonization during soybean nodule development. *Fixed and cleared soybean roots were GUS stained and imaged at stage 1-1 (A), 1-2 (B), 2 (C) and 4 (D).*

At stage 2, the blue staining is darker in the center of the primordium indicating a higher bacterial abundance and suggesting colonization of the primordium by the bacteria (Figure 3.4.2-1c). Interestingly, the enrichment in *B. diazoefficiens* GUS correlates with a very low and specific ACRO ratio present in the stage 2 primordium. Unfortunately,

stage 3 was disregarded as we were unable to obtain enough images representative of this developmental stage.

The central zone and the inner middle zone of the stage 4 nodules displayed bacteria colonization while the surrounding zones did not (Figure 3.4.2-1d), in agreement with previous study (Suzaki et al., 2012). Note that the stage 4 staining appears less intense due to tissue thickness attenuating the signal intensity. The low average ACRO ratio and the *B. diazoefficiens* GUS colonization are both occurring at stage 2 in the primordium, suggesting a causal relationship between these processes. To further study the ACRO ratio requirements and dynamics during nodulation we investigated roots displaying a reduced sensitivity to auxin and an enhanced sensitivity to cytokinin.

3.4.3. AuxCysensor STTM160 roots have more but delayed nodule primordium and altered average ACRO ratio

3.4.3.1. AuxCysensor STTM160 roots phenocopies STTM160 roots associated with a diminution of miR160's expression

In 2015 we created miR160 silenced roots (STTM160) that had higher relative expression levels of the ARF 10/16/17 gene family members. In agreement with the prediction of ARF10/1/6/17 family members as repressors of auxin responsive gene expression, STTM160 roots were less sensitive to auxin (Nizampatnam, Schreier et al.

2015). Interestingly, there were also more sensitive to cytokinin and produced more nodule primordia that appeared have a delay in maturation.

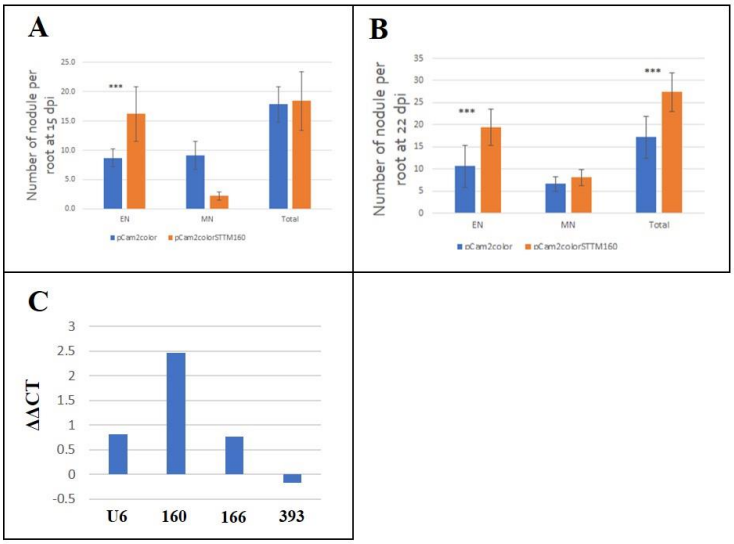

Figure 3.4.3-1: Nodulation phenotype in AuxCysensor STTM160. *Average number of emerging, mature and total nodule per root at 15 (A) and 22 dpi (B) in AuxCysensor and AuxCysensor STTM160 roots. (C): Relative qPCR expression of miR160, miR166, miR393 and U6 in AuxCysensor and AuxCysensor STTM160 roots. Error bars represent standard deviation of the mean. P value of * is <0.05, ** is <= 0.01, *** is <= 0.001 and **** is <= 0.0001.*

We characterized ACRO ratios in these roots to determine potential roles of miR160 in regulating ACRO ratios dynamics during nodulation.

The number of emerging and mature nodules in AuxCysensor STTM160 roots were counted at 15 and 22dpi to confirm that they have a similar nodulation phenotype as

the STTM160 roots at 14 and 21dpi (Nizampatnam, Schreier et al. 2015). At 15dpi, AuxCysensor STTM160 roots had significantly more emerging nodules (16.19±4.64) compared to the vector control (8.71±1.54), and significantly less mature nodules (2.24±0.70) than the vector control (9.10±2.39; Figure 3.4.3-1a). At 22 dpi, STTM160 roots had significantly more emerging and total nodules (19.33±4.10 and 27.38±4.35 respectively) when compared to the vector control (10.62±4.71 and17.19±4.73, Figure 3.4.3-1b). The average number of mature nodules at 22dpi in AuxCysensor STTM160 (8.05±1.80) and vector control roots (6.57±1.68) was similar (Figure 3.4.3-1b), corroborating the maturation delay previously characterized in STTM160 at 21dpi.

To further confirm that this phenotype was due to a miR160 reduction, we quantified the relative presence of mature miR160 in the AuxCysensor STTM160 roots compared to the vector control roots. miR160 is 2.5 less present in AuxCysensor STTM160 compared vector control (Figure 3.4.3-1c). There was no significant difference in the levels of miR166, miR393 and the house kipping geneU6 indicating that STTM160 specifically reduced miR160 levels (Figure 3.4.3-1c). Hence, AuxCysensor STTM160 roots with a higher number of emerging nodules that are delayed in their maturity were used to investigate relative ACRO ratios during nodule organogenesis.

3.4.3.2. AuxCysensor STTM160 nodule primordium initials have low average ACRO ratio and display altered ACRO ratio patterns in stage 3 and 4

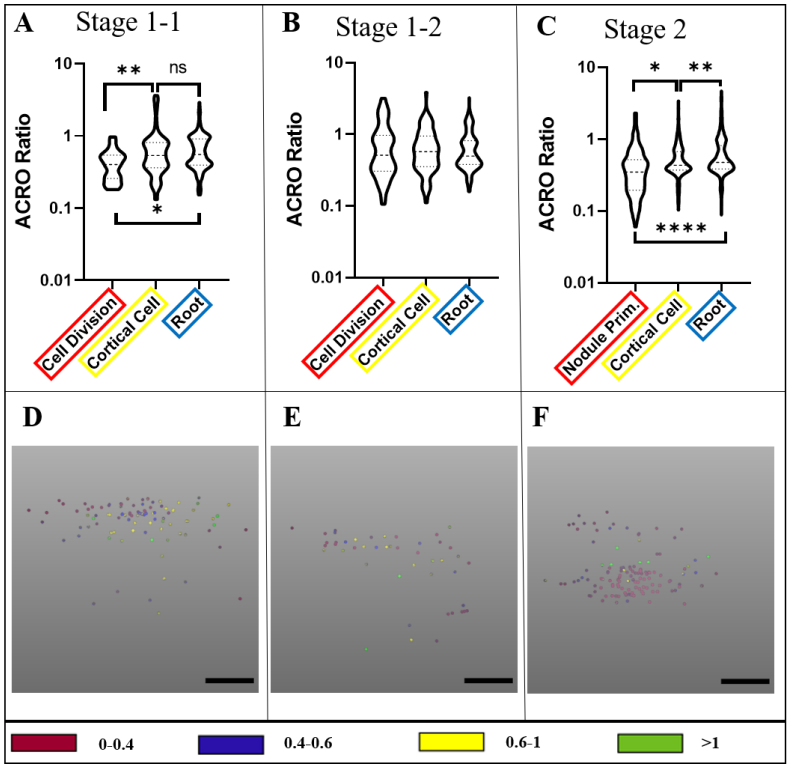

Figure 3.4.3-2: Average ACRO ratios in AuxCysensor STTM160 during soybean nodule primordium initiation. *Average ACRO ratios in dividing, cortical and root cells at the stages 1-1 (A), 1-2 (B) and 2 (C). A to C were represented via violin plots where lines at the median and quartile showed distribution of the values. (D to F): Root single nuclei 4-color map scale image at stages 1-1, 1-2 and 2 respectively. Scale bar=100µm. Statistical analysis using one way-ANOVA with multiple comparison using Tukey test with confidence level 0.05. P value of * is <0.05, ** is <= 0.01, *** is <= 0.001 and **** is <= 0.0001, ns means non-significant.*

In 2015, our lab reported that miR160 activity was sparsely detected at the base of emerging nodule and widely in mature nodule using a miR160 GFP sensor

(Nizampatnam, Schreier et al. 2015). In AuxCysensor STTM160 roots, three types seem primarily impacted. The dividing cells during early primordium formation (stage 1), the primordium during nodule maturation (stage 3 and 4) which then becomes infection zone at the PMN stage and PMN vascular bundles. Contrary to the stage 1-1 AuxCysensor (Figure 3.4.3-2a), the average ACRO ratio in the AuxCysensor STTM160 stage1-1 dividing cells (0.43±0.03) was significantly lower compared to their surrounding cortical cells (0.70±0.06) and the rest of the root (0.67±0.03; Figure 3.4.3-2a). No differences were observed between the different cell types of the AuxCysensor STTM160 at stage 1-2 (Figure 3.4.3-2b), while the dividing cells at stage 1-2 in the AuxCysensor roots had a higher average ACRO ratio compared to the rest of the root (Figure 3.4.1.1b). Indeed, the green (ACRO ratio higher than 1) nuclei files present in the dividing cells at both stages 1 in the AuxCysensor roots (Figure 3.4.1.1c and 3.4.1.1d) were not present in the AuxCysensor STTM160 and these nuclei have a red to yellow coloration (ACRO ratio from 0 to 1; Figure 3.4.3-2d and 3.4.3-2e). Similar to stage 2 AuxCysensor primordia (Figure 3.4.1.1c), average ACRO ratio of stage 2 AuxCysensor STTM160 primordia (0.43±0.03) was significantly lower compared to that in the surrounding cortical cells (0.55±0.02) and arranged as a cluster of red nuclei (Figure 3.4.3-2c). In case of the stage 2 AuxCysensor STTM160 the average ACRO ratio of the cortical cells (0.55±0.02) is also significantly lower compared to the rest of the root (0.67±0.02; Figure 3.4.3-2c).

AuxCysensor STTM1610 stage 3 primordium were presenting two distinct patterns after imaging. Five of the ten were looked predominantly cytokinin enriched and the 5 others

auxin enriched. The average ACRO ratios was significantly higher in the central zone (0.47±0.02) compared to the peripheral zone (0.56±0.01; Figure 3.4.3-3a). More importantly, the ACRO ratios distribution represented by violin plots showed two segregating population within each zone (Figure 3.4.3-3a). Indeed, ACRO ratios were not following a normal distribution and one population presented a positive ACRO ratio close to 1, and the other had a negative ACRO (Figure 3.4.3-3a). The 4-color map scale ACRO ratio indicated that five of the ten AuxCysensor STTM160 roots stage 3 nodule primordia, showed a very low ACRO ratio (nuclei principally red, similar to AuxCysensor roots stage 2 primordia) while the other 5 showed a pattern similar to the stage 3 AuxCysensor nodule primordia: a neutral ACRO ratio in the center (yellow) and a lower ratio surrounding it (blue to red) (Figure 3.4.1-2e and 3.4.3-3d).

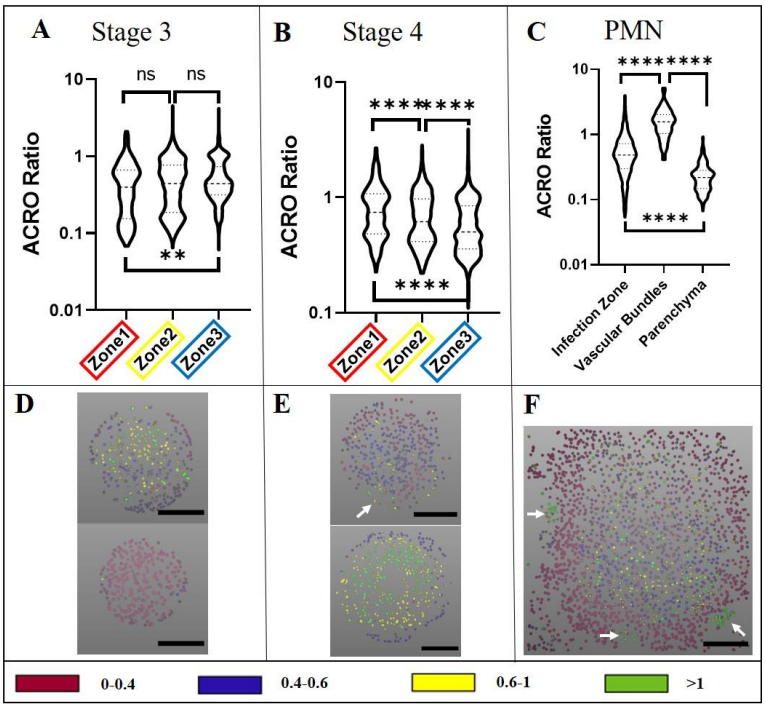

Figure 3.4.3-3: Average ACRO ratios in AuxCysensor STTM160 during soybean nodule primordium development. *Average ACRO ratios in Zone 1, 2 and 3 at the stage 3 (A) and 4 (B) and in the infection zone, vascular bundles and parenchyma in PMN (C). A to C were represented via violin plots where lines at the median and quartile showed distribution of the values. Single nuclei 4-color map scale image of zones 1, 2 and 3 at stage 3 (D) and 4 (E) and whole PMN section (F). Note that in stage 3 and in stage 4, the 4-color map scale images are equally distributed into two representative and exclusive categorizes. White arrow indicates putative vascular bundle. Scale bar=100µm. Statistical analysis using one way-ANOVA with multiple comparison using Tukey test with confidence level 0.05. P value of * is <0.05, ** is <= 0.01, *** is <= 0.001 and **** is <= 0.0001, ns means non-significant.*

AuxCysensor STTM1610 stage 3 primordium were presenting two distinct patterns after imaging. Five of the ten were looked predominantly cytokinin enriched and the 5 others auxin enriched. The average ACRO ratios was significantly higher in the central zone (0.47±0.02) compared to the peripheral zone (0.56±0.01; Figure 3.4.3-3a). More importantly, the ACRO ratios distribution represented by violin plots showed two segregating population within each zone (Figure 3.4.3-3a). Indeed, ACRO ratios were not following a normal distribution and one population presented a positive ACRO ratio close to 1, and the other had a negative ACRO (Figure 3.4.3-3a). The 4-color map scale ACRO ratio indicated that five of the ten AuxCysensor STTM160 roots stage 3 nodule primordia, showed a very low ACRO ratio (nuclei principally red, similar to

AuxCysensor roots stage 2 primordia) while the other 5 showed a pattern similar to the stage 3 AuxCysensor nodule primordia: a neutral ACRO ratio in the center (yellow) and a lower ratio surrounding it (blue to red) (Figure 3.4.1-2e and 3.4.3-3d).

At stage 4 two distinct population were also observed. Overall, the ACRO ratios were higher in the central zone and gradually decreased towards the periphery (0.84±0.02, 072±0.01 and 0.62±0.01 respectively; Figure 3.4.3-3b). In each zone one population of ACRO ratio was close to 1 and the other to 0.5 and the ACRO ratios were not following a normal distribution Figure 3.4.3-3b). Three of the seven stage 4 AuxCysensor STTM160 root nodule primordia, were similar to the stage 3 AuxCysensor roots as they have a high ACRO ratio in the center (higher than 1), that declines toward a lower ACRO ratio in the periphery (1 to 0.4) (Figure 3.4.3-3d and 3.4.3-3e). The 4 other primordia had ACRO patterns similar to the stage 4 AuxCysensor nodule primordium: an ACRO ratio between 0.4 and 0.6 at their center (blue) and a lower ACRO ratio at their periphery (red) at the exception of little groups of green and yellow nuclei (Figure 3.4.1-2f and 3.4.3-3e).

ACRO ratios of AuxCysensor STTM160 PMNs were very broad, going from 0.1 to 1 with an average at 0.59±0.02 (Figure 3.4.3-3c). Contrary to AuxCysensor roots (Figure 3.4.1-3b), the ACRO ratio of AuxCysensor STTM160 PMNs in the infection zone was significantly higher than in the parenchyma (0.24±0.01; Figure 3.4.3-3c). Like

AuxCysensor PMNs, the average ACRO ratio of the vascular bundles (1.64±0.11) is significantly higher than the other cell types (Figure 3.4.1-3b and 3.4.3-3c).

PMNs vascular bundles in AuxCysensor (Figure 3.4.1-3c) and AuxCysensor STTM160 (Figure 3.4.3-3f) are both represented by cluster of green nuclei in the PMN. However, AuxCysensor identity in the infection zone (red nuclei) and parenchyma (blue nuclei) seem to be switched in AuxCysensor STTM160 (from yellow to red and red respectively, Figure 3.4.1-3c and 3.4.3-3f). AuxCysensor and AuxCysensor STTM160 roots were compared to further investigate the impact on the ACRO ratio for these roots having an altered auxin and cytokinin sensitivity.

3.4.3.3. STTM160 impacts the ACRO ratios in most of nodule cell types

Direct comparison of the average ACRO ratios between AuxCysensor and AuxCysensor STTM160 roots confirmed the significative reduction in the dividing cells of AuxCysensor STTM160 compared to AuxCysensor at stage 1-1 and 1-2 respectively (0.43±0.03 VS 0.96±0.06

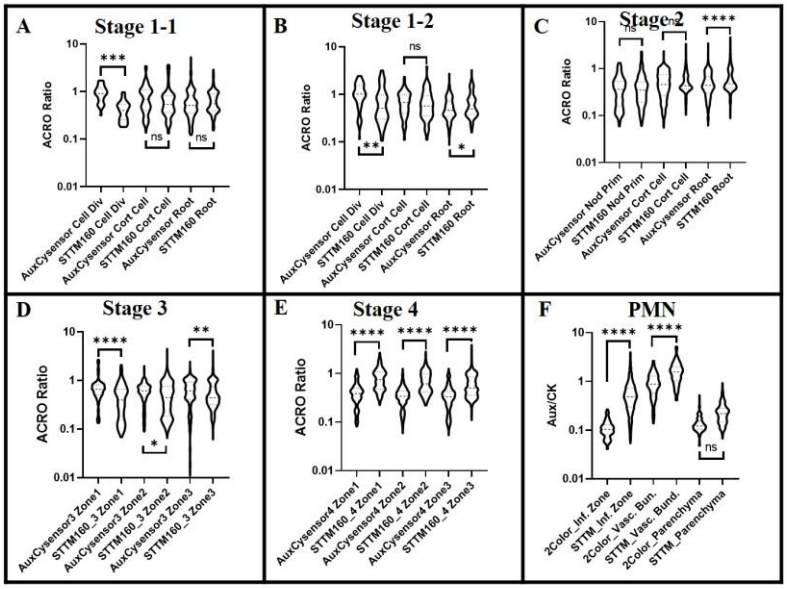

Figure 3.4.3-4: Cell type comparison of the average ACRO ratios between AuxCysensor and AuxCysensor STTM160. *Stage 1-1 (A), 1-2 (B), 2 (C), 3 (D), 4 (E) and PMN (F) were compared. At stage 1-1 and 1-2 dividing, cortical and roots cells were compared between AuxCysensor and AuxCysensor STTM160. At stage 2 nodule primordia, cortical and roots cells were compared between AuxCysensor and AuxCysensor STTM160. At stage 3 and 4, zone1, 2 and 3 were compared between AuxCysensor and AuxCysensor STTM160. In PMN, infection zone, vascular bundles and roots were compared between AuxCysensor and AuxCysensor STTM160. A to F were represented via violin plots where lines at the median and quartile showed distribution of the values. Statistical analysis using one way-ANOVA with multiple comparison using Tukey test with confidence level 0.05. P value of * is <0.05, ** is <= 0.01, *** is <= 0.001 and **** is <= 0.0001.*

and 0.79±0.09 VS 1.07±0.07; Figure 3.4.3-4a and 3.4.3-4b). Interestingly, the other cell types do not differ at the exception of the root cells at stage 1-2, for which AuxCysensor STTM160 average ACRO ratio (0.68±0.04) is slightly higher than in AuxCysensor (0.56±0.01; Figure 3.4.3-4b).

At stage 2, there were no significant differences in ACRO ratios in cell division and cortical cell, AuxCysensor STTM160 average ACRO ratio in root cells (0.69±0.03) was significantly higher than in AuxCysensor roots (0.52±0.01); Figure 3.4.3-4c). Note that even though AuxCysensor STTM160 produce more primordia, the ACRO ratio is not impacted at stage2. Total stage 3 AuxCysensor STTM160 zones 1, 2 and 3 have significantly a lower average ACRO ratio (0.47±0.02, 0.53±0.01 and 0.56±0.01) than in stage 3 AuxCysensor zones 1, 2 and 3 (0.72±0.03, 0.60±0.01 and 0.64±0.02 respectively; Figure 3.4.3-4d). It is the opposite in total stage 4 primordium, as AuxCysensor STTM160 roots zones 1, 2 and 3 have significantly higher average ACRO ratios (0.84±0.02, 0.72±0.01 and 0.62±0.01 respectively) than in AuxCysensor roots (0.41±0.01, 0.35±0.01 and 0.35±0.01 respectively; Figure 3.4.3-4e).

The average ACRO ratio of AuxCysensor STTM160 PMNs in the infection zone (0.59±0.02) and in the vascular bundles (1.64±0.11) is significantly higher than in AuxCysensor roots (0.11±0.00 and 0.95±0.05 respectively), while the average ACRO ratio in the parenchyma is not altered (0.14±0.00 and 0.24±0.01; Figure 3.4.3-4f). Interestingly, a higher number of nodule primordium is associated with a lower ACRO

ratio during early primordium organogenesis, while delayed maturation is associated with a higher ACRO ratio.

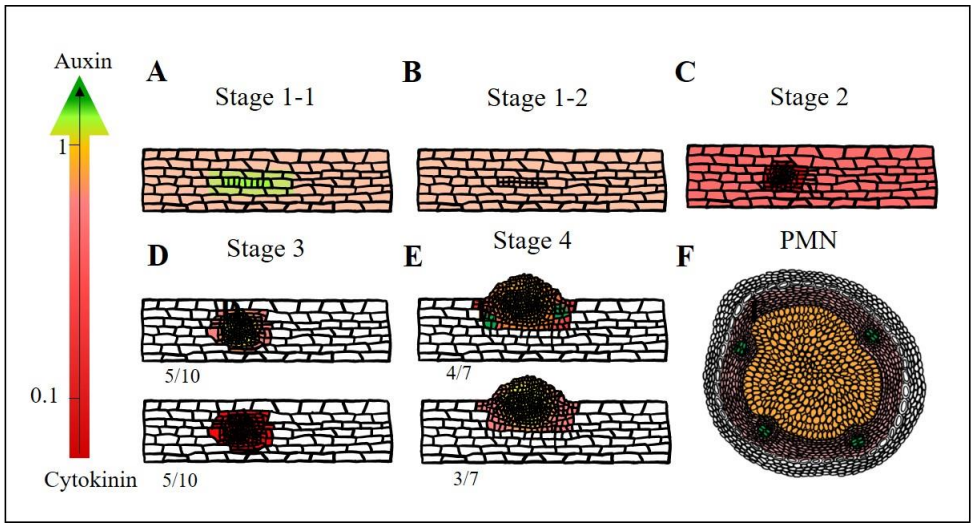

Figure 3.4.3-5: Schematic representation of the ACRO ratios in AuxCysensor during nodule development. *Average ACRO ratios were represented at stage 1-1 (A), 1-2 (B), 2 (C), 3 (D), 4 (E) and PMN (F). Note that stage 3 and stage 4 are equally distributed into two representative and exclusive categorizes. Average ACRO ratios are represented by a color scale going from dark red associated with a low ACRO ratio to dark green associated with a high ACRO ratio.*

In summary, the AuxCysensor STTM160 initial dividing cells seem to have a lower ACRO ratio (Figure 3.4.3-5a and 3.4.3-5b) and a subset of the stage 3 and 4 primordia show an altered ACRO ratio phenotype (Figure 3.4.3-5d and 3.4.3-5e), while AuxCysensor STTM160 PMNs have an unexpectedly broad ACRO ratio (Figure 3.4.3-5f).

3.4.3.4. STTM160 vascular bundle surface area is reduced in PMNs

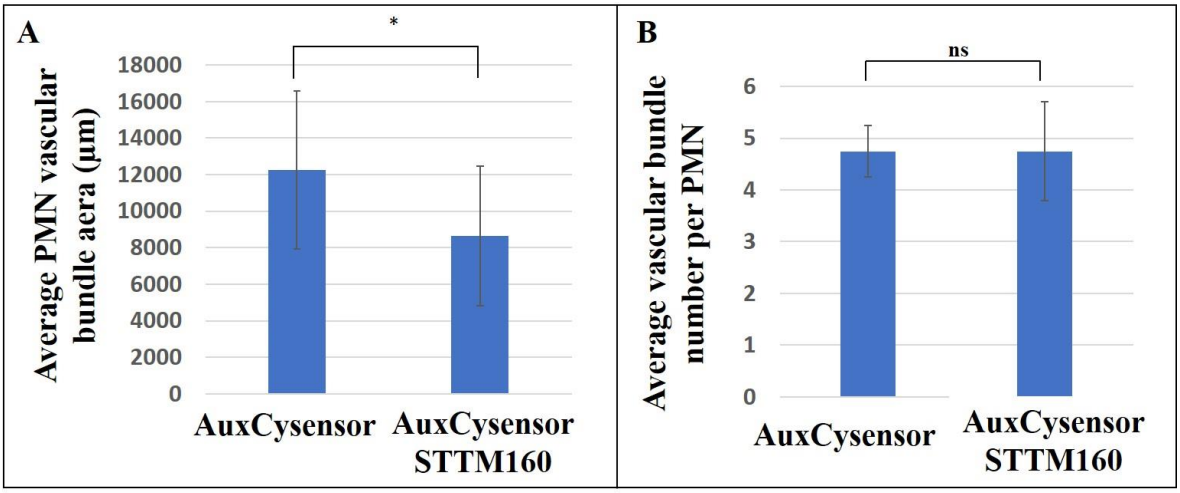

Figure 3.4.3-6: Average vascular bundle surface area and number comparison between AuxCysensor and AuxCysensor STTM160 PMNs. *(A): Average vascular bundle surface area in AuxCysensor and AuxCysensor STTM160 PMNs. (B): Average vascular bundle number per PMN in AuxCysensor and AuxCysensor STTM160 PMNs. Error bars represent standard deviation of the mean. P value of * is <0.05. ns= non-significant.*

In the STTM160 mature nodule, Nizampatnam et al 2015 hypothesized that a vasculature deficit was responsible of the nodule development delay. To address this question, PMNs vascular bundles were digitally sectioned counted and their area were calculated. It is reduced in PMNs AuxCysensor STTM160 (Figure 3.4.3-6a). The mean

area for 15 vascular bundles out of 4 independents AuxCysensor PMNs is 12243±4315µm which is significantly higher compared to 8622±3820µm, the mean of 15 vascular bundles out of 4 independent AuxCysensor STTM160 PMNs. Interestingly the number of vascular bundles per PMN was similar between AuxCysensor (4.75±0.5) and AuxCysensor STTM160 (4.75±0.9; Figure 3.4.3-6b).

3.5. Discussion

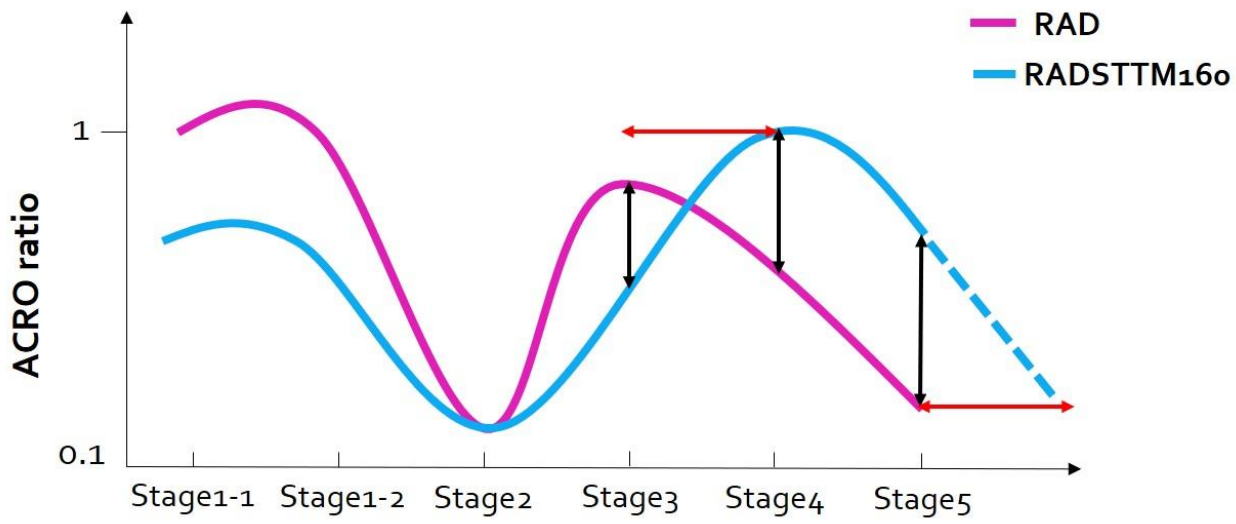

Figure 3.5-1: *Dynamic of the ACRO ratio in AuxCysensor and AuxCysensor STTM160 over different nodule developmental stages.*

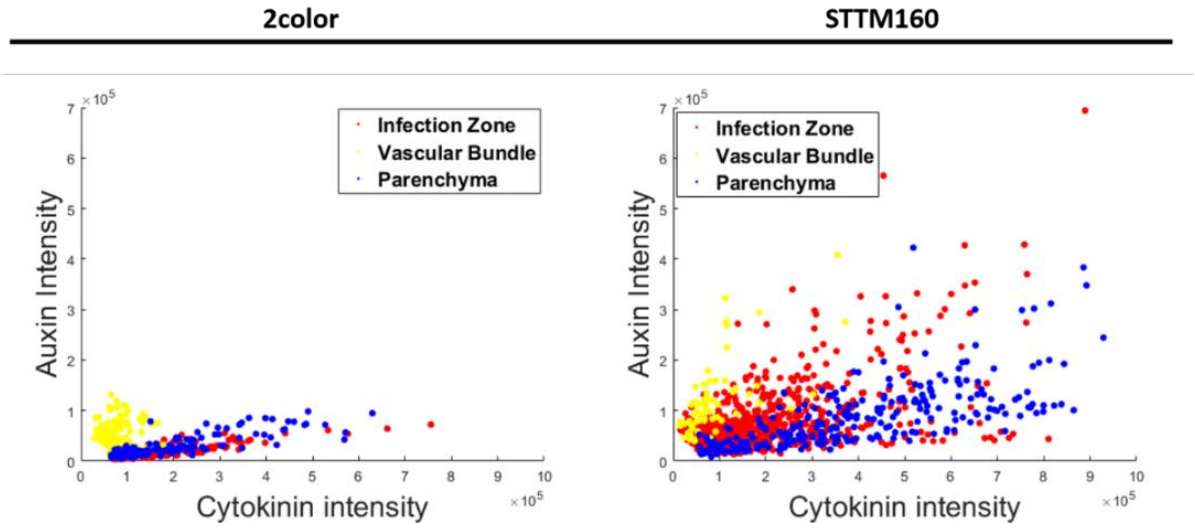

Figure 3.5-2: *Auxin and cytokinin intensity in AuxCysensor and AuxCysensor STTM160 PMNs.*

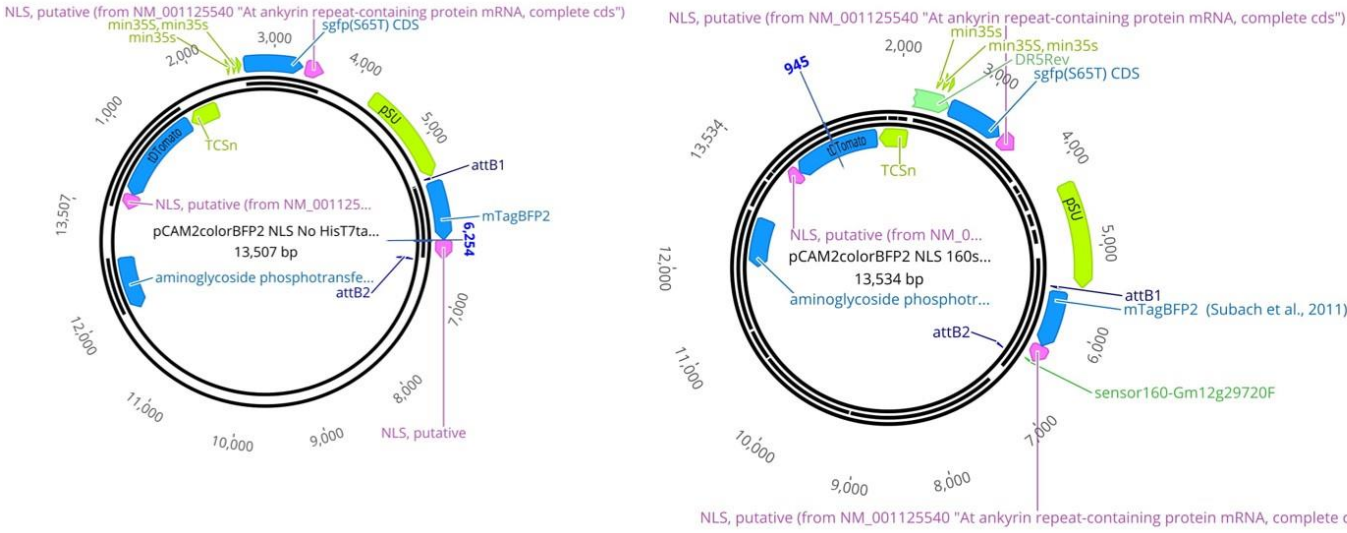

Figure 3.4.3: *AuxCysensor coupled to a fluorescent miR160 sensor. AuxCymBFP2-NLS-NOmiR160sensor in the left AuxCyBFP2-NLS-miR160sensor on the right.*

Previously, our team demonstrated that microRNA 160 controls the number and maturation of nodules via the regulation of the auxin/CK sensitivity. Here, we characterized auxin/CK ratios in individual cells of different nodule zones at different nodule developmental stages. To determine how these ratios are altered by miR160, we also evaluated these ratios in roots with reduced levels of miR160. Different cell types and nodule zones showed very specific auxin/CK ratios associated with specific stages of nodule development. At stage 1-1 and 1-2, the dividing cells have a high ACRO ratio, while the rest of the root has a lower ACRO ratio. Similarly, founder cell identity establishment during the initiation of lateral root primordia is correlated with auxin maxima (De Smet, Tetsumura et al. 2007). Such auxin accumulation is probably necessary to trigger cell division to give rise to nodule primordium initiation. Note that even though the root QC has a very high ACRO ratio, cell division is repressed by the cell cycle switch gene CCS52A2 (Vanstraelen, Baloban et al. 2009, Fisher, Gaillard et al. 2018).

At stage 2, the primordium has very low ACRO ratio, compared to the stage 1-1 and 1-2 and compared to the rest of the root. This is consistent with previous studies in *L. japonicus*, where cytokinin responses were observed during primordium initiation in the outer cortex and the third cortical cell layer (Szczyglowski, Shaw et al. 1998, van Spronsen, Grønlund et al. 2001). As observed in Figure 3.4.1-1c, stage 2 primordium are infected by rhizobia, and this coincides with low ACRO ratios. It is possible that this cytokinin accumulation might be required to produce a primordium with differentiated

cells able to host the bacteria. Moreover, cytokinin treated roots or roots presenting a high cytokinin sensitivity produce psendonodule and more initial primordia respectively (Cooper and Long 1994, Heckmann, Sandal et al. 2011, Nizampatnam, Schreier et al. 2015). Therefore, cytokinin might promote the transition of primordia from stage 1 to stage 2 and lead to successful nodulation. Indeed, cytokinin is present in the cortex after inoculation and auto-active cytokinin receptor mutants are able to produced nodule in the absence of the symbiotic bacteria (Tirichine, Sandal et al. 2007).

At the stage 3, the center of the primordium has a relatively higher ACRO ratio compared to its periphery. It is conceivable that the ACRO ratio drops associated with stage 2, might needs to be followed by a higher ACRO ratio in order to form a transient meristem responsible a providing enough cells to create a new organ. The periphery of the primordia has a relatively lower ACRO ratio. This looks similar to soybean lateral root primordia (LRP), or soybean root apical meristem for which central cells have a high ACRO ratio that triggers cell division to give rise to a new organ and/or promotes its growth. In the periphery cells of the LRP and RAM cells have a low ACRO ratio as they are entering in their differentiation program (Fisher, Gaillard et al. 2018).

Stage 4 has a similar trend as stage 3, where the highest ACRO ratio is at the center and it lowers at the periphery. At stage 4, the primordium is emerging from the root and becoming more mature. It is possible that in the central zone of stage 4 nodules, most of the cells have been produced, the meristem has stopped its activity, and the auxin enrichment is no longer present. Additionally, the overall cells require a lower ACRO

ratio in order to be differentiated and go towards nodule maturation. Thus stage 4 zones might have lower ACRO ratios compared to their respective stage 3 zones due to these combined effects. The peripheric region of the stage 4 presents a low ACRO ratio where cells have probably acquired different cell identities such as parenchyma and endodermis. Interestingly we can notice that the peripheral cells are not infected and are mostly likely acting as an oxygen barrier to favor the nitrogen fixation, while the central zone is colonized indicating that nitrogen fixation has probably started to occur. If we were to make a parallel between nodule primordium and lateral root primordium, we could say that in both cases the peripheral cells emerging from the root are associated with cytokinin enrichment and cell differentiation involved in nodule epidermis and root cap identity respectively. Note that clusters of local auxin maxima are also detected in the periphery of the stage 4. These are most likely responsible of the vasculature bundle establishment. Concomitant to the creation of a sclereid layer that insulates the infection zone from the surrounding tissues, the nodule creates a vasculature to enable exchange between the inside and the outside.

In the PMN, the different ACRO ratios are correlated with different tissue types. The central zone that has infected cells and uninfected cells showed a low ACRO ratio. The parenchyma is also cytokinin enriched but relatively lesser than the center of the nodule. Vascular bundles clearly identifiable in PMN periphery show a clearly higher auxin output (Fisher, Gaillard et al. 2018). Indeed, it has been reported that auxin is required to the creation of xylem cells present in the vascular bundles (Kondo, Tamaki et

al. 2014). Therefore, the high ACRO ratio is present in the vascular bundle to allow cell division and the creation of a vasculature surrounding the nodule.

Altogether, these data support the hypothesis made by Nizampatnam et al.; 2015 suggesting that “an initial pulse of auxin causes primordium cell division, after which auxin activity is suppressed in the nodule primordium and cytokinin activity is largely responsible for its subsequent development, and that auxin activity is relegated to nodule parenchyma, where it promotes cell differentiation, including formation of vascular bundles”.

The AuxCysensor STTM160 roots present a silenced miR160 activity and are associated with a modified auxin/CK balance and nodulation phenotypes. miR160 functions to reduce the transcript levels of the ARF10/16/17 gene family which are thought to be repressors of auxin response. In the STTM160 roots, reduced miR160 levels lead to higher levels of repressor ARF10/16/17 resulting in auxin hyposensitive roots (Nizampatnam, Schreier et al. 2015).

Unlike AuxCysensor, the diving cells of AuxCysensor STTM160 at stages 1-1 and 1-2 do not present an auxin maximum. In fact, they showed a lower ACRO ratio than the surrounding cortex cells. This is consistent with the auxin hyposensitive, cytokinin hypersensitive phenotype previously described for the STTM160 roots. Interestingly these cells are still able to divide to initiate nodule primordium which agrees with Libbenga et al., 1973 that described that both auxin and cytokinin were necessary to

trigger cell divisions in pea cortex cell explants (Libbenga, van Iren et al. 1973). Moreover, Zhang et al 2013, have also demonstrated that cytokinin can promote cell division in the root via the QC auxin transport regulation (Zhang, Swarup et al. 2013). It would be interesting to look at the rhizobia staining in AuxCysensor STTM160 at these stages to see if the infection is affected. Previous studies have reported that the root hair curling is not impacted while there is a higher number of infection thread in STTM160 roots (Nizampatnam, Schreier et al. 2015).

At stage 2, the ACRO ratio is similar in the cortical cells, but different in the overall roots cells of AuxCysensor STTM160 compared to AuxCysensor. It was unexpected as STTM160 roots have been described as auxin hyposensitive, but we have to keep in mind that this was based on whole root imaging and not cell type specific imaging (Nizampatnam, Schreier et al. 2015).

Interestingly, half of the stage 3 AuxCysensor STTM160 nodule primordium had lower ACRO ratios compared to stage 3 AuxCysensor. In these primordia where the negative ARF10/16/17 auxin regulator is favored, the primordia lack the auxin accumulation characteristic of the AuxCysensor stage 3 primordium. As previously discussed, a low ACRO ratio might be required to engage the first stage1 nodule initials into further development and maturation. Therefore, the AuxCysensor STTM160 roots being more sensitive to cytokinin, they might allow more primordium to continue their development resulting in the higher number of emerging nodules observed in STTM160 and AuxCysensor STTM160.

On the contrary, in the case of AuxCysensor, as their ACRO is higher, it is possible that a lower number of primordia transitions resulting in a higher abortion rate and a relatively lower number of emerging nodules. Interestingly, auxin treatment of the STTM160 roots was able to partially reduce the abnormal nodule number and restore the phenotype compared to the vector control (Nizampatnam, Schreier et al. 2015). This supports the role of a low ACRO ratio as a promotor of nodule organogenesis.

In stage 4 AuxCysensor STTM160 3 out of 7 primordia present a different pattern compared to stage 4 AuxCysensor primordia and 4 out of 7 look similar. It is possible that the AuxCysensor STTM160 stage 3 primordia which were initially not able to increase their auxin output levels are able to do it, but at a later stage, at the stage 4. Similarly, AuxCysensor STTM160 PMNs have a higher ACRO ratio in the infection zone and vascular bundles suggesting that these primordia haven't accomplished their maturation and are delayed compared to AuxCysensor PMNs. It seems that the delay initiated during the transition from stage 2 to stage 3 is still present at the PMN stage which could explain the overall nodule maturation delay observed in the AuxCysensor STTM160 roots (Figure 3.5-1). Here again, it would be interesting to look at the rhizobia abundance in AuxCysensor at stage 4 and PMNs to evaluate the impact of a higher ACRO ratio on the rhizobia occupation.

To better understand this phenotype, we need to closely examine the pattern of miR160 expression at the same cellular resolution. miR160 expression is downregulated in the roots upon rhizobia inoculation (Subramanian, Fu et al. 2008). This is consistent

with the low ACRO ratio observed in early nodule primordia, the low ACRO ratio observed in AuxCysensor STTM160 and associated with a higher number of emerging nodules. Moreover, miR160's level of expression is relatively low during early nodule formation and high in mature nodules. Using a fluorescence miRNA sensor revealed that miR160 is active the base of the nodule and in the nodule parenchyma of emerging nodules (stage 4) and broadly active in mature nodule. Additionally, emerging and mature STTM160 nodules show a reduction of their auxin transcriptional outputs compared to vector control (Nizampatnam, Schreier et al. 2015).

Surprisingly, AuxCysensor STTM160 present a higher ACRO ratio at the PMN stage due to an overall higher auxin intensity (Figure 3.5-2). However, mature STTM160 nodule expressing DR5rev:GUS presented a reduced auxin output in the vascular bundles (Nizampatnam, Schreier et al. 2015). This lower auxin signal observed in STTM160 nodule is most likely due to a lower vascular bundle area as measured in AuxCysensor STTM160. Moreover, in the case of DR5rev:eGFP2-NLS, the use fluorescence microscopy coupled with the nuclear localization signals on the fluorophores enables detection and quantification of cellular level of auxin outputs. This reporter strategy provides a higher response resolution than DR5:GUS nodule sections observed using a bright field under a compound microscope that only provide a qualitative description at the tissue-type level.

To have better representation of the role played by miR160's activity on the ACRO ratios we attempted to combine a sensor construct for miR160 to the

AuxCysensor (AuxCyBFP2-NLS-miR160sensor). As the AuxCysensor comprises eGFP and tdTomato, we chose a blue fluorophore to avoid spectral overlapping (Subach, Cranfill et al. 2011). In this fluorescent miR160 sensor the soybean superubiquitin promotor constitutively expresses BFP2 that is addressed to the nucleus (NLS) and fused to a miR160 binding site in the 3' UTR (Figure 3.5-3) (Parizotto, Dunoyer et al. 2004). We also created an AuxCyBFP2-NLS-miR160sensor without the miR160 binding site (AuxCyBFP2-NLS-NOmiR160sensor) (Figure 3.5-1).

AuxCyBFP2-NLS-NOmiR160sensor sensor was used to confirm proper BFP2 expression and to compare its fluorescence intensity to the AuxCyBFP2-NLS-miR160sensor. A reduction/absence of BFP2 fluorescence was expected to reveal miR160 activity in AuxCyBFP2-NLS-miR160sensor. Unfortunately, imaging of AuxCyBFP2-NLS-miR160sensor or AuxCyBFP2-NLS-NOmiR160sensor couldn't provide any signal most likely due to its high susceptibility to photobleaching (Day and Davidson 2009). Alternatively, we replaced BFP2 by mCer3, another fluorescent protein in the blue spectral range (Markwardt, Kremers et al. 2011). However, no signal was detected for this fluorophore in the nucleus, while blue cell wall autofluorescence was observed indicating functional imaging methodology. AuxCymCer3-NLS-miR160sensor and AuxCymCer3-NLS-NOmiR160sensor roots were harvested and mCer3 mRNAs and proteins will be quantified to verify accurate mCer3 expression.

The number of vascular bundles per PMN is similar between AuxCysensor STTM160 PMNs and AuxCysensor PMNs (Figure 3.4.3-6b). Hence, the vasculature

initiation didn't seem to be impacted as observed in half of the stage 4 primordia (Figure 3.4.3-3e). However, the vasculature area of AuxCysensor STTM160 PMNs is reduced compared to AuxCysensor PMNs (Figure 3.4.3-6a). This decrease is associated with an auxin enrichment. It is most likely that AuxCysensor STTM160 PMNs vasculature is in an active cell division phase and that the cell differentiation is reduced, contrary to AuxCysensor PMNs that are in a more advanced stage. Consequently, this results in a delayed maturation and a smaller vasculature area in AuxCysensor STTM160 PMNs.

The differences observed in the AuxCysensor STTM160 ratios before and after the stage 2 might come from the constitutive silencing of miR160 levels solely, and/or from a combined effect of miR160 alteration and modified bacteria colonization. To address this, AuxCysensor STTM160 inoculated with *B. diazoefficiens* GUS will be imaged at stage 1-1 to 4, to examine if the infection and colonization pattern is impacted. Moreover, AuxCysensor and AuxCysensor STTM160 PMNs will also be sectioned and stained with a fluorescent dye to quantify and compare the relative bacterial abundance.

To summarize, a higher number of nodule primordium is associated with a lower auxin/CK ratio during early primordium organogenesis, while delayed maturation is associated with a higher auxin/CK ratio. Biological Nitrogen fixation enables legumes to obtain part of their nitrogen requirement from the atmospheric dinitrogen via a symbiotic relation with diazotrophic bacteria. This association occurs in a specific organ named nodule; however, it doesn't provide enough nitrogen to meet the overall plant demand (Harper 1974). Therefore, generation of optimal yield in legume crops is also relying on

fertilizer application which is costly and can be a source of pollution. Consequently, enhancing nodule capacity to fix more nitrogen is crucial to increase the soybean production in an ecofriendly manner. This study could lead to the creation of crop producing more nodule that are fixing for a longer period.

3.6. References

Axtell, M. J. (2013). "Classification and comparison of small RNAs from plants." Annu Rev Plant Biol **64**: 137-159.

Benkova, E. and J. Hejatko (2009). "Hormone interactions at the root apical meristem." Plant Mol Biol **69**(4): 383-396.

Bensmihen, S. (2015). "Hormonal Control of Lateral Root and Nodule Development in Legumes." Plants (Basel) **4**(3): 523-547.

Boivin, S., T. Kazmierczak, M. Brault, J. Wen, P. Gamas, K. S. Mysore and F. Frugier (2016). "Different cytokinin histidine kinase receptors regulate nodule initiation as well as later nodule developmental stages in Medicago truncatula." Plant Cell Environ **39**(10): 2198-2209.

Collier, R., B. Fuchs, N. Walter, W. Kevin Lutke and C. G. Taylor (2005). "Ex vitro composite plants: an inexpensive, rapid method for root biology." Plant J **43**(3): 449-457.

Cooper, J. B. and S. R. Long (1994). "Morphogenetic Rescue of Rhizobium meliloti Nodulation Mutants by trans-Zeatin Secretion." The Plant cell **6**(2): 215-225.

Day, R. N. and M. W. Davidson (2009). "The fluorescent protein palette: tools for cellular imaging." Chem Soc Rev **38**(10): 2887-2921.

De Smet, I., T. Tetsumura, B. De Rybel, N. Frei dit Frey, L. Laplaze, I. Casimiro, R. Swarup, M. Naudts, S. Vanneste, D. Audenaert, D. Inze, M. J. Bennett and T. Beeckman (2007). "Auxin-dependent regulation of lateral root positioning in the basal meristem of Arabidopsis." Development **134**(4): 681-690.

Ferguson, B. J., A. Indrasumunar, S. Hayashi, M. H. Lin, Y. H. Lin, D. E. Reid and P. M. Gresshoff (2010). "Molecular analysis of legume nodule development and autoregulation." J Integr Plant Biol **52**(1): 61-76.

Fisher, J., P. Gaillard, C. R. Fellbaum, S. Subramanian and S. Smith (2018). "Quantitative 3D imaging of cell level auxin and cytokinin response ratios in soybean roots and nodules." Plant Cell Environ **41**(9): 2080-2092.

Gao, Y. and M. L. Kilfoil (2009). "Accurate detection and complete tracking of large populations of features in three dimensions." Opt Express **17**(6): 4685-4704.

Harper, J. E. (1974). "Soil and Symbiotic Nitrogen Requirements for Optimum Soybean Production1." Crop Science **14**(2): cropsci1974.0011183X001400020026x.

Heckmann, A. B., N. Sandal, A. S. Bek, L. H. Madsen, A. Jurkiewicz, M. W. Nielsen, L. Tirichine and J. Stougaard (2011). "Cytokinin induction of root nodule primordia in Lotus japonicus is regulated by a mechanism operating in the root cortex." Mol Plant Microbe Interact **24**(11): 1385-1395.

Hirsch, A. M., T. V. Bhuvaneswari, J. G. Torrey and T. Bisseling (1989). "Early nodulin genes are induced in alfalfa root outgrowths elicited by auxin transport inhibitors." Proceedings of the National Academy of Sciences of the United States of America **86**(4): 1244-1248.

Joshi, P. A., G. Caetano-Anollés, E. T. Graham and P. M. Gresshoff (1991). "Ontogeny and ultrastructure of spontaneous nodules in alfalfa (Medicago sativa)." Protoplasma **162**(1): 1-11.

Kondo, Y., T. Tamaki and H. Fukuda (2014). "Regulation of xylem cell fate." Front Plant Sci **5**: 315.

Laplaze, L., E. Benkova, I. Casimiro, L. Maes, S. Vanneste, R. Swarup, D. Weijers, V. Calvo, B. Parizot, M. B. Herrera-Rodriguez, R. Offringa, N. Graham, P. Doumas, J. Friml, D. Bogusz, T. Beeckman and M. Bennett (2007). "Cytokinins act directly on lateral root founder cells to inhibit root initiation." Plant Cell **19**(12): 3889-3900.

Libbenga, K. R., F. van Iren, R. J. Bogers and M. F. Schraag-Lamers (1973). "The role of hormones and gradients in the initiation of cortex proliferation and nodule formation in Pisum sativum L." Planta **114**(1): 29-39.

Livak, K. J. and T. D. Schmittgen (2001). "Analysis of relative gene expression data using real-time quantitative PCR and the 2(-Delta Delta C(T)) Method." Methods **25**(4): 402-408.

Mallory, A. C., D. P. Bartel and B. Bartel (2005). "MicroRNA-directed regulation of Arabidopsis AUXIN RESPONSE FACTOR17 is essential for proper development and modulates expression of early auxin response genes." The Plant cell **17**(5): 1360-1375.

Marin, E., V. Jouannet, A. Herz, A. S. Lokerse, D. Weijers, H. Vaucheret, L. Nussaume, M. D. Crespi and A. Maizel (2010). "miR390, Arabidopsis TAS3 tasiRNAs, and their AUXIN RESPONSE FACTOR targets define an autoregulatory network quantitatively regulating lateral root growth." Plant Cell **22**(4): 1104-1117.

Markwardt, M. L., G.-J. Kremers, C. A. Kraft, K. Ray, P. J. C. Cranfill, K. A. Wilson, R. N. Day, R. M. Wachter, M. W. Davidson and M. A. Rizzo (2011). "An improved cerulean fluorescent protein with enhanced brightness and reduced reversible photoswitching." PloS one **6**(3): e17896-e17896.

Muller, D. and O. Leyser (2011). "Auxin, cytokinin and the control of shoot branching." Ann Bot **107**(7): 1203-1212.

Nizampatnam, N. R., S. J. Schreier, S. Damodaran, S. Adhikari and S. Subramanian (2015). "microRNA160 dictates stage-specific auxin and cytokinin sensitivities and directs soybean nodule development." Plant J **84**(1): 140-153.

Oldroyd, G. E. (2013). "Speak, friend, and enter: signalling systems that promote beneficial symbiotic associations in plants." Nat Rev Microbiol **11**(4): 252-263.

Parizotto, E. A., P. Dunoyer, N. Rahm, C. Himber and O. Voinnet (2004). "In vivo investigation of the transcription, processing, endonucleolytic activity, and

functional relevance of the spatial distribution of a plant miRNA." Genes & development **18**(18): 2237-2242.

Riou-Khamlichi, C., R. Huntley, A. Jacqmard and J. A. Murray (1999). "Cytokinin activation of Arabidopsis cell division through a D-type cyclin." Science **283**(5407): 1541-1544.

Su, Y. H., Y. B. Liu and X. S. Zhang (2011). "Auxin-cytokinin interaction regulates meristem development." Mol Plant **4**(4): 616-625.

Subach, O. M., P. J. Cranfill, M. W. Davidson and V. V. Verkhusha (2011). "An enhanced monomeric blue fluorescent protein with the high chemical stability of the chromophore." PLoS One **6**(12): e28674.

Subramanian, S., Y. Fu, R. Sunkar, W. B. Barbazuk, J. K. Zhu and O. Yu (2008). "Novel and nodulation-regulated microRNAs in soybean roots." BMC Genomics **9**: 160.

Suzaki, T., M. Ito and M. Kawaguchi (2013). "Genetic basis of cytokinin and auxin functions during root nodule development." Front Plant Sci **4**: 42.

Szczyglowski, K., R. S. Shaw, J. Wopereis, S. Copeland, D. Hamburger, B. Kasiborski, F. B. Dazzo and F. J. de Bruijn (1998). "Nodule Organogenesis and Symbiotic Mutants of the Model Legume Lotus japonicus." Molecular Plant-Microbe Interactions® **11**(7): 684-697.

Takanashi, K., A. Sugiyama and K. Yazaki (2011). "Involvement of auxin distribution in root nodule development of Lotus japonicus." Planta **234**(1): 73-81.

Teale, W. D., I. A. Paponov and K. Palme (2006). "Auxin in action: signalling, transport and the control of plant growth and development." Nat Rev Mol Cell Biol **7**(11): 847-859.

Tirichine, L., N. Sandal, L. H. Madsen, S. Radutoiu, A. S. Albrektsen, S. Sato, E. Asamizu, S. Tabata and J. Stougaard (2007). "A gain-of-function mutation in a cytokinin receptor triggers spontaneous root nodule organogenesis." Science **315**(5808): 104-107.

Turner, M., N. R. Nizampatnam, M. Baron, S. Coppin, S. Damodaran, S. Adhikari, S. P. Arunachalam, O. Yu and S. Subramanian (2013). "Ectopic expression of miR160 results in auxin hypersensitivity, cytokinin hyposensitivity, and inhibition of symbiotic nodule development in soybean." Plant Physiol **162**(4): 2042-2055.

van Spronsen, P. C., M. Grønlund, C. P. Bras, H. P. Spaink and J. W. Kijne (2001). "Cell Biological Changes of Outer Cortical Root Cells in Early Determinate Nodulation." Molecular Plant-Microbe Interactions® **14**(7): 839-847.

Vanstraelen, M., M. Baloban, O. Da Ines, A. Cultrone, T. Lammens, V. Boudolf, S. C. Brown, L. De Veylder, P. Mergaert and E. Kondorosi (2009). "APC/C^{CCS52A} complexes control meristem maintenance in the Arabidopsis root." Proceedings of the National Academy of Sciences **106**(28): 11806-11811.

Wang, Y., K. Li, L. Chen, Y. Zou, H. Liu, Y. Tian, D. Li, R. Wang, F. Zhao, B. J. Ferguson, P. M. Gresshoff and X. Li (2015). "MicroRNA167-Directed Regulation

of the Auxin Response Factors GmARF8a and GmARF8b Is Required for Soybean Nodulation and Lateral Root Development." Plant physiology **168**(3): 984-999.

Zhang, W., R. Swarup, M. Bennett, G. E. Schaller and J. J. Kieber (2013). "Cytokinin induces cell division in the quiescent center of the Arabidopsis root apical meristem." Curr Biol **23**(20): 1979-1989.

CHAPTER IV

4. *In vivo* quantification of the relative auxin cytokinin ratios enabled by AuxCysensor plants. (status: manuscript in preparation[c])

4.1. Abstract

The plant hormones auxin and cytokinin control cell proliferation and differentiation to promote plant development. Organs such as shoot apical meristems (SAM), root apical meristems (RAM) or lateral root primordia (LRP) are composed of different cell types ensuring specific function. Auxin and cytokinin dictate cell identity in these organs to determine organ initiation and development. Moreover, these hormones are known to act antagonistically and/or synergistically to control and regulate several plant developmental processes such as embryogenesis and shoot/root meristem maintenance. Although auxin and cytokinin have been individually extensively studied in plants, their relative ratios in specific cell types are unknown. We developed a strategy based on

[c] Gaillard P, Nurmalasari NPD, Smith S, Subramanian S (2020) Auxin and cytokinin response ratios in soybean nodule primordium at different developmental stages (tentative).

nuclear-localized fluorescent reporters coupled with multi photon microscopy and quantitative 3-dimensional imaging to quantify *in vivo* transcriptional auxin-cytokinin relative outputs at the cellular level. The ACRO ratios estimated in Arabidopsis root tips, Medicago root tips, lateral roots tips, lateral root primordia and mature nodule in this study agreed with previously reported studies based on the individual fluorescent reporters. It indicated that the methodology is reliable and accurate. Further, we determined that specific ACRO ratios were associated with specific cell types in the different organs mentioned above. Interestingly, these specific cell type ACRO ratios also coincided with specific cell type functions (e.g. high ACRO in quiescent center associated with stem cell identity and stem cell maintenance and low ACRO ratios associated with lateral root cap and mature cell in the RAM). Additionally, we demonstrated that the Arabidopsis AuxCysensor line provide to dose-dependent response to exogenous auxin or cytokinin treatments. Finally, we used the AuxCysensor lines to illustrate instances where auxin and cytokinin might be controlling physiological processes such as stomata opening and closure and where the characterization of specific ACRO ratios might be crucial to understand these mechanisms.

4.2. Introduction

Auxin and cytokinin are two plant hormones involved in cell division and differentiation. Traditionally, these two hormones have been used in tissue culture and plant propagation where low auxin/cytokinin ratio induces shoots production and high

auxin/cytokinin triggers roots development (Skoog and Miller 1957). Distinct *in planta* auxin/cytokinin relative outputs determine shoot versus root meristematic identity. The shoot apical meristem (SAM) is the source of aboveground organs and the root apical meristem (RAM) along with lateral root primordia determine root system architecture.

The SAM is composed of different regions corresponding to the central zone (CZ), the organizing center (OC), the peripheral zone (PZ), and the rib zone (RZ) (reviewed by (Fletcher and Meyerowitz 2000, Clark 2001, Sablowski 2007)). The CZ is at the top and center of the SAM where cells divide slowly. The bottom of the CZ overlaps with the top of the OC to form a reservoir of stem cells. At the periphery of the CZ, cells have a higher cell division rate in PZ and this balance is responsible for the organ size and number. Below the CZ and the OC, the RZ supplies multipotent cells with a higher cell division rate that generate a stem that support the SAM. The SAM size and structure result from the balance between cell division and differentiation. High levels of cytokinin in the OC are well known to the maintain stem cell identity in the SAM (Riou-Khamlichi, Huntley et al. 1999, Kurakawa, Ueda et al. 2007) and consistently, the cytokinin reporter Two-Component-Output-Sensor: Green Fluorescent Protein (TCS:GFP) is expressed in OC cells (Yoshida, Mandel et al. 2011).

On the other hand, the auxin peak associated with organ initiation and visualized by DR5:3xVENUS-N7 is detected in the leaf primordia (Heisler, Ohno et al. 2005). Therefore, the distribution of these two hormones coincides with different regions that are clearly separated and have different functions within the SAM. However, this

apparent dichotomy must be nuanced as auxin and cytokinin also act synergistically in the OC where auxin is enhancing cytokinin sensitivity.

A perception sensor degraded in the presence of auxin also reports auxin maxima at the primordial tips from which new lateral organ are initiated (Vernoux, Brunoud et al. 2011). It has been accepted that auxin patterning dictates primordia position. Young primordia act as auxin sinks and deplete auxin accumulation within surrounding cells. The new primordia are initiated by auxin maxima created via the action of auxin transporters and are located in the periphery of the SAM, well away from preexisting primordia.

Like the SAM, the RAM possesses different regions involved in cell division and differentiation. The OC of the SAM has its equivalent in the RAM, the quiescent center (QC), a stem cell niche surrounded by cells having a low mitotic rate near the root tip (reviewed by (Benkova and Hejatko 2009, Stahl and Simon 2010)). There is also a proximal meristem where cells are dividing to continuously produce cells and ensure root growth. As cells progress along the proximo-distal axis, cells lower their division rate, start to elongate once they enter the elongation zone (EZ) and differentiate in the differentiation zone (DZ). Note that the proximal meristem zone and the elongation zone are separated by the transition zone (TZ) which is crucial for proper cell division and differentiation.

An auxin maximum is observed in the QC and it gradually decreases towards the TZ. It is responsible for the QC cell identity and maintenance of mitotic activity in the proximal meristem. Cytokinin accumulates in the TZ and induces cell differentiation. Interestingly, cytokinin regulates auxin transport while auxin negatively regulates cytokinin signaling and biosynthesis in plant roots. It creates two mutually inhibitory domains of actions required to create a balance between cell division and differentiation and control to root growth.

Lateral roots are initiated along the longitudinal axis of the root from the RAM to the elongation zone depending on the plant species (Ilina, Kiryushkin et al. 2018). During this process, auxin accumulation can also be observed in at the opposite of a protoxylem pole in root pericycle (De Smet, Tetsumura et al. 2007). This often results in the "priming" of lateral root cells founders. Once initiated, cell division associated with high auxin levels is observed to promote primordia formation and its emergence. Cytokinin negatively regulates root primordium initiation in inhibiting lateral root founder cell priming. However, cytokinin activity is detectable at the base of the lateral root primordia and later in the vasculature, columella and root cap of emerging lateral root (Dobisova, Hrdinova et al. 2017).

To summarize, even though SAM and RAM have very similar function and rely on specific hormonal requirements, the role of auxin and cytokinin in RAM and SAM are apparently reversed. The OC in the SAM is associated with high cytokinin accumulation while the QC of the RAM presents an auxin maximum. Similarly, cell differentiation

requires auxin in the periphery of the SAM, while cytokinin is responsible root cell identity. Additionally, auxin and cytokinin can regulate each other's level and activity to control cell identity and specific auxin/CK ratios are responsible of specific developmental programs. Consequently, there is an urge to concomitantly characterize the activity of these hormones involved in every aspects of plant development.

To the best of our knowledge, 4 teams have independently developed sensors to qualitatively report auxin and cytokinin levels over the last 4 years (Pernisová, Klíma et al. 2009, Muller, Larsson et al. 2017, Nadzieja, Stougaard et al. 2019, Smet, Sevilem et al. 2019). This represents interesting advancements in the understanding of the role played by auxin and cytokinin, however their balance has never been quantified. Here, we provide an advanced tool to calculate *in vivo* and cellular Auxin-cytokinin relative output (ACRO) ratios using transcriptional output sensors named "AuxCysensor".

The primary focus of our lab is to understand hormonal control of nodule development during the legume-rhizobia symbiosis. Nodules are specialized plant organs commonly produced by legumes through rhizobia symbiosis. Legumes derive a major portion of their nitrogen through symbiotic nitrogen fixation in nodules. Nodules are divided into two main categories:(i) determinate (presence of a transient meristem) or (ii) indeterminate (presence of a persistent and apical meristem) respectively (Ferguson, Indrasumunar et al. 2010). Auxin and cytokinin regulate multiple aspects of the legume-rhizobia interaction including nodule initiation and development, but how they interact

during this process is still unclear. Hence, we generated AuxCysensor roots to understand these dynamics.

We previously reported that distinct ACRO ratios corresponded to distinct nodule cell types in soybean (*Glycine max*) that produces determinate nodules (Fisher, Gaillard et al. 2018). We presently studied barrel clover (*Medicago truncatula*) indeterminate nodule to investigate if its different nodule cell types were also associated with specific ACRO ratios. Moreover, AuxCysensor *Arabidopsis thaliana* homozygote lines were created upon the request of the scientific community. Arabidopsis has been extensively used to study plant developmental due to its rapid seeds to seeds cycle, small genome and large mutant bank as reviewed by (Koornneef and Meinke 2010). Moreover, its anatomy is composed of few cell layers making it a perfect tool for *in situ* imaging.

In this article, we present the AuxCysensor strategy applied to multiple Arabidopsis organs and Medicago root tips, primordia and nodules. The auxin/CK ratios reported agreed with previous studies and enabled a cell specific characterization of auxin and cytokinin relative sensitivity providing new insights in the study of plant development.

4.3. Material and methods

4.3.1. Plasmid construct

BAR resistance gene was PCR amplified from pBAR-Tnos vector, cloned into pCR8/GW/TOPO and recombined with the binary destination vector AuxCysensor containing DR5:GFP-NLS, TCSn:tdTomato-NLS, and pSubi:GW (Fisher, Gaillard et al. 2018).

4.3.2. Plant transformation

AuxCysensor *Arabidopsis thaliana* stable lines were generated after transformation of the ecotype Columbia-O with the AuxCysensor plasmid (Fisher, Gaillard et al. 2018) carrying the *bar* gene conferring resistance to the herbicide bialaphos. Arabidopsis transformation was done using the floral dip method as described by (Clough and Bent 1998). A17 *Medicago truncatula* transgenic composite plant were generated using the same method as proposed by Collier at al., 2005 for soybean. Medicago seeds were scarified with sandpaper, both *Arabidopsis thaliana* and *Medicago truncatula* seeds were surface-sterilized with 70% ethanol for 2minutes, placed in ½ Murashige and Skoog plates (Caisson Laboratories) with 1% sucrose and 0.8% agar and stratified for 2 days at 4°C in the dark. *Arabidopsis thaliana* containing plates were vertically placed at 21°C for 5 days with 16 hours days 8 hours night and Medicago plates left horizontally in the dark for 4 days. Medicago seedlings were place in pots with Sunshine mix soil and placed at 21°C with 16 hours days 8 hours night. Four weeks after transformation, Medicago plants were screened for the presence of tdTomato epifluorescence at the root tip. Medicago composite plants were planted into 4″ pots

containing sterilized 3:1 vermiculite: perlite mix and watered with nitrogen free plant nutrient solution (N− PNS).

4.3.3. Hormone and rhizobia treatments

Responses to exogenous hormones were evaluated by treatment with 1-Naphthaleneacetic acid (NAA, a synthetic form of auxin) and 6-Benzylaminopurine (BAP, a synthetic form of cytokinin). Five-day-old seedlings were transferred to new media containing either no addition or one of the following treatments: 10nM NAA (1-Naphthaleneacetic acid), 100nM NAA, 1µM NAA, 10µM NAA, 100µM NAA, 10nM BAP (6-Benzylaminopurine), 100nM BAP or 1µM BAP for 24 hours then imaged. Concentrated stock solutions of 10 mM of these additives were dissolved in ethanol (NAA), or water (BAP) and added to agar medium cooled to 50°C. Seven days after transfer, each plant was inoculated with 25ml of *Sinorhizobium meliloti* cells resuspended in N− PNS to OD_{600nm} of 0.15.

4.3.4. Sample preparation and microscopic acquisition

Twenty-four hours after treatment, Arabidopsis AuxCysensor lines were collected for imaging. For imaging Medicago nodules, plants were carefully removed from pots two or three weeks after inoculation and placed in petri dishes containing distilled water prior nodule sectioning. Mature Medicago nodules were sectioned longitudinally (Figure

4.4.7-1a) or transversally (Figure 4.4.7-1b) prior to imaging. Due to very high autofluorescence in the infection zone, detection parameters were individually optimized for each image. Biological samples were 3D imaged with multiphoton microscope as described in Fisher et al., 2018 to report eGFP2 and tdTomato presence along with light imaging.

4.3.5. Image analysis

For the detection methodology refer to Chapter III "Image post-processing".

Auxin to cytokinin ratio was analyzed based on specific regions of interest (ROIs). For cylindrical ROI, Auxin to Cytokinin ratio was measured radially (a disk ROI) or integrated over a distance from the tip of the meristem (a pipe ROI). Radius (r) is calculated using the equation above, while distance (D) from the root tip to meristem is calculated using the equation below. x_1, y_1, z_1 are the center of the cylinder on the root tip/top cylinder, x_2, y_2, z_2 are the center of the cylinder on the bottom, and x,y,z are the centroid of nuclei inside the cylinder.

$$D = \frac{(x - x_1)(x_2 - x_1) + (y - y_1)(y_2 - y_1) + (z - z_1)(z_2 - z_1)}{\sqrt{(x_2 - x_1)^2 + (y_2 - y_1)^2 + (z_2 - z_1)^2}}$$

For an annular or donut ROI, 2 concentric cylinders with different radii were chosen, the nuclei in the donut were measured by subtracting nuclei found using a smaller

cylinder with those found in the larger cylinder. Raw images were overlapped with the detected nuclei by LMDM and rendered in 3D by Arivis Vision 4D to optimize the parameters.

4.3.5.1. Medicago analysis

Medicago lateral root tip (LRT) and primary root tip (PRT) were analyzed by using parameters with a mask of 7x7x9 voxels validated based on manually inspecting the raw images and nuclei detected in 3D renderings. The ROI for Medicago LRT and PRT were three cylinders with a radius of 15µm; from the tip, meristem and vasculature. The cylinders were defined by connecting four coordinates that define the center four circles which when connected create the three cylindrical ROI's. The middle slice of the image will show a rectangular slice of the ROI's. The average of auxin to cytokinin ratio 3 to 5 PRT and LRT was determined by normalizing each root by scaling the QC to the same size. ROI for Medicago stage VI vs emerged lateral root tip (LRP) was one cylinder with radius 15µm, this can be created by defining two points of the center for the top and base circle caps of the cylinder. The average of auxin to cytokinin ratio for LRP was calculated by overlapping all auxin to cytokinin ratio over distance. All segmented nuclei in PRT, LRT and LRP were characterized as a function of distance from the root apex along the drawn vector. Images of Medicago LRT, PRT and LRP were quite clear and no-autofluorescence is observed in these ROIs; the LMDM was detecting the nuclei with high accuracy.

Medicago longitudinal nodule and Medicago nodule sections had very high intensity not only on the nuclei but also in the cytoplasm which lead to false positives. For Medicago longitudinal nodules, we compared 2 ROIs in the infection zone at the center and meristem at the apex, we detected the nuclei separately based on ROIs and adjusted the intensity threshold to eliminate false positives but at the same time detect all nuclei. The ROIs were cylinders defined by elongating a circle by 15 µm for meristem and 40 µm for infection zone, in either direction along the z-axis, in this case, the radius of the cylinder is varied base on ROI size. For Medicago nodule section the ROIs for infection zone and vascular bundles are cylinders with a height of 15 µm. Each image for Medicago longitudinal nodule and Medicago nodule section was adjusted and validated manually. The drawback of this routine was that were not able to distinguish nuclei from background fluorescence above the intensity threshold.

4.3.5.2. Arabidopsis analysis

The parameters used to detect Arabidopsis roots were a mask with size 7x7x9 voxels, minimum separation diameter/2 and 50,000 intensity threshold. The goal was to calculate auxin to cytokinin ratio in columella, lateral cap, QC, epidermis and vasculature. We used cylindrical ROIs in columella, QC, and vasculature. Donut shape ROIs were used for lateral cap and epidermis. The donut shape ROI was created by drawing two cylinders at the same center with different radii, the nuclei in the donut shape were acquired by subtracting nuclei in the smaller radius cylinder from those in the larger radius cylinder.

The primary output of the LMDM are auxin to cytokinin ratio which plots at different concentrations. In addition, the number of nuclei is detected from 4-6 roots at certain concentrations are also compared.

Auxin cytokinin ratio was mapped and compared statistically at different stages of nodule development. In this analysis, violin plots were generated using GraphPad Prism version 8 which shows the frequency distribution of data and plot lines at the median and quartiles. (Unpaired t) test and one-way ANNOVA (Tukey test) were used to measure statistical analysis of two groups and more than two groups of data respectively. P-value higher than 0.05 means the value is not significant (ns), P value less than or equal to ≤0.05, ≤0.01, ≤0.001 and ≤0.0001 mean significant difference which correspond to *, **, ***, and **** respectively.

4.4. Results

4.4.1. Arabidopsis AuxCysensor pattern in different organs display the typical auxin and CK pattern

Patterns of auxin and cytokinin transcriptional outputs in RAM and SAM of intact Arabidopsis AuxCysensor lines were evaluated using intravital multiphoton imaging. Cytokinin output was detected in the RZ which is associated with meristematic activity (Figure 4.4.1-1a). Additionally, cytokinin output was also present in the OC and the overlap between OC and CZ, where SAM stem cells are located (Figure 4.4.1-1a). Auxin outputs was detected in the CZ where it is involved in maintaining stem cell homeostasis

(Figure 4.4.1-1a). Moreover, auxin output was also reported in the peripheric zone, peaked at initiation site of leaf primordium and young leaf primordia (Figure 4.4.1-1a). In the RAM cytokinin outputs were primarily associated with the root cap where cells are differentiated (Figure 4.4.1-1b).

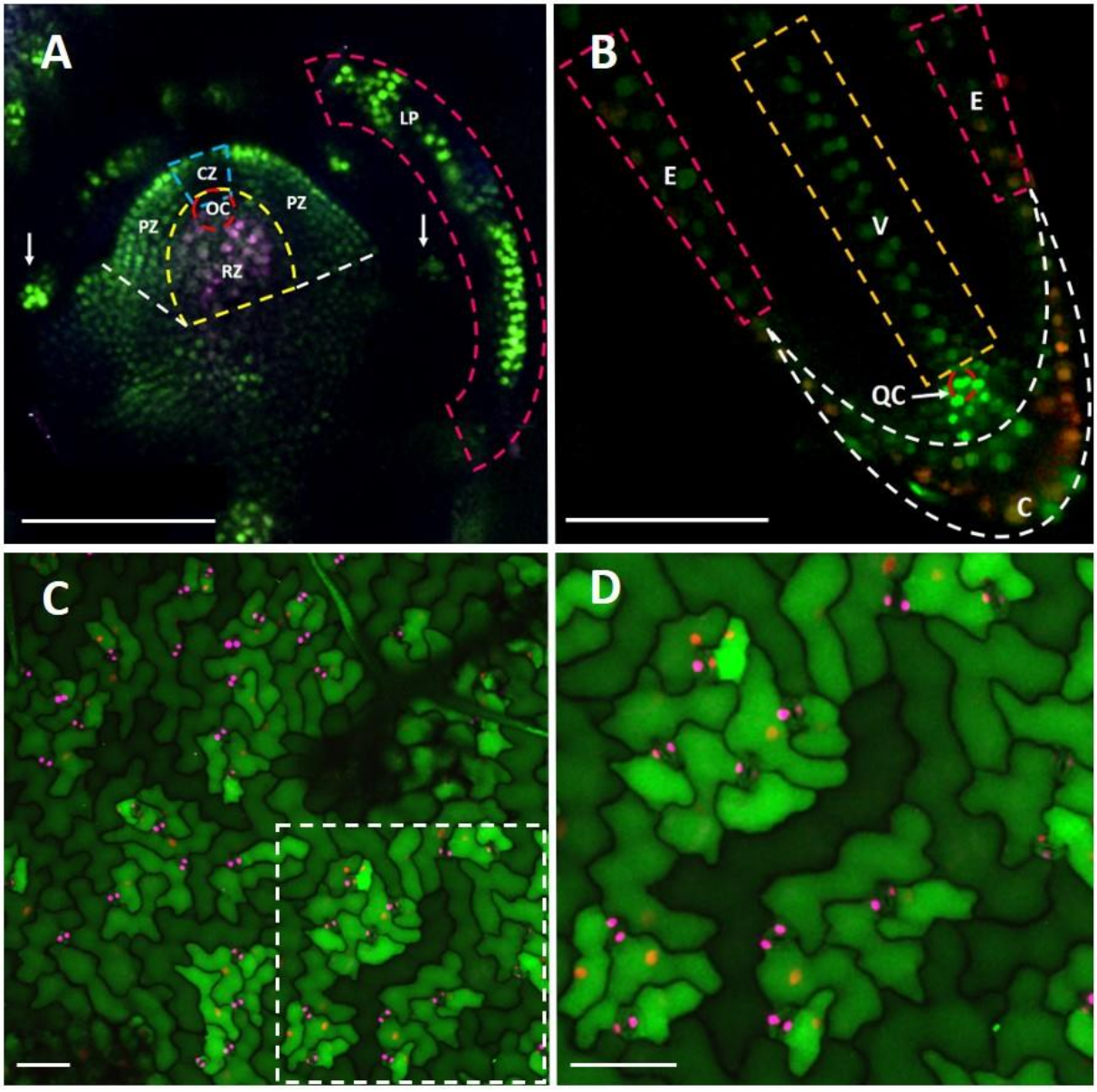

Figure 4.4.1-1: AuxCysensor in different organs of Arabidopsis thaliana. *(A): Shoot apical meristem, blue dashed area indicates the central zone (CZ), red dashed circle indicates the organization center (OC), yellow dashed area indicates the rib zone (RZ), white dashed lines indicate the peripheral zone (PZ), white arrows indicate young leaf primordia and pink dashed area indicates the lateral primordium (LP). (B): Root apical meristem, red dashed circle contains the quiescent center (QC), orange dashed area contains proximal meristem and the vasculature (V), white dashed shape delimits the root cap (C) and pink dashed areas contain the epidermis (E). (C): Top view of leave epidermis. (D): close-up of dashed area in (C). (A): magenta represents tdTomato and green DR5ev (B): red represents tdTomato and green DR5ev. (C and D) magenta represents tdTomato, red DR5ev and green autofluorescence in the blue spectra. Scale bar: 100µm for (A and B) and 50µm for (C and D).*

Auxin outputs climaxed in the quiescent center where stem cells are located (Figure 4.4.1-1b). Furthermore, auxin outputs were present in the epidermal and the vasculature cells (Figure 4.4.1-1b). Interestingly both auxin and cytokinin outputs were spatially distinct in RAM and SAM and did not visually overlap.

Patterns of auxin and cytokinin transcriptional outputs in RAM and SAM of intact Arabidopsis AuxCysensor lines were evaluated using intravital multiphoton imaging. Cytokinin output was detected in the RZ which is associated with meristematic activity (Figure 4.4.1-1a). Additionally, cytokinin output was also present in the OC and the overlap between OC and CZ, where SAM stem cells are located (Figure 4.4.1-1a). Auxin

outputs was detected in the CZ where it is involved in maintaining stem cell homeostasis (Figure 4.4.1-1a). Moreover, auxin output was also reported in the peripheric zone, peaked at initiation site of leaf primordium and young leaf primordia (Figure 4.4.1-1a). In the RAM cytokinin outputs were primarily associated with the root cap where cells are differentiated (Figure 4.4.1-1b). Auxin outputs climaxed in the quiescent center where stem cells are located (Figure 4.4.1-1b). Furthermore, auxin outputs were present in the epidermal and the vasculature cells (Figure 4.4.1-1b). Interestingly both auxin and cytokinin outputs were spatially distinct in RAM and SAM and did not visually overlap.

Leaf epidermis was imaged to provide an example of this technology applied to an organ where auxin and cytokinin pattern are still unclear. Autofluorescence in the blue spectra was false-colored in green and used to visualize cell morphology and determine cell identity (Figure 4.4.1-1c and 4.4.1-1d). The magenta color coding for cytokinin outputs was associated with guard cells and the red auxin signal to leaf epidermis (Figure 4.4.1-1c and 4.4.1-1d). Here is a concrete case where the AuxCysensor strategy could be used to study auxin and cytokinin regulation of a physiological process such as stomatal opening and closure for which their roles are uncertain.

4.4.2. Arabidopsis AuxCysensor shows a dose-dependent response to exogenous hormone treatments

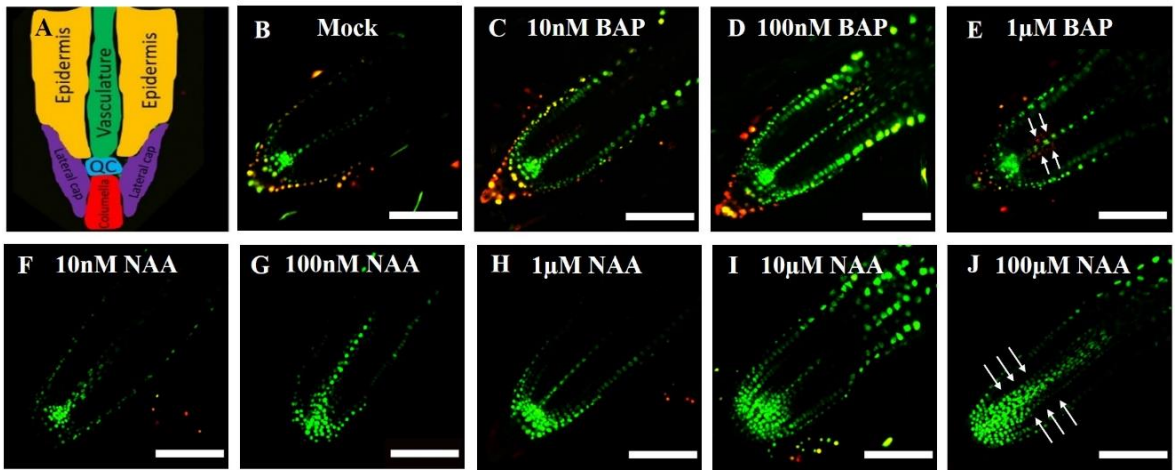

Figure 4.4.2-1: ACRO responses in the AuxCysensor lines treated with exogenous auxin or cytokinin. *(A): representation of the different root tissue types including the epidermis, the vasculature, the quiescent center (QC), the lateral root cap and the columella. (B to J): Representative images of the AuxCysensor roots with mock, 10nM BAP, 100nM BAP, 1µM of BAP, 10nM NAA, 100nM NAA, 1µM of NAA, 10µM of NAA or 100µM of NAA treatment respectively. For each categories 3 to 8 roots were imaged. White arrows represent peripheric vasculature in E. Scale bar is 100µm.*

To evaluate the sensitivity of the AuxCysensor to report auxin and cytokinin transcriptionnal outputs, we applied a range of exogenous auxin and cytokinin treatments (10nM BAP, 100nM BAP, 1µM of BAP, 10nM NAA, 100nM NAA, 1µM of NAA, 10µM of NAA or 100µM of NAA). The responses to the diverse treatments were qualitatively compared in the different root tissue types corresponding to the epidermis, the vasculature, the quiescent center (QC), the lateral root cap and the columella (Figure 4.4.2-1a).

Roots treated with 10nM BAP and 100nM BAP had a higher cytokinin output signal in the root cap compared to mock treated roots (Figure 4.4.2-1b to 4.4.2-1d). 1µM BAP-treated roots did not present the root cap ctyokinin enrichment but showed an abnormal cytokinin output in cell files bordeing the vasculature (Figure 4.4.2-1e). The BAP treatment did not induce drastic differences for the auxin output reports as the cell types reporting auxin acivity were the same among the different treatments (primarly QC, epidermis and 1-2 central cell files of the vasculature) (Figure 4.4.2-1b to 4.4.2-1e).

NAA treatment did not visually induce cytokinin outputs, but the auxin reporter was presenting a dose-dependent response. In mock treated roots the strongest auxin reponse was observed in the QC and this response was present in additional cell types as the hormonal concentrations were increased. After the 10nM NAA treatment, the auxin response was observed in the QC and also the proximal mreristem and the columella. In 100nM NAA treated roots, the response was present in the QC, surronding cells, and also observed in several layers of cortical, endodermal, epidermal, lateral root cap and columella initials cells (Figure 4.4.2-1g). The response at 1µM of NAA was present in the same cells types as in the 100nM NAA treated roots (Figure 4.4.2-1g) and was extended to 3-4 additionnal cell layers (Figure 4.4.2-1h). After a tratement of 10µM of NAA, most of the diving cells presented an auxin response in the proximal meristematic cells and all initial cells (Figure 4.4.2-1i). 100µM NAA treated roots showed an auxin output response in every cell types except some cell that were most likely cortical and endodermal cells as inidcated by the white arrows in Figure 4.4.2-1j.

Based on these qualitative observations, the AuxCysensor line seemed to specifically respond to diverse hormone concentrations. After 10nM BAP or 100nM BAP teatments, AuxCysensor lines reported additionnal cytokinin transcriptionnal outputs in the lateral root cap. Similarly, 1µM BAP treatment elicited a cytokinin transcriptionnal outputs in the vasculature, but none of the BAP treatments induced an auxin transcriptionnal output compared to the mock treatment. After NAA treatments the overall auxin transcriptionnal outputs were induced in a dose-dependent maner, but the cytokinin transcriptionnal outputs were similar to the mock treatment.

4.4.3. Arabidopsis AuxCysensor a tool to quantify auxin-cytokinin relative output (ACRO) and perceive hormone sensitivity

AuxCysensor line not only gives the ability to visualize concomitant presence of auxin and cytokinin transcriptional outputs, it also provides the opportunity to quantify these. To further charaterize the AuxCysensor reponsivness to different auxin or cytokinin treatments, the relative intensity of the auxin and cytokinin transcriptionnal output reporters were measured and compared. The roots imaged were divided into different regions of interests (ROIs)

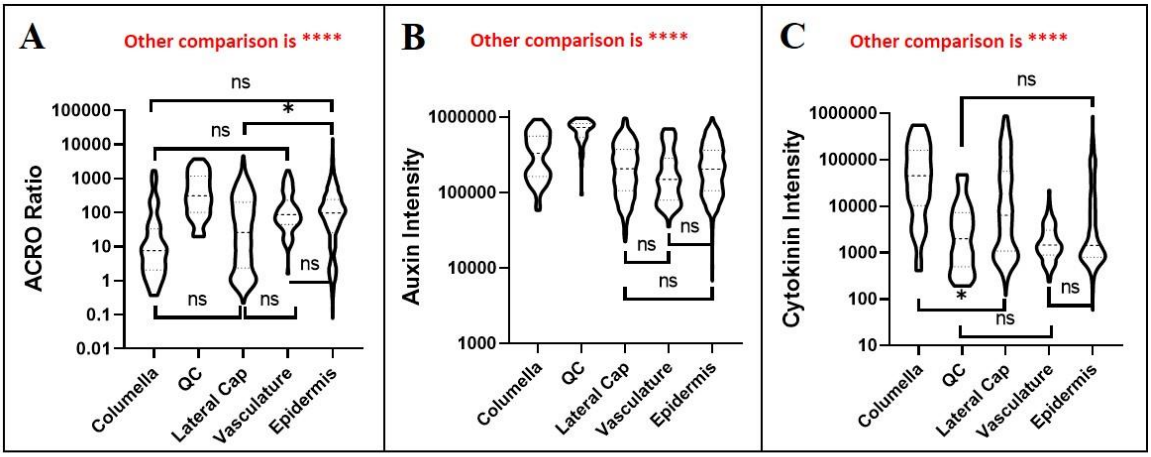

Figure 4.4.3-1: Comparison of the average ACROs ratio between different cell types in the AuxCysensor. *(A): average ACRO ratio comparison between the 5 different cell types considered. (B and C): intensity detected in the different RAM tissues types of auxin and cytokinin respectively. Statistical analysis using one way-ANOVA with multiple comparison using Tukey test with confidence level 0.05. Non-significant differences are illustrated by ns, absence of ns indicates a significative difference at a P value of <= 0.0001.*

corresponding to the different cell types indicated in Figure 4.4.2-1a. We calculated the ACROs in the root columella, the lateral root cap, the QC, the vascular tissue (4 cell files going from the proximal meristem to the elongation zone), and epidermis comprising the remaining peripheral vasculature, the pericycle, the endodermis, the cortex and the epidermis (Figure 4.4.3-1a).

In the AuxCysensor line roots, all the ACROs cell types were significantly different between each other. The lowest average ACROs ratios was present in the columella (88.8±31.4) and in the lateral root cap (186.2±14.5), two tissue types associated with cytokinin activity (Figure 4.4.3-1b). In the epidermis (269±16.8) and the vasculature (228±35.1) the average ACRO ratios were intermediate, while in the QC, a cell type reported to have the highest auxin accumulation, the average ACRO ratio was high (730±108; Figure 4.4.3-1b).

As ACRO ratios result from average auxin and cytokinin outputs, auxin and cytokinin output intensities were separately analyzed. This enabled to determine if the specificities observed among the different cell types were the effect of changes in the output of either hormone individually, or a combined effect. Concerning the columella, it had the lowest average ACRO ratio, even though its auxin intensity (368653±27758) was significantly higher compared to the lateral root cap, vasculature and epidermis (259357±6550, 218665±19519 and 260186±4178 respectively) and was significantly lower than the QC (678888±23868; Figure 4.4.3-1c). Indeed cytokinin intensity in the columella (105424±16654) was primarily responsible of this high ACRO ratio as it was significantly higher than in the QC, the lateral root cap, the vasculature and the epidermis (6862±1428, 70903±5142, 2457±320 and 23701±1543 respectively; Figure 4.4.3-1d).

Concerning the QC its high ACRO ratio was principally the results of a specific auxin accumulation. QC had the highest auxin intensity (678888±23868), compared to columella, lateral root cap, vasculature and epidermis (368653±27758, 259357±6550,

218665±19519 and 260186±4178 respectively; Figure 4.4.3-1c). In addition, QC's cytokinin intensity (6862±1428) was statistically similar to the vasculature and the epidermis (2457±320 and 23701±1543 respectively). QC's cytokinin intensity (6862±1428) was significantly higher than the lateral root cap (70903±5142) and significantly lower than the columella that was standing out (105424±16654; Figure 4.4.3-1d).

The lateral root cap auxin intensity (259357±6550) was statistically similar to vasculature and epidermis (218665±19519 and 260186±4178 respectively) and lower than columella and QC that had the highest values (368653±27758 and 678888±23868 respectively; Figure 4.4.3-1c). Concerning the cytokinin intensity in the lateral root cap (70903±5142), it was significantly lower than the columella (105424±16654), but significantly higher than QC, vasculature and epidermis (6862±1428, 2457±321 and 23701±1543 respectively; Figure4.4.3-1d). Consequently, the cytokinin accumulation in lateral root cap was primarily responsible of its relatively low ACRO ratio.

Even though vasculature and epidermis had different average ACRO ratios, their auxin and cytokinin intensities were statistically similar. Auxin intensities in the vasculature (218665±19519) and the epidermis (260186±4178) were similar to the lateral root cap (259357±6550) but significantly lower compared to the columella and the vasculature (368653±27758 and 678888±23868 respectively; Figure 4.4.3-1c). The cytokinin intensities of the vasculature (2457±321) and the epidermis (23701±1543) were statistically similar between themselves and with the QC (6862±1428) and significantly

lower than the columella (105424±16654) and the lateral root cap (70903±5142; Figure 4.4.3-1d). Therefore, the relative cytokinin abundance explained why average ACRO ratios in the vasculature and the epidermis were higher compared to lateral root cap.

To summarize, low ACRO ratio in lateral root cap was due to a relatively high relative cytokinin intensity, high ACRO ratio in the QC was caused by a relatively high auxin intensity. Between these two extremes, vasculature and epidermis are quite similar between each other but diverge from lateral root cap as the latter has a higher cytokinin intensity. The effect of exogenous hormone treatments was then quantified in these different cell types to assess their sensitivity.

4.4.4. Cell-type response of the AuxCysensor after auxin or cytokinin treatments

Transcriptional outputs within the different AuxCysensor root cell types treated with 10nM NAA, 100µM NAA, 10nM BAP or 1µM BAP were selected to assess the specificity of their sensitiveness. The average ACRO ratios in columella cells after treatment were not significantly different compared to mock treated columella cells. They were relatively low and comprised between 12.6±4.7 and 158±46 (Figure 4.4.4-1a).

In the lateral root cap, the average ACRO ratios were significantly higher after NAA treatment with 291±17.6 and 348±18 at 10nM and 10µM respectively and significantly lower after BAP treatment with 87.4±5.4 and 129±12 at 10nM and 1µM respectively when compared to mock treated roots (186.2±14.5; Figure 4.4.4-1b). Even

though we observed a dose dependent response in the case of NAA treatment, BAP treatments were not significatively different from each other in the lateral root cap.

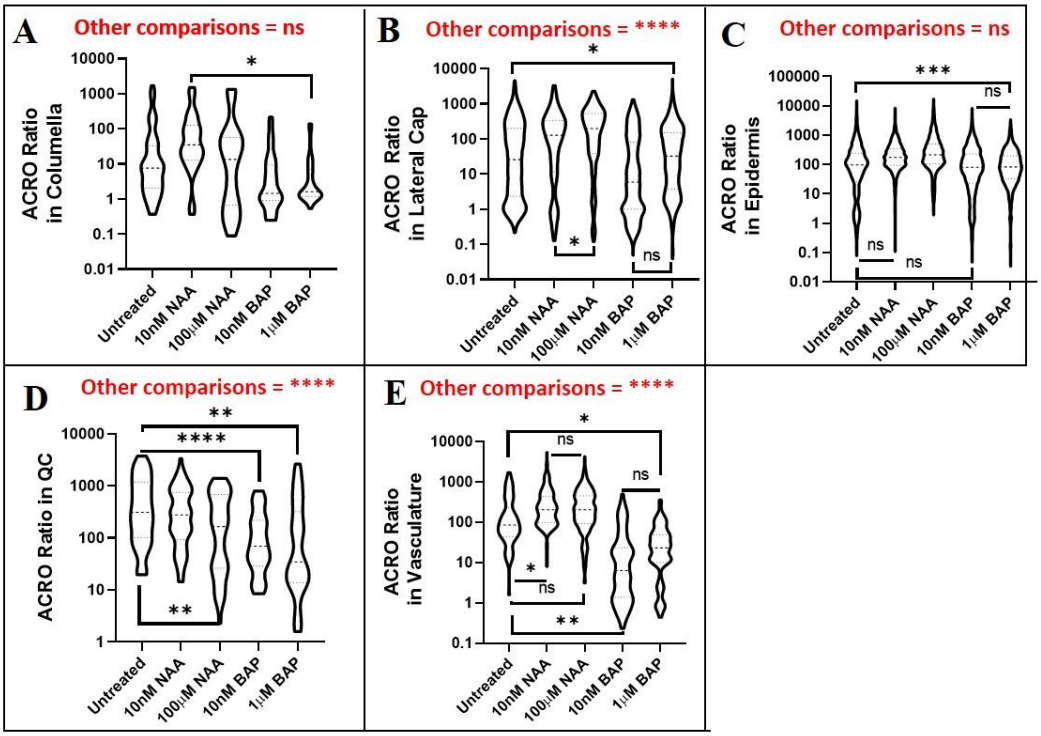

Figure 4.4.4-1: ACRO ratios in the different cell types of the AuxCysensor lines after different treatments with auxin, or cytokinin. *(A to E): comparison of the average ACRO ratio in the columella, lateral root cap, epidermis, QC and vasculature respectively. Roots were mock treated or treated with 10nM BAP, 1µM of BAP, 10nM NAA or 100µM of NAA. Statistical analysis using one way-ANOVA with multiple comparison using Tukey test with confidence level 0.05. P value of * is <0.05, ** is <= 0.01, *** is <= 0.001 and **** is <= 0.0001, ns corresponds to non-significant.*

In the epidermis, only the highest treatment concentrations significantly modified the ACRO ratios. Indeed, the average ACRO ratio in mock treated root (269±16.8) was similar to 10nM NAA (310±9.6) and 10nM BAP (215±8.8) treated roots, but 100µMNAA had a higher (551.1±21.3) and 1µM BAP a lower (168±5.8) average ACRO ratio compared to mock treated roots (Figure 4.4.4-1c).

Concerning the QC, the average ACRO ratio in the mock treated roots (730±108) was very high and statistically similar to the 10nM NAA treatment (472±59.4), and surprisingly 100µM NAA treated roots had a lower average ACRO ratio in the QC (340±53; Figure 4.4.4-1d). There was a response after BAP treatment as the average ACRO ratio in 10nM BAP treated roots (166±33.4) was significantly lower compared to mock treated roots (730±108). Moreover, average ACRO ratio at 1µM BAP (309±76.5) was significantly higher compared to 10nM BAP (166±33.4) and significantly lower compared mock treated root (730±108; Figure 4.4.4-1d).

Vasculature of 10nM NAA treated roots (370±41.1) had a significantly higher average ACRO ratio compared to mock treated roots (238±35.1) and 100µM NAA treated roots (343±19.3) are statistically similar to 10nM NAA treated roots (370±59.4) and mock treated roots (288±35.1; Figure 4.4.4-1e). On the other hand, 10nM BAP and 1µM BAP treated roots (34.7±5.4 and 40.9±5.8 respectively) had significantly lower average ACRO ratios than mock treated roots (Figure 4.4.4-1e). Furthermore, exogenous auxin treatment triggered auxin responses in additional cells of the vasculature.

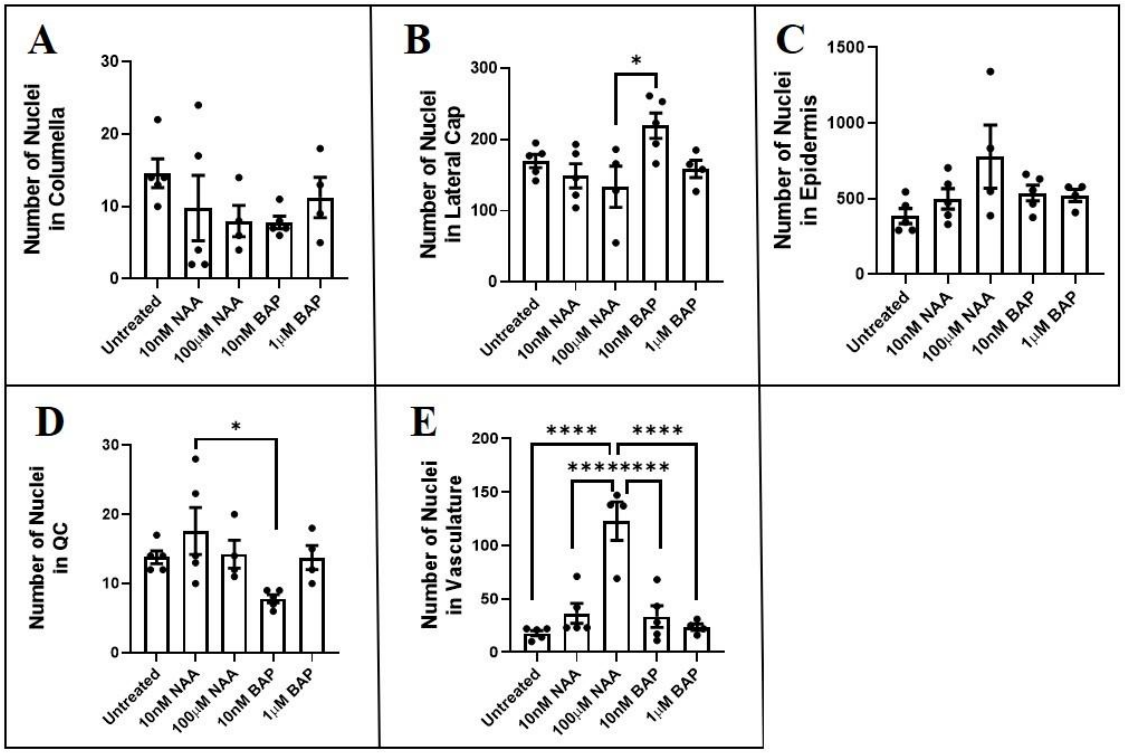

Figure 4.4.4-2: Number of nuclei showing a response to auxin and/or cytokinin in AuxCysensor roots. *(A to E): Comparison of the number of nuclei detected between mock, 10nM BAP, 1µM of BAP, 10nM NAA and 100µM of NAA treated AuxCysensor roots in the columella, lateral root cap, epidermis, QC and vasculature respectively. Bars represent mean of the average number of nuclei, line is the standard error and dots are the absolute value. Statistical analysis using one way-ANOVA with multiple comparison using Tukey test with confidence level 0.05. P value of * is <0.05 and **** is <= 0.0001.*

Even though the average ACRO ratio in the vasculature of 100µM NAA treated roots was like mock treated roots, it had significantly more nuclei detected (123±18) compared to the mock treated roots (18±2.5; Figure 4.4.4-2e). This suggests that 100µM

NAA treatment was able to trigger an auxin transcriptional response in additional cells. No other differences were observed for the number of nuclei detected within a specific cell type after a NAA or BAP treatments compared to the mock treated roots.

There were more nuclei detected in the QC region after a 10nM NAA treatment compared to a 10nM BAP treatment (Figure 4.4.4-2d) and in the lateral root cap, after a 10nM BAP treatment compared to a 100µM NAA treatment (Figure 4.4.4-2b). Therefore, exogenous hormonal treatments appear to induce or repress transcriptional outputs already active in specific cells, and also expand the tissue domain of response.

4.4.5. AuxCysensor applied to Medicago truncatula primary root tip

Our laboratory being interested in the hormonal regulation of nodule development, we also created AuxCysensor roots in the plant model *Medicago truncatula*. AuxCysensor primary root tips were imaged to assess the reliability of this methodology in Medicago transgenic roots and compare the expression patterns to soybean transgenic roots. ACRO ratios were quantified in three tissues types similarly to previous soybean study (Fisher et al, 2018).

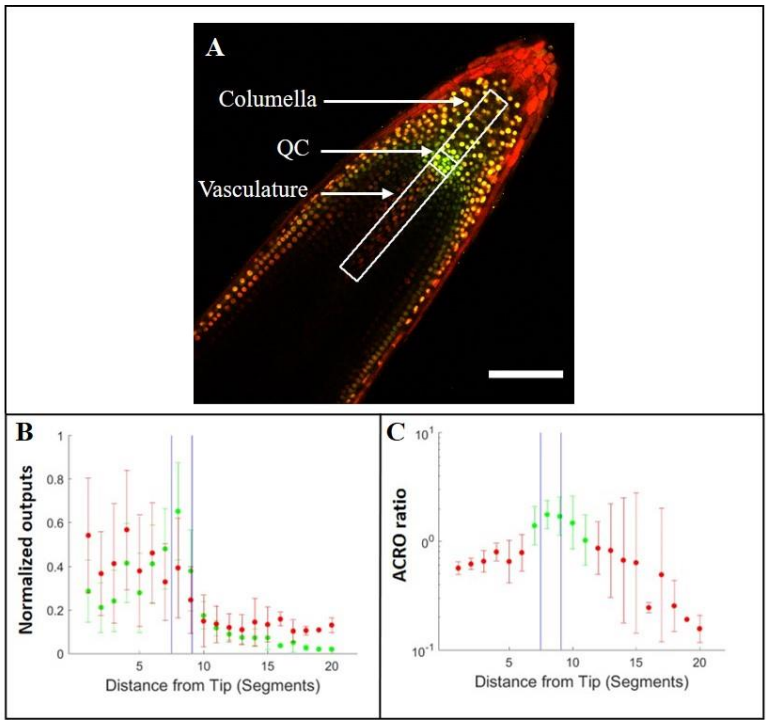

Figure 4.4.5-1: Quantification of auxin and CK outputs and average ACRO ratios along the central root axis of AuxCysensor primary root tip. *(A): Representative image of a primary root tip, white rectangles correspond to tissue specific ROIs root columella, QC and vasculature. Vertical blue lines indicate the boundaries of root cap columella, QC, and proximal meristem. (B): Average auxin and CK outputs and (C): ACRO ratios obtained from four independent transgenic roots (n=4). Auxin and CK outputs and ACRO ratios in nuclei from 20 normalized segments (≈31µm each) in each root along the root axis were determined and averaged. Segments along the root axis for each root were normalized by scaling the QCs to the same size. Scale bar at 100µm.*

Cytokinin outputs were visible in the columella, lateral root cap and the epidermis, while auxin outputs were apparent in the QC, the initials and epidermal cells

(Figure 4.4.5-1a). ACROs ratio of four independent roots were quantified, normalized by scaling the QCs to the same size and plotted as a function of distance from the tip (Figure 4.4.5-1b and 4.4.5-1c). The columella had an ACRO ratio below 1 and the lowest was present at the tip. The closer the columella cells were to the QC, the higher were their ACRO ratios (Figure 4.4.5-1c). As observed in soybean, QC cells had higher ACRO ratios compared to columella and had relatively higher auxin output vs. cytokinin output (Figure 4.4.5-1b and 4.4.5-1c). In the transition between QC and vasculature, cells had a high ACRO ratio that rapidly and gradually decreased toward a negative ACRO ratio (Figure 4.4.5-1c). To assess ACRO ratios in root lateral organs of Medicago, AuxCysensor lateral root tips and nodules were imaged.

4.4.6. AuxCysensor applied to Medicago truncatula lateral root tip and primordia

Primary root tips and lateral root tips had similar cell tissue types. Hence, similar ROIs were selected in lateral root tips including the columella, the QC and the vasculature (Figure 4.4.6-1a). Primary root tips and lateral root tips had similar cell tissue types. Hence, similar ROIs were selected in lateral root tips including the columella, the QC and the vasculature (Figure 4.4.6-1a). The pattern reported in the case of Medicago AuxCysensor lateral root tip (Figure 4.4.6-1a and 4.4.6-1c) was similar in Medicago AuxCysensor primary root tip (Figure 4.4.6-1a and 4.4.4-6c).

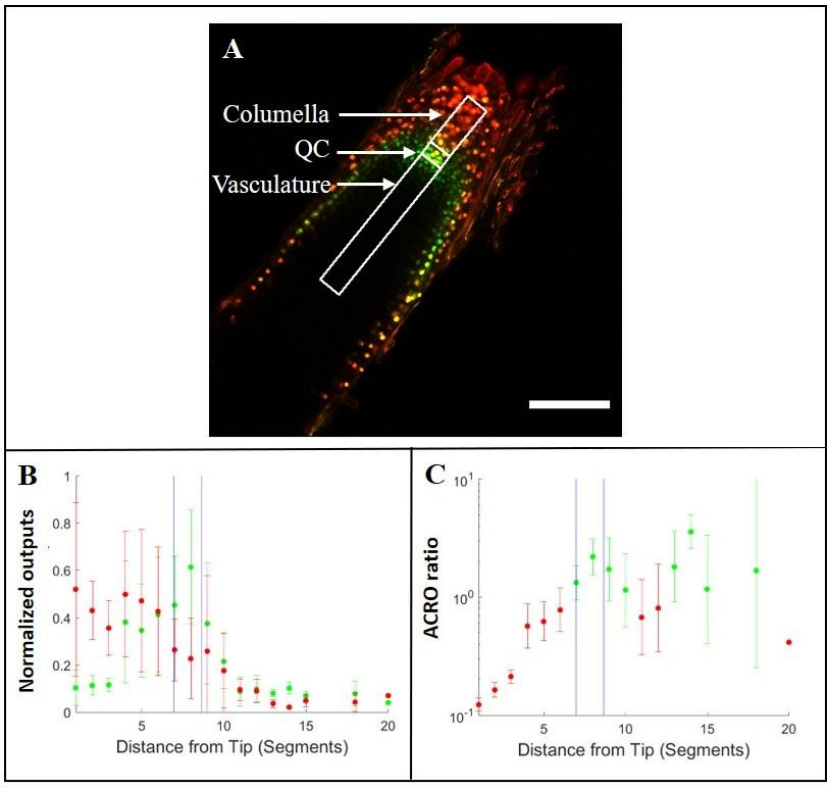

Figure 4.4.6-1: Quantification of auxin and CK outputs and ACRO ratios along the central root axis of AuxCysensor lateral root tips. *(A): Representative image of lateral root, white rectangles correspond to tissue specific ROIs, root columella, QC and vasculature. Vertical blue lines indicate the boundaries of root cap columella, QC, and proximal meristem. (B): Average auxin and CK outputs and (C): ACRO ratios obtained from three independent transgenic roots (n=3). Auxin and CK outputs and ACRO ratios in nuclei from 20 normalized segments (≈17µm each) in each root along the root axis were determined and averaged. Segments along the root axis for each root were normalized by scaling the QCs to the same size. Scale bar at 100µm.*

Meaning average ACRO ratios below 1 in the columella, a gradual transition from the root tip to the QC in which average ACRO ratios become higher than 1 and plateaued at the transition from QC to vasculature and a decrease of the average ratios (Figure 4.4.6-1c). Primary root being more thick than lateral, additional cell types might be present within similar ROIs volume. It resulted in variation of the ACRO ratios present in the columella and vasculature. Indeed, average columella ACRO ratio goes from 0.56±0.07 to 1.46±0.19 and from 0.12±0.01 to 0.78±0.27 in the primary and lateral root tip respectively. Additionally, vasculature ACRO ratios goes from 0.89±0.26 to 0.16±0.04 and from 1.80±0.89 to 0.41± 0.00 in the primary and lateral root tip respectively. To further investigate on the ACRO ratios and cell types sensitiveness in Medicago AuxCysensor, lateral roots primordia were imaged at two different developmental stages.

Lateral root primordia (LRP) emergence is associated with a specific cytokinin enrichment in newly root cap cells in soybean (Fisher et al 2018). Here, we evaluated two lateral root primordia developmental stages in Medicago to assess if similar hormonal specifications were present. At stage V, LRPs had reached the epidermis and were about to breached from the primary root (Herrbach, Remblière et al. 2014). They were primarily showing an auxin-related signal (Figure 4.4.6-2a). Interestingly, stage VI lateral roots primordia that had just breached the epidermal cells, the signal was mostly related to auxin and the exception of the nascent root vasculature were a red signal was present and the root cap cells presenting both hormonal outputs (Figure 4.4.6-2b).

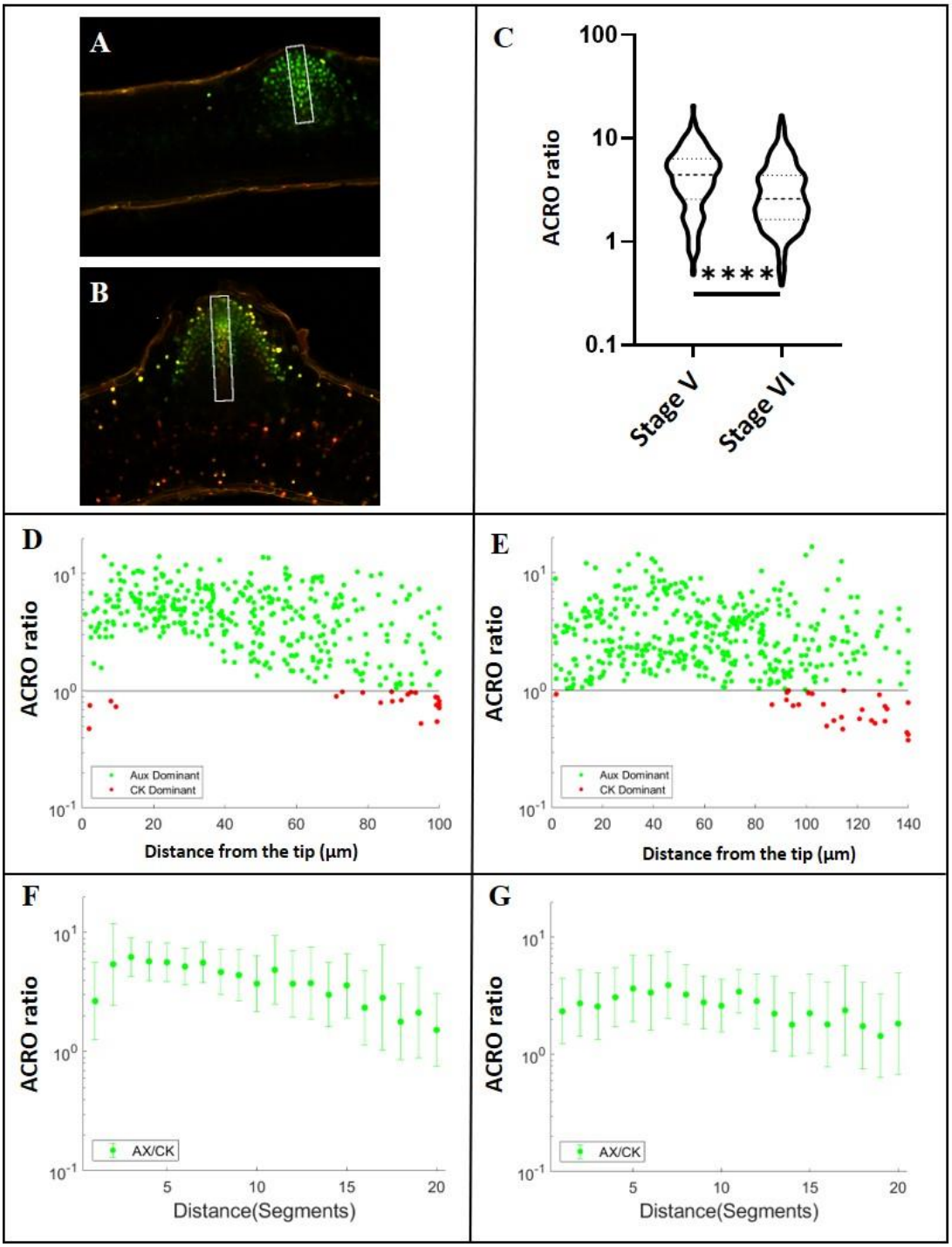
A
B
C
100
10
1
0.1
ACRO ratio
****
Stage V
Stage VI
D
ACRO ratio
Aux Dominant
CK Dominant
Distance from the tip (µm)
E
ACRO ratio
Aux Dominant
CK Dominant
Distance from the tip (µm)
F
ACRO ratio
AX/CK
Distance(Segments)
G
ACRO ratio
AX/CK
Distance(Segments)

Figure 4.4.6-2: ACRO ratios in stage V and stage VI AuxCysensor lateral root primordia. *(A): Representative image of stage V lateral root primordia (B): Representative image of stage VI lateral root primordia. (A and B): white rectangles correspond to ROIs drawn along the central axis of lateral root primordia. (C): Average ACRO ratio in stage V compared to stage VI lateral root primordia. (D and E): ACRO ratios in each nucleus plotted as a function of distance from the tip of the lateral root primordia in stage V and VI lateral root primordia respectively. Each dot represents a nucleus. (F and G): Average ACRO ratios obtained from four independent transgenic roots (n=4) in stage V and stage VI lateral root primordia respectively by adding all the auxin to cytokinin ratio over distance. ACRO ratios in nuclei from 20 normalized segments (≈5µm for stage V and 7µm for stage VI) in each root along the lateral root axis were determined and averaged. Statistical analysis using method similar to Figure 4.4.4-2. P value of * is <0.05, ** is <= 0.01, *** is <= 0.001 and **** is <= 0.0001, ns means non-significant. Scale bar at 100µm.*

Average ACRO ratios along the central lateral root primordia axis is higher (4.8±0.15) in stage V primordia than in stage VI ones (3.4±0.12; Figure 4.4.6-2c). Regarding the distribution of the ACRO ratio along that central axis, the majority of the nuclei had ACRO ratios higher than 1 at both stages (Figure 4.4.6-2d and 4.4.6-2e). Few nuclei were presenting ACRO ratios below 1 in the primordia tip, none is the meristematic zone, and some more in the vasculature in both stage VI and stage V lateral root primordia (Figure 4.4.6-2d and 4.4.6-2e). Average ACRO ratio declined from the tip

of the lateral root primordia toward the vasculature at both stages (Figure 4.4.6-2f and 4.4.6-2g). Note that stage VI lateral root primordia were not significantly cytokinin-enriched in the root cap or the vasculature contrary to soybean ones (Figure 4.4.6-2g; Fisher at al 2018). Medicago nodules were also imaged to determine if their different cell types were presenting specific ACRO signature.

4.4.7. AuxCysensor applied to sectioned Medicago truncatula root nodules

Medicago is the model plant for indeterminate nodule development studies. Here, AuxCysensor Medicago nodules were sectioned longitudinally (Figure 4.4.7-1a) or transversally (Figure 4.4.7-1b) and imaged. Longitudinal sections present a visible and active meristem at the nodule apex, that is followed by an infection and differentiation zone constituted of few cell layers only (Figure 4.4.7-1a and 4.4.7-1b). The infection zones of longitudinal sections occupy most of the nodule and a senescent zone is present before the nodule connects to the root (Figure 4.4.7-1a and 4.4.7-1c). Transversal sections were effectuated in the center of the nodule and are composed of the infection zone at the center and circular vascular bundles in the periphery (Figure 4.4.7-1b and 4.4.7-1d). The average ACRO ratio in the meristem (16.7±1.3) is significantly higher than in the related infection zone (0.8±0.02±; Figure 4.4.7-1e) and the average ACRO ratio in the vascular bundles (4.8±0.5) is significantly higher than in the related infection zone (0.9±0.03±; Figure 4.4.7-1f).

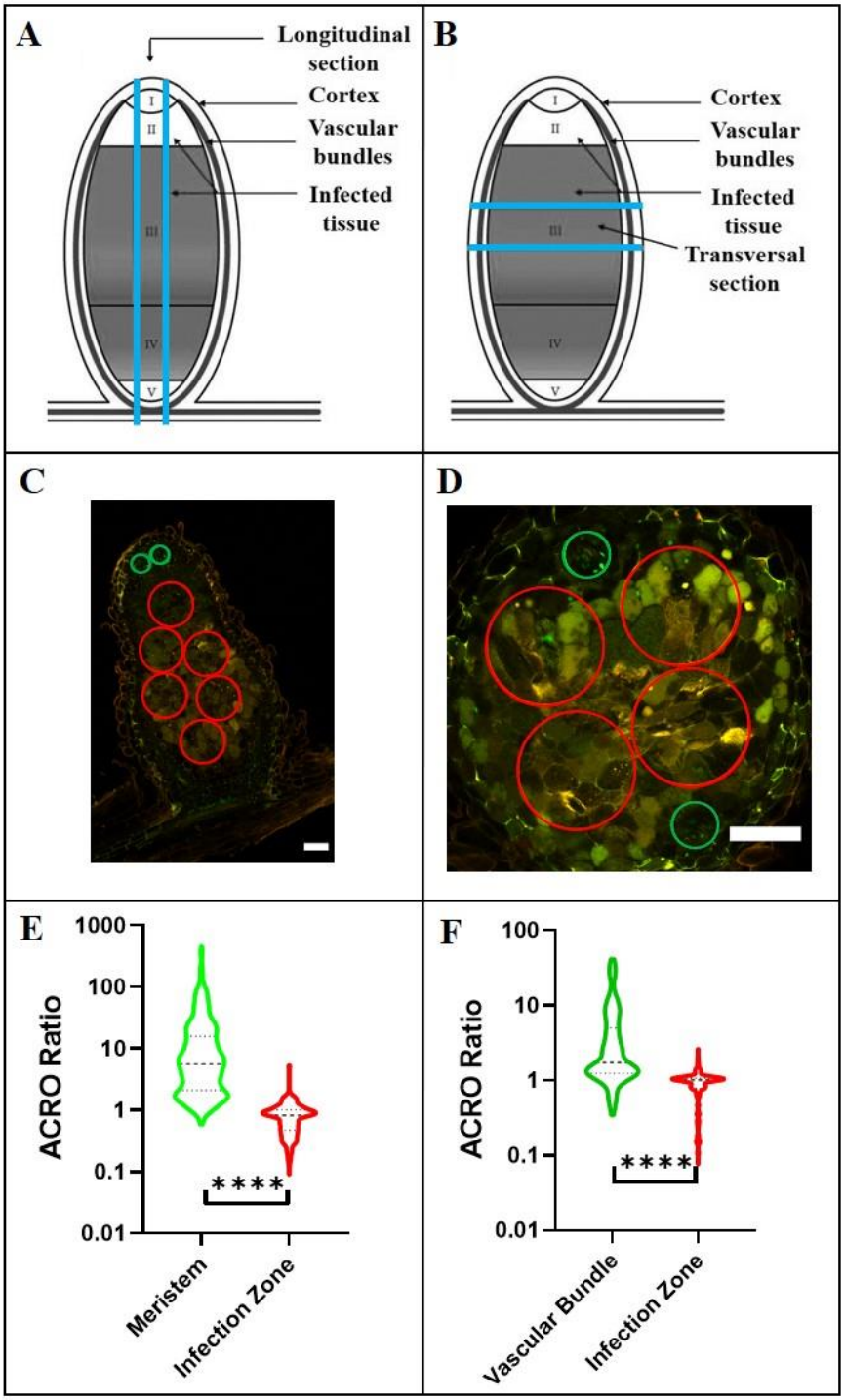
A
Longitudinal section
Cortex
Vascular bundles
Infected tissue
I
II
III
IV
V
B
Cortex
Vascular bundles
Infected tissue
Transversal section
C
D
E
ACRO Ratio
1000
100
10
1
0.1
0.01
****
Meristem
Infection Zone
F
ACRO Ratio
100
10
1
0.1
0.01
****
Vascular Bundle
Infection Zone

Figure 4.4.7-1: ACRO ratios in AuxCysensor Medicago nodules. *(A and B): schematic representation of indeterminate nodule comprising five different tissues zones, adapted from Dupont et al. 2012. I: apical meristem, II: infection and differentiation zone, III: fixation zone, IV: senescent zone and V: saprophytic zone. Nodule present a cortical cell layer, vascular bundles and central infected tissues. Blue line indicates the section made longitudinally (A) or transversally (B). (C and D:) Imaging of auxin (green dots), cytokinin (red dots) in longitudinal and transversal cross section respectively. Green circles represent ROIs containing the meristem and the vascular bundle in C and D respectively. Red circles represent ROIs corresponding to the infection zone (C and D). (E): average ACRO ratios comparison between the root nodule apical meristem and the infection zone of AuxCysensor nodule longitudinally sectioned. (F): average ACRO ratios comparison between the root nodule vascular bundle and the infection zone of AuxCysensor nodule transversally sectioned. Statistical analysis using one way-ANOVA with multiple comparison using unpaired t test with confidence level 0.05. P value of * is <0.05, ** is <= 0.01, *** is <= 0.001 and **** is <= 0.0001, ns means non-significant. Scale bar at 100µm.*

4.5. Discussion

Here we present AuxCysensor *Arabidopsis thaliana*, a line able to report auxin-CK relative outputs. This strategy has already been successfully used in soybean transgenic root of composite plants (Fisher, Gaillard et al. 2018). In that study we showed

that auxin and cytokinin patterns in soybean primary root tips and lateral root primordia agreed with previous studies underscoring the usefulness of AuxCysensor construct to monitor cell level auxin-cytokinin outputs. Moreover, we showed that relative quantification of auxin and cytokinin output was accurate and cell specific in these organs and in soybean pre-mature root nodule.

In the present article, we report auxin and cytokinin patterns in the SAM and RAM of Arabidopsis AuxCysensor lines. As expected, cytokinin outputs were detected in the RZ (Figure 4.4.1-1a) a tissue associated with meristematic activity and cellular division (Barton 2010). High cytokinin outputs were also detected in the OC and the overlap between OC and CZ (Figure 4.4.1-1a), where high cytokinin has been reported to maintain stem cells identity (Kurakawa, Ueda et al. 2007). Transcriptional auxin activity was detected in the peripheral zone (Figure 4.4.1-1a), where its accumulation is required to initiate new primordia, and in the CZ (Figure 4.4.1-1a) to ensure stem cell homeostasis (Yoshida, Mandel et al. 2011, Adibi, Yoshida et al. 2016). Additionally, high auxin outputs were also reported in the leaf primordium (Figure 4.4.1-1a) even though its role in regulating leaf dorsoventrality is still controversial (Bhatia, Åhl et al. 2019). Here we imaged the transcriptional output of auxin in relation to cytokinin to report their relative patterns and abundance and provide new insights of these.

In the RAM auxin outputs culminate in the quiescent center where auxin is responsible for maintaining stem cell identity (Figure 4.4.1-1b). Auxin was also located in the proximal meristem (Figure 4.4.1-1b) where it acts to promote cell division (Lewis,

Negi et al. 2011). In the primary root tip, cytokinin can be detected in the lateral root cap and in the columella (Figure 4.4.1-1b) where it is associated with cell maturation and differentiation (Dobisova, Hrdinova et al. 2017). Imaging of the AuxCysensor reporter in the RAM and SAM agreed with literatures studies and is therefore a reliable tool to investigate concomitant auxin and cytokinin activity in these contexts. Moreover, auxin and cytokinin transcriptional outputs were spatially distinct in RAM and SAM and did not visually overlap. This agrees with their functions described as antagonistic toward each other, reviewed by (Su, Liu et al. 2011). Furthermore, the hormone tissue-specific prevalence indicates the crucial role played by auxin and cytokinin to control cell identity in an exclusive and opposite manner.

The sensitivity of the AuxCysensor reporter line was then tested via exogenous auxin and cytokinin treatments at different concentrations. Cytokinin treatments induced a cytokinin response in the lateral root cap except at 1µM of BAP where it was observed in lateral vascular cells (Figure 4.4.2-1b to 4.4.2-1e). Regulatory mechanisms might be involved in the repression of the cytokinin reposnse in lateral root cap after the 1µM of BAP treatment to maintain cellular homeostasis. Additionnaly, it seems that vascular cells might be responsive to high cytokinin concentrations in the vasculature. It appears that AuxCysensor is responding to increased cytokinin concentration and can be a tool to estimate the state of cytokinin activity *in situ*. Similar observation was made after auxin treatment. The AuxCysensor reported a dose-dependent response to the various NAA

concentrations applied. Indeed, the more NAA concentrations were applied, the more cells were responding, until most of the root tip presented an auxin transcriptional output.

In mock treated roots, the auxin output was primarly observed in the QC (Figure 4.4.2-1a). After the 10nM NAA treatment, the auxin output was broadened and comprised the QC and surrondings cells (Figure 4.4.2-1e). In 100nM NAA treated roots, the response was present in the QC, surrounding cells, and in several layers of cortical, endodermal, epidermal, lateral root cap and columella initials cells (Figure 4.4.2-1f). Auxin response at 1µM of NAA was observed in similar cells types as in the 100nM NAA treated roots (Figure 4.4.2-1f) but in a broader number of cells (Figure 4.4.2-1g). After a tratement of 10µM of NAA, majority of the cells present in the proximal meristematic cells and all initial cells were reporting an auxin related signal (Figure 4.4.2-1h). After a 100µM of NAA treatement, the overal root showed a positive auxin output signal except some cortical and endodermal cells (Figure 4.4.2-1i). It is possible that cortical and endodermal cells have a very low sensitivity to auxin and might not be able to reponsd to the 100µM of NAA treatement which is beyond physiological concentrations. Note that treatements were exogenous and that these tissue types might have a different accessibilities resulting in different outputs but not sensnitivity.

Overall, the AuxCysensor provided a positive response to cytokinin treatments and a dose-dependent response to auxin treatments. Consequently, AuxCysensor lines could be used to classify different cell types according to their sensitivity to auxin or

cytokinin treatments. ACRO ratios were then quantified to further investigate the auxin/CK specificities from cell type to cell type and their responsiveness specificities.

Auxin and cytokinin are involved in most of the plant growth and developmental processes and the abundance of one hormone over the other usually dictates specific developmental programs. They often interact in complex ways and although they have been independently described, their relative ratios are currently ignored. Therefore, we quantified the average ACRO ratios within different root cell types to identify specific ACRO ratios profiles. When compared to each other, the cell types present in the root tip (columella, lateral root cap, QC, the vascular tissue and epidermis) felt into three main categories according to their average ACRO ratios (Figure 4.4.3-1a and 4.4.3-1b).

The first group was composed of the columella and lateral root cap that had the lowest ACRO ratios. The cells composing these tissues are predominantly mature and a high cytokinin transcriptional activity was expected in agreement with cytokinin's role in cell differentiation (Figure 4.4.3-1b). Vasculature and the epidermis have been reported to show a slight response using auxin transcriptional output reporter (Lewis, Negi et al. 2011). Just as expected, vasculature and the epidermis were part of the second group and had medium average ACRO ratio. The QC represented the third category with a high ACRO ratio, a cell type where the auxin transcriptional outputs maxima had been reported multiples times (Ge, Peer et al. 2010, Lewis, Negi et al. 2011, Hayashi, Nakamura et al. 2014). Individual auxin and cytokinin outputs (intensity) were also

analyzed to understand if the respective ACRO ratios were the result of one hormone over the other or both effects combined.

It appears that the hormone predominantly driving the cell function is also driving the ACRO ratio. In the case of the lateral root cap, the low average ACRO ratio was due to a high cytokinin intensity and not to a low auxin intensity (Figure 4.4.3-1c and 4.4.3-1d). This is consistent as root cap functions as a protective layer of mature cells and cytokinin is involved in cell differentiation. High average ACRO ratio in the QC was caused by a high auxin intensity and not a low cytokinin intensity (Figure 4.4.3-1c and 4.4.3-1d). This also agrees with auxin's role in high concentration in the root which is to maintain and ensure stem cell identity, reviewed by (Stahl and Simon 2010). Between these two extremes, vasculature and epidermis are quite similar between each other but diverge from lateral root cap as the latest has a higher cytokinin intensity (Figure 4.4.3-1c and 4.4.3-1d). Once again this in agreement with the role of cytokinin which is to trigger cell differentiation like in the case of lateral root cap cell identity. Vasculature being in transition from dividing to elongation cells an average ACRO ratio involving both hormones was expected. Auxin transcriptional outputs in the epidermis were in agreement with previous study (Lewis, Negi et al. 2011). Epidermal auxin is involved in key aspects of plant development and responses such as root hair elongation (Santelia, Vincenzetti et al. 2005) and gravitropism (Swarup, Kramer et al. 2005).

The ACRO ratios after exogenous hormone treatments were calculated to quantify the responsiveness specificity in the different cell types. To evaluate the sensitivity of the

AuxCysensor line, we selected the lowest and highest treatment concentrations (10nM BAP and 1µM BAP) for cytokinin and (10nM NAA or 100µM NAA) for auxin. No differences between 10nM BAP and 1µM BAP treatments in all the root tissues considered (Figure 4.4.4-1a to 4.4.4-1e). This suggests that 10nM BAP might be enough to trigger a cytokinin response maxima, or that beyond 10nM BAP, a negative feedback might happen. Considering that auxin and cytokinin are interdependently regulating their concentration in the RAM, comparisons between treatments should be taken with caution and emphasize should be made on the comparison from treated to mock treated roots.

Columella cells are in an advanced differentiation state and their average ACRO ratios were relatively low and were not significatively impacted by any of the treatments compared to mock treated roots (Figure 4.4.4-1a). These cells don't seem to be responsive to the treatments applied. This cellular identity is associated with a low auxin and cytokinin responsiveness that might be maintained and required to ensure their function. In the lateral root cap, a dose dependent response was observed after the NAA treatment (Figure 4.4.4-1b). Although lateral root cap cells are fully mature, they are still sensitive to both hormones. They responded to the NAA and BAP treatment, even though this cell type had a relatively low average ACRO ratio in the mock treated roots (Figure 4.4.4-1b).

Lateral root cap cells presented an auxin and cytokinin sensitivity, that might be involved in their function. The epidermis seems to be less sensitive to both hormones, as only high hormonal treatment concentrations induced a response in the AuxCysensor

lines (Figure 4.4.4-1c). The QC of mock treated roots is characterized by the highest average ACRO ratio. BAP treatments reduced the high auxin response (Figure 4.4.4-1d) and suggests a sensitivity to cytokinin. QC of 10nM NAA treated roots had a similar average ACRO ratio as in the QC of mock treated roots (Figure 4.4.4-1d). The average ACRO ratio being already very high in the mock treated root QC, this suggests that the auxin might be plateaued. Indeed, Hayashi et al 2014 did not report a visual increase of the auxin transcriptional output in the QC after a 10nM NAA root treatment (Hayashi, Nakamura et al. 2014). Surprisingly, 100µMNAA treated roots had a lower average ACRO compared to mock treated roots (Figure 4.4.4-1d). This might be due to negative feedback regulatory mechanisms in order to maintain the auxin maxima within physiological concentration in the RAM.

In the vasculature, BAP treated roots had a lower average ACRO ratio, 10nM NAA treated roots had a higher average ratio, but 100µM NAA treated roots had a similar average ratio compared to the mock treated ones (Figure 4.4.4-1e). Thus, vasculature cells were responsive to BAP treatments and 100nM NAA treatment which makes sense as they relied on this sensitivity to both hormones to acquire new identities during their migration out of the meristem. 100µM NAA treatment did not induced a higher ACRO ratio but it induced a significatively higher number of cells providing a signal in the vasculature (Figure 4.4.4-1e and 5e).

Interestingly, this is the only cell type for which a treatment had induced an altered number of nuclei detected compared to the mock treated roots. The vasculature of

100µM NAA treated roots presented a significantly higher number of cells reporting an output compared to the mock treated roots (Figure 4.4.4-2e). Considering that cells within the vasculature were transitioning from an active cell division state associated with high auxin and low cytokinin to an elongation state correlated with less auxin and more cytokinin it is not surprising that the cells remained auxin sensitive (Dello Ioio, Linhares et al. 2007). The cells detected were most likely composed of a gradient of cells going from cell dividing to cell elongating and they might have different auxin sensitivities. Therefore, the highest number of cells detected is probably composed of a population of cells having different sensitivities. This could explain why the average ACRO ratio in the vasculature at 100µM NAA is not significantly different from the ones present in roots treated with 10nM NAA or mock treated roots.

To summarize, the different cell types at the exception of the columella responded to the hormonal treatment. These results agreed with Tobisova et al., 2017 that also reported an increased cytokinin transcriptional outputs after BAP treatment in the lateral root cap, quiescent center, vasculature and epidermis (Dobisova, Hrdinova et al. 2017). Moreover, similar to our results, higher auxin transcriptional outputs after NAA treatment in the lateral root cap, the epidermis and the vasculature were also previously reported (Hayashi, Nakamura et al. 2014).

This helped to validate the accuracy of the methodology and the sensitivity of the AuxCysensor line. Additionally, the different ACRO ratios observed in different cell types concurs with the gradient of cytokinin observed along the root tip axe and the cell

type specific auxin/CK antagonistic relationship previously described (Antoniadi, Plačková et al. 2015). Furthermore, we reported the presence of specific average ACRO ratios being associated with specific cell types and mostly likely responsible of their identity. These ratios seem to be the driving force of plant development and to dictate plant cell and plant development status. It would be interesting to look at known auxin and/or cytokinin mutants with developmental phenotypes to characterize these in light of both hormones individually as well as their average ACRO ratios.

Arabidopsis leaf epidermis imaging of concomitant auxin and cytokinin outputs was realized for the first time. Interestingly, cytokinin output seems to be associated with guard cells and the auxin to leaf epidermis (Figure 4.4.1-1c). As both of these cell types are differentiated and have a low division rate, this might indicate a potential involvement of these hormones in the regulation of physiological processes. The role played by auxin and cytokinin in stomatal opening and closure is ambiguous and cytokinin has been proposed to regulate the differentiation of stomatal cell lineages (Daszkowska-Golec and Szarejko 2013). Hence, the AuxCysensor can not only be used to assess auxin and cytokinin roles in plant development, but it also can be used to study their function.

Here, leaf epidermal imaging gave an overview of the capability of the technique: auxin and cytokinin outputs imaging of intact plants to study their function *in vivo*. It would be interesting to place the AuxCysensor lines under (a)biotic stresses to observe the cell type ACRO ratios responses and if they are associated with stomal opening and closure. Such a philosophy could be extended to other plant functions in which auxin and

cytokinin transcriptional activity is important or ignored as long as imaging techniques allows it.

The AuxCysensor was then evaluated in Medicago, a model plant of the symbiosis between rhizobia and legumes to assess auxin/CK root specificities and auxin and cytokinin requirements involved in nodule development. Medicago ACROs ratios patterns were similar in lateral and primary root tips (Figure 4.4.5-1c and 4.4.5-1e and figure 4.4.6-1c and 4.4.6-1e): low the columella, high in the QC and low in the vasculature. Note that there was a substantial variation in lateral root tip vasculature tissues and imaging a larger number of roots should provide a better representation of the ACRO ratios in this cell type.

Additionally, these patterns were also observed in Arabidopsis and soybean primary root tip. In the case of soybean primary root tip and Medicago primary and lateral root tips, ACRO ratios in the columella (Figure 4.4.5-1c and 4.4.5-1c; Figure 4.4.6-1c and 4.4.6-1e; (Fisher, Gaillard et al. 2018)) and vasculature (Figure 4.4.5-1c and 4.4.5-1e; Figure 4.4.6-1c and 4.4.6-1e; (Fisher, Gaillard et al. 2018)) were lower than 1, but not in the case of Arabidopsis (Figure 4.4.3-1b). This indicates that similar tissues types ensuring similar biological functions have slightly different hormonal sensitiveness, especially in the case of cytokinin. However, the overall pattern is identical, justifying the importance of considering auxin and cytokinin as a ratio and not individually. That observation was also observed in the case of lateral root primordia emergence.

Fisher et al., 2018 described this process being associated with a specific cytokinin enrichment in newly root cap cells in soybean (Fisher, Gaillard et al. 2018). Here, non-emerged stage V Medicago primordia were primarily auxin enriched (Figure 4.4.6-2a, 4.4.6-2d and 4.4.6-2f) like in soybean (Fisher, Gaillard et al. 2018). However, Medicago stage VI emerged lateral root primordia were not presenting the cytokinin accumulation in root cap cells and nascent vasculature contrary to soybean (Fisher, Gaillard et al. 2018). Consequently, it appears that cytokinin sensitivity is not only species but also organ specific. The Medicago ACRO patterns being overall consistent with other plant species and literature reports, the accuracy of the methodology was validated, and we applied it to Medicago nodules for which less is known about auxin and cytokinin.

Medicago produces indeterminate nodules type. These nodules have a persistent apical meristem that maintains mitotic activity and sustains nodule growth resulting in oblong nodule shape (Figure 4.4.7-1a). On the contrary, determinate nodules possess a transient meristem that initiates nodule organogenesis but ceases mitotic activity during nodule development resulting in a spherical nodule. Despite this difference, both nodules share similar functions ensured by two tissue types. Nitrogen is fixated by rhizobia in the infection zone and nutrients are exchanged between the infection zone and the rest of the plant tissues via vascular bundles. Fisher et al 2018 reported that these two tissues had specific auxin/ck relative ratios in determinate type nodules of soybean pre-mature

nodules (Fisher, Gaillard et al. 2018). We decided to study if these traits were conserved in indeterminate and images AuxCysensor mature nodules.

Mature Medicago nodule have a higher average ACRO ratio in the apical meristem compared to the infection zone. Even though auxin and cytokinin have been reported in indeterminate nodule apical meristem (Plet, Wasson et al. 2011, Kohlen, Ng et al. 2018), we reported that auxin transcriptional outputs are relatively higher than cytokinin ones. As mentioned, the presence of auxin in the meristem agreed with previous reports (Ng and Mathesius 2018) and is in agreement with auxin function in indeterminate nodule meristem: ensuring continuous nodule growth.

Indeed, root and nodule meristems both ensure cell division to generate organ growth and this activity relies on auxin enrichment. Similarly to soybean, the infection zone of Medicago nodules presented a low average ACRO ratio (Figure 4.4.7-1c; (Fisher, Gaillard et al. 2018)). Additionally, vascular bundles of Medicago were associated with a high ACRO ratios (Figure 4.4.7-1d) as previously observed (Ng and Mathesius 2018) and observed in soybean (Fisher, Gaillard et al. 2018). Hence, even though soybean and Medicago have different nodule types, the same tissue types with similar functions and are associated with similar aux/CK balance.

Multi-photon microscopy combined with the AuxCysensor line strategy enables to image in a non-destructive way living tissue and various developmental processes can be followed over time. This is particularly important in contexts where both hormones are

involved in developmental and/or functional processes, but their relationships are ignored or unclear. We demonstrated that specific ACRO ratio were associated with specific cell type in Arabidopsis and Medicago roots. Moreover, these specific ACRO ratios were associated with specific function (e.g. high average ACRO ratio associated with meristematic activity). Additionally, we demonstrated how the methodology can be to study plant development processes like LRP emergence where slight ACRO changes are associated with drastic developmental changes. Finally, we illustrated how the AuxCysensor lines could be used to study physiological processes such as stomata opening and closure where specific ACRO ratios might be crucial to control.

Concomitant auxin and cytokinin output quantification in processes where unknown auxin/ck relative ratio regulates specific developmental programs could fill these gaps in knowledge and provide a wide range of discoveries and application. Stable AuxCysensor line have been obtained for *Arabidopsis thaliana* and *Medicago truncatula* and are currently being developed in wheat (*Triticum aestivum*), tomato (*Solanum lycopersicum*), soybean and peanut (*Arachis hypogaea*). Additionally, the AuxCysensor can be used in composite plant (Fisher, Gaillard et al. 2018) and our lab have used it in *Agrobacterium*-mediated transient expression in tobacco leaves (unpublished).

4.6. References

Abdel-Lateif, K., D. Bogusz and V. Hocher (2012). "The role of flavonoids in the establishment of plant roots endosymbioses with arbuscular mycorrhiza fungi, rhizobia and Frankia bacteria." Plant Signal Behav **7**(6): 636-641.

Adibi, M., S. Yoshida, D. Weijers and C. Fleck (2016). "Centering the Organizing Center in the Arabidopsis thaliana Shoot Apical Meristem by a Combination of Cytokinin Signaling and Self-Organization." PLoS One **11**(2): e0147830.

Antoniadi, I., L. Plačková, B. Simonovik, K. Doležal, C. Turnbull, K. Ljung and O. Novák (2015). "Cell-Type-Specific Cytokinin Distribution within the Arabidopsis Primary Root Apex." The Plant Cell **27**(7): 1955-1967.

Ariel, F., M. Brault-Hernandez, C. Laffont, E. Huault, M. Brault, J. Plet, M. Moison, S. Blanchet, J. L. Ichante, M. Chabaud, S. Carrere, M. Crespi, R. L. Chan and F. Frugier (2012). "Two direct targets of cytokinin signaling regulate symbiotic nodulation in Medicago truncatula." Plant Cell **24**(9): 3838-3852.

Axtell, M. J. (2013). "Classification and comparison of small RNAs from plants." Annu Rev Plant Biol **64**: 137-159.

Barton, M. K. (2010). "Twenty years on: the inner workings of the shoot apical meristem, a developmental dynamo." Dev Biol **341**(1): 95-113.

Benkova, E. and J. Hejatko (2009). "Hormone interactions at the root apical meristem." Plant Mol Biol **69**(4): 383-396.

Bensmihen, S. (2015). "Hormonal Control of Lateral Root and Nodule Development in Legumes." Plants (Basel) **4**(3): 523-547.

Bhatia, N., H. Åhl, H. Jönsson and M. G. Heisler (2019). "Quantitative analysis of auxin sensing in leaf primordia argues against proposed role in regulating leaf dorsoventrality." eLife **8**: e39298.

Boivin, S., C. Fonouni-Farde and F. Frugier (2016). "How Auxin and Cytokinin Phytohormones Modulate Root Microbe Interactions." Frontiers in plant science **7**: 1240-1240.

Boivin, S., T. Kazmierczak, M. Brault, J. Wen, P. Gamas, K. S. Mysore and F. Frugier (2016). "Different cytokinin histidine kinase receptors regulate nodule initiation as well as later nodule developmental stages in Medicago truncatula." Plant Cell Environ **39**(10): 2198-2209.

Bond, L. (1948). "Origin and Development Morphology of Root Nodules of Pisum sativum." Botanical Gazette **109**(4): 411-434.

Boot, K. J. M., A. A. N. van Brussel, T. Tak, H. P. Spaink and J. W. Kijne (1999). "Lipochitin Oligosaccharides from Rhizobium leguminosarum bv. viciae Reduce Auxin Transport Capacity in Vicia sativa subsp. nigra Roots." Molecular Plant-Microbe Interactions® **12**(10): 839-844.

Boualem, A., P. Laporte, M. Jovanovic, C. Laffont, J. Plet, J.-P. Combier, A. Niebel, M. Crespi and F. Frugier (2008). "MicroRNA166 controls root and nodule development in Medicago truncatula." The Plant Journal **54**(5): 876-887.

Breakspear, A., C. Liu, S. Roy, N. Stacey, C. Rogers, M. Trick, G. Morieri, K. S. Mysore, J. Wen, G. E. D. Oldroyd, J. A. Downie and J. D. Murray (2014). "The root hair "infectome" of Medicago truncatula uncovers changes in cell cycle genes and reveals a requirement for Auxin signaling in rhizobial infection." The Plant cell **26**(12): 4680-4701.

Brunoud, G., D. M. Wells, M. Oliva, A. Larrieu, V. Mirabet, A. H. Burrow, T. Beeckman, S. Kepinski, J. Traas, M. J. Bennett and T. Vernoux (2012). "A novel sensor to map auxin response and distribution at high spatio-temporal resolution." Nature **482**(7383): 103-106.

Bustos-Sanmamed, P., G. Mao, Y. Deng, M. Elouet, G. A. Khan, J. Bazin, M. Turner, S. Subramanian, O. Yu, M. Crespi and C. Lelandais-Brière (2013). "Overexpression of miR160 affects root growth and nitrogen-fixing nodule number in Medicago truncatula." Functional Plant Biology **40**(12): 1208-1220.

Cai, Z., Y. Wang, L. Zhu, Y. Tian, L. Chen, Z. Sun, I. Ullah and X. Li (2017). "GmTIR1/GmAFB3-based auxin perception regulated by miR393 modulates soybean nodulation." New Phytologist **215**(2): 672-686.

Capoen, W., J. Den Herder, S. Rombauts, J. De Gussem, A. De Keyser, M. Holsters and S. Goormachtig (2007). "Comparative transcriptome analysis reveals common and specific tags for root hair and crack-entry invasion in Sesbania rostrata." Plant Physiol **144**(4): 1878-1889.

Clark, S. E. (2001). "Cell signalling at the shoot meristem." Nat Rev Mol Cell Biol **2**(4): 276-284.

Clough, S. J. and A. F. Bent (1998). "Floral dip: a simplified method for Agrobacterium-mediated transformation of Arabidopsis thaliana." Plant J **16**(6): 735-743.

Collier, R., B. Fuchs, N. Walter, W. Kevin Lutke and C. G. Taylor (2005). "Ex vitro composite plants: an inexpensive, rapid method for root biology." Plant J **43**(3): 449-457.

Combier, J.-P., F. Frugier, F. de Billy, A. Boualem, F. El-Yahyaoui, S. Moreau, T. Vernié, T. Ott, P. Gamas, M. Crespi and A. Niebel (2006). "MtHAP2-1 is a key transcriptional regulator of symbiotic nodule development regulated by microRNA169 in Medicago truncatula." Genes & development **20**(22): 3084-3088.

Cooper, J. B. and S. R. Long (1994). "Morphogenetic Rescue of Rhizobium meliloti Nodulation Mutants by trans-Zeatin Secretion." The Plant cell **6**(2): 215-225.

D'Haeseleer, K., G. Den Herder, C. Laffont, J. Plet, V. Mortier, C. Lelandais-Briere, S. De Bodt, A. De Keyser, M. Crespi, M. Holsters, F. Frugier and S. Goormachtig (2011). "Transcriptional and post-transcriptional regulation of a NAC1 transcription factor in Medicago truncatula roots." New Phytol **191**(3): 647-661.

Damodaran, S., C. S. Westfall, B. A. Kisely, J. M. Jez and S. Subramanian (2017). "Nodule-Enriched GRETCHEN HAGEN 3 Enzymes Have Distinct Substrate

Specificities and Are Important for Proper Soybean Nodule Development." Int J Mol Sci **18**(12).

Daszkowska-Golec, A. and I. Szarejko (2013). "Open or close the gate - stomata action under the control of phytohormones in drought stress conditions." Frontiers in plant science **4**: 138-138.

Day, R. N. and M. W. Davidson (2009). "The fluorescent protein palette: tools for cellular imaging." Chem Soc Rev **38**(10): 2887-2921.

de Billy, F., C. Grosjean, S. May, M. Bennett and J. V. Cullimore (2001). "Expression studies on AUX1-like genes in Medicago truncatula suggest that auxin is required at two steps in early nodule development." Mol Plant Microbe Interact **14**(3): 267-277.

De Smet, I., T. Tetsumura, B. De Rybel, N. Frei dit Frey, L. Laplaze, I. Casimiro, R. Swarup, M. Naudts, S. Vanneste, D. Audenaert, D. Inze, M. J. Bennett and T. Beeckman (2007). "Auxin-dependent regulation of lateral root positioning in the basal meristem of Arabidopsis." Development **134**(4): 681-690.

Dello Ioio, R., F. S. Linhares, E. Scacchi, E. Casamitjana-Martinez, R. Heidstra, P. Costantino and S. Sabatini (2007). "Cytokinins determine Arabidopsis root-meristem size by controlling cell differentiation." Curr Biol **17**(8): 678-682.

Demina, I. V., P. J. Maity, A. Nagchowdhury, J. L. P. Ng, E. van der Graaff, K. N. Demchenko, T. Roitsch, U. Mathesius and K. Pawlowski (2019). "Accumulation of and Response to Auxins in Roots and Nodules of the Actinorhizal Plant

Datisca glomerata Compared to the Model Legume Medicago truncatula." Frontiers in Plant Science **10**(1085).

Di Giacomo, E., C. Laffont, F. Sciarra, M. A. Iannelli, F. Frugier and G. Frugis (2017). "KNAT3/4/5-like class 2 KNOX transcription factors are involved in Medicago truncatula symbiotic nodule organ development." New Phytol **213**(2): 822-837.

Dobisova, T., V. Hrdinova, C. Cuesta, S. Michlickova, I. Urbankova, R. Hejatkova, P. Zadnikova, M. Pernisova, E. Benkova and J. Hejatko (2017). "Light Controls Cytokinin Signaling via Transcriptional Regulation of Constitutively Active Sensor Histidine Kinase CKI1." Plant Physiol **174**(1): 387-404.

Dolgikh, A. V., A. N. Kirienko, I. A. Tikhonovich, E. Foo and E. A. Dolgikh (2019). "The DELLA Proteins Influence the Expression of Cytokinin Biosynthesis and Response Genes During Nodulation." Frontiers in plant science **10**: 432-432.

Dolgikh, E. A., P. G. Kusakin, A. B. Kitaeva, A. V. Tsyganova, A. N. Kirienko, I. V. Leppyanen, A. V. Dolgikh, E. L. Ilina, K. N. Demchenko, I. A. Tikhonovich and V. E. Tsyganov (2020). "Mutational analysis indicates that abnormalities in rhizobial infection and subsequent plant cell and bacteroid differentiation in pea (Pisum sativum) nodules coincide with abnormal cytokinin responses and localization." Ann Bot.

Ferguson, B. J., A. Indrasumunar, S. Hayashi, M. H. Lin, Y. H. Lin, D. E. Reid and P. M. Gresshoff (2010). "Molecular analysis of legume nodule development and autoregulation." J Integr Plant Biol **52**(1): 61-76.

Ferguson, B. J., E. M. Wiebe, R. J. Neil Emery and F. C. Guinel (2005). "Cytokinin accumulation and an altered ethylene response mediate the pleiotropic phenotype of the pea nodulation mutant R50 (sym16)." Canadian Journal of Botany **83**(8): 989-1000.

Fisher, J., P. Gaillard, C. R. Fellbaum, S. Subramanian and S. Smith (2018). "Quantitative 3D imaging of cell level auxin and cytokinin response ratios in soybean roots and nodules." Plant Cell Environ **41**(9): 2080-2092.

Fletcher, J. C. and E. M. Meyerowitz (2000). "Cell signaling within the shoot meristem." Curr Opin Plant Biol **3**(1): 23-30.

Franssen, H. J., T. T. Xiao, O. Kulikova, X. Wan, T. Bisseling, B. Scheres and R. Heidstra (2015). "Root developmental programs shape the Medicago truncatula nodule meristem." Development **142**(17): 2941-2950.

Friml, J. (2003). "Auxin transport - shaping the plant." Curr Opin Plant Biol **6**(1): 7-12.

Fukuhara, H., Y. Minakawa, S. Akao and K. Minamisawa (1994). "The Involvement of Indole-3-Acetic Acid Produced by Bradyrhizobium elkanii in Nodule Formation." Plant and Cell Physiology **35**(8): 1261-1265.

Gage, D. J. (2004). "Infection and invasion of roots by symbiotic, nitrogen-fixing rhizobia during nodulation of temperate legumes." Microbiol Mol Biol Rev **68**(2): 280-300.

Gamas, P., M. Brault, M. F. Jardinaud and F. Frugier (2017). "Cytokinins in Symbiotic Nodulation: When, Where, What For?" Trends Plant Sci **22**(9): 792-802.

Gao, Y. and M. L. Kilfoil (2009). "Accurate detection and complete tracking of large populations of features in three dimensions." Opt Express **17**(6): 4685-4704.

Gauthier-Coles, C., R. G. White and U. Mathesius (2018). "Nodulating Legumes Are Distinguished by a Sensitivity to Cytokinin in the Root Cortex Leading to Pseudonodule Development." Front Plant Sci **9**: 1901.

Ge, L., W. Peer, S. Robert, R. Swarup, S. Ye, M. Prigge, J. D. Cohen, J. Friml, A. Murphy, D. Tang and M. Estelle (2010). "Arabidopsis ROOT UVB SENSITIVE2/WEAK AUXIN RESPONSE1 is required for polar auxin transport." Plant Cell **22**(6): 1749-1761.

Gonzalez-Rizzo, S., M. Crespi and F. Frugier (2006). "The Medicago truncatula CRE1 Cytokinin Receptor Regulates Lateral Root Development and Early Symbiotic Interaction with Sinorhizobium meliloti." The Plant Cell **18**(10): 2680-2693.

Guan, D., N. Stacey, C. Liu, J. Wen, K. S. Mysore, I. Torres-Jerez, T. Vernié, M. Tadege, C. Zhou, Z.-y. Wang, M. K. Udvardi, G. E. D. Oldroyd and J. D. Murray (2013). "Rhizobial infection is associated with the development of peripheral vasculature in nodules of Medicago truncatula." Plant physiology **162**(1): 107-115.

Harper, J. E. (1974). "Soil and Symbiotic Nitrogen Requirements for Optimum Soybean Production1." Crop Science **14**(2): cropsci1974.0011183X001400020026x.

Hayashi, K., S. Nakamura, S. Fukunaga, T. Nishimura, M. K. Jenness, A. S. Murphy, H. Motose, H. Nozaki, M. Furutani and T. Aoyama (2014). "Auxin transport sites are

visualized in planta using fluorescent auxin analogs." Proc Natl Acad Sci U S A **111**(31): 11557-11562.

Heckmann, A. B., N. Sandal, A. S. Bek, L. H. Madsen, A. Jurkiewicz, M. W. Nielsen, L. Tirichine and J. Stougaard (2011). "Cytokinin induction of root nodule primordia in Lotus japonicus is regulated by a mechanism operating in the root cortex." Mol Plant Microbe Interact **24**(11): 1385-1395.

Heisler, M. G., C. Ohno, P. Das, P. Sieber, G. V. Reddy, J. A. Long and E. M. Meyerowitz (2005). "Patterns of auxin transport and gene expression during primordium development revealed by live imaging of the Arabidopsis inflorescence meristem." Curr Biol **15**(21): 1899-1911.

Held, M., H. Hou, M. Miri, C. Huynh, L. Ross, M. S. Hossain, S. Sato, S. Tabata, J. Perry, T. L. Wang and K. Szczyglowski (2014). "Lotus japonicus Cytokinin Receptors Work Partially Redundantly to Mediate Nodule Formation." The Plant Cell **26**(2): 678-694.

Herrbach, V., X. Chirinos, D. Rengel, K. Agbevenou, R. Vincent, S. Pateyron, S. Huguet, S. Balzergue, A. Pasha, N. Provart, C. Gough and S. Bensmihen (2017). "Nod factors potentiate auxin signaling for transcriptional regulation and lateral root formation in Medicago truncatula." Journal of experimental botany **68**(3): 569-583.

Herrbach, V., C. Remblière, C. Gough and S. Bensmihen (2014). "Lateral root formation and patterning in Medicago truncatula." Journal of Plant Physiology **171**(3): 301-310.

Hirsch, A. M., T. V. Bhuvaneswari, J. G. Torrey and T. Bisseling (1989). "Early nodulin genes are induced in alfalfa root outgrowths elicited by auxin transport inhibitors." Proceedings of the National Academy of Sciences of the United States of America **86**(4): 1244-1248.

Hofferek, V., A. Mendrinna, N. Gaude, F. Krajinski and E. A. Devers (2014). "MiR171h restricts root symbioses and shows like its target NSP2 a complex transcriptional regulation in Medicago truncatula." BMC Plant Biology **14**(1): 199.

Huo, X., E. Schnabel, K. Hughes and J. Frugoli (2006). "RNAi Phenotypes and the Localization of a Protein::GUS Fusion Imply a Role for Medicago truncatula PIN Genes in Nodulation." Journal of Plant Growth Regulation **25**(2): 156-165.

Hwang, I., J. Sheen and B. Muller (2012). "Cytokinin signaling networks." Annu Rev Plant Biol **63**: 353-380.

Ilina, E. L., A. S. Kiryushkin, V. A. Semenova, N. P. Demchenko, K. Pawlowski and K. N. Demchenko (2018). "Lateral root initiation and formation within the parental root meristem of Cucurbita pepo: is auxin a key player?" Annals of botany **122**(5): 873-888.

Jardinaud, M. F., S. Boivin, N. Rodde, O. Catrice, A. Kisiala, A. Lepage, S. Moreau, B. Roux, L. Cottret, E. Sallet, M. Brault, R. J. Emery, J. Gouzy, F. Frugier and P.

Gamas (2016). "A Laser Dissection-RNAseq Analysis Highlights the Activation of Cytokinin Pathways by Nod Factors in the Medicago truncatula Root Epidermis." Plant Physiol **171**(3): 2256-2276.

Jones, B., S. A. Gunneras, S. V. Petersson, P. Tarkowski, N. Graham, S. May, K. Dolezal, G. Sandberg and K. Ljung (2010). "Cytokinin regulation of auxin synthesis in Arabidopsis involves a homeostatic feedback loop regulated via auxin and cytokinin signal transduction." Plant Cell **22**(9): 2956-2969.

Joshi, P. A., G. Caetano-Anollés, E. T. Graham and P. M. Gresshoff (1991). "Ontogeny and ultrastructure of spontaneous nodules in alfalfa (Medicago sativa)." Protoplasma **162**(1): 1-11.

Kohlen, W., J. L. P. Ng, E. E. Deinum and U. Mathesius (2017). "Auxin transport, metabolism, and signalling during nodule initiation: indeterminate and determinate nodules." Journal of Experimental Botany **69**(2): 229-244.

Kohlen, W., J. L. P. Ng, E. E. Deinum and U. Mathesius (2018). "Auxin transport, metabolism, and signalling during nodule initiation: indeterminate and determinate nodules." J Exp Bot **69**(2): 229-244.

Kondo, Y., T. Tamaki and H. Fukuda (2014). "Regulation of xylem cell fate." Front Plant Sci **5**: 315.

Koornneef, M. and D. Meinke (2010). "The development of Arabidopsis as a model plant." The Plant Journal **61**(6): 909-921.

Kouchi, H., H. Imaizumi-Anraku, M. Hayashi, T. Hakoyama, T. Nakagawa, Y. Umehara, N. Suganuma and M. Kawaguchi (2010). "How many peas in a pod? Legume genes responsible for mutualistic symbioses underground." Plant Cell Physiol **51**(9): 1381-1397.

Kurakawa, T., N. Ueda, M. Maekawa, K. Kobayashi, M. Kojima, Y. Nagato, H. Sakakibara and J. Kyozuka (2007). "Direct control of shoot meristem activity by a cytokinin-activating enzyme." Nature **445**(7128): 652-655.

Laplaze, L., E. Benkova, I. Casimiro, L. Maes, S. Vanneste, R. Swarup, D. Weijers, V. Calvo, B. Parizot, M. B. Herrera-Rodriguez, R. Offringa, N. Graham, P. Doumas, J. Friml, D. Bogusz, T. Beeckman and M. Bennett (2007). "Cytokinins act directly on lateral root founder cells to inhibit root initiation." Plant Cell **19**(12): 3889-3900.

Lerouge, P., P. Roche, C. Faucher, F. Maillet, G. Truchet, J. C. Prome and J. Denarie (1990). "Symbiotic host-specificity of Rhizobium meliloti is determined by a sulphated and acylated glucosamine oligosaccharide signal." Nature **344**(6268): 781-784.

Lewis, D. R., S. Negi, P. Sukumar and G. K. Muday (2011). "Ethylene inhibits lateral root development, increases IAA transport and expression of PIN3 and PIN7 auxin efflux carriers." Development **138**(16): 3485-3495.

Libbenga, K. R., F. van Iren, R. J. Bogers and M. F. Schraag-Lamers (1973). "The role of hormones and gradients in the initiation of cortex proliferation and nodule formation in Pisum sativum L." Planta **114**(1): 29-39.

Livak, K. J. and T. D. Schmittgen (2001). "Analysis of relative gene expression data using real-time quantitative PCR and the 2(-Delta Delta C(T)) Method." Methods **25**(4): 402-408.

Lorteau, M. A., B. J. Ferguson and F. C. Guinel (2001). "Effects of cytokinin on ethylene production and nodulation in pea (Pisum sativum) cv. Sparkle." Physiol Plant **112**(3): 421-428.

Mallory, A. C., D. P. Bartel and B. Bartel (2005). "MicroRNA-directed regulation of Arabidopsis AUXIN RESPONSE FACTOR17 is essential for proper development and modulates expression of early auxin response genes." The Plant cell **17**(5): 1360-1375.

Marin, E., V. Jouannet, A. Herz, A. S. Lokerse, D. Weijers, H. Vaucheret, L. Nussaume, M. D. Crespi and A. Maizel (2010). "miR390, Arabidopsis TAS3 tasiRNAs, and their AUXIN RESPONSE FACTOR targets define an autoregulatory network quantitatively regulating lateral root growth." Plant Cell **22**(4): 1104-1117.

Marin, E., V. Jouannet, A. Herz, A. S. Lokerse, D. Weijers, H. Vaucheret, L. Nussaume, M. D. Crespi and A. Maizel (2010). "miR390, Arabidopsis TAS3 tasiRNAs, and their AUXIN RESPONSE FACTOR targets define an autoregulatory network quantitatively regulating lateral root growth." The Plant cell **22**(4): 1104-1117.

Markwardt, M. L., G.-J. Kremers, C. A. Kraft, K. Ray, P. J. C. Cranfill, K. A. Wilson, R. N. Day, R. M. Wachter, M. W. Davidson and M. A. Rizzo (2011). "An improved cerulean fluorescent protein with enhanced brightness and reduced reversible photoswitching." PloS one **6**(3): e17896-e17896.

Mashiguchi, K., K. Tanaka, T. Sakai, S. Sugawara, H. Kawaide, M. Natsume, A. Hanada, T. Yaeno, K. Shirasu, H. Yao, P. McSteen, Y. Zhao, K.-i. Hayashi, Y. Kamiya and H. Kasahara (2011). "The main auxin biosynthesis pathway in Arabidopsis." Proceedings of the National Academy of Sciences of the United States of America **108**(45): 18512-18517.

Mathesius, U., H. R. Schlaman, H. P. Spaink, C. Of Sautter, B. G. Rolfe and M. A. Djordjevic (1998). "Auxin transport inhibition precedes root nodule formation in white clover roots and is regulated by flavonoids and derivatives of chitin oligosaccharides." Plant J **14**(1): 23-34.

Mathesius, U., J. J. Weinman, B. G. Rolfe and M. A. Djordjevic (2000). "Rhizobia can induce nodules in white clover by "hijacking" mature cortical cells activated during lateral root development." Mol Plant Microbe Interact **13**(2): 170-182.

Miri, M., P. Janakirama, M. Held, L. Ross and K. Szczyglowski (2016). "Into the Root: How Cytokinin Controls Rhizobial Infection." Trends Plant Sci **21**(3): 178-186.

Mortier, V., A. Wasson, P. Jaworek, A. De Keyser, M. Decroos, M. Holsters, P. Tarkowski, U. Mathesius and S. Goormachtig (2014). "Role of LONELY GUY

genes in indeterminate nodulation on Medicago truncatula." New Phytol **202**(2): 582-593.

Muller, C. J., E. Larsson, L. Spichal and E. Sundberg (2017). "Cytokinin-Auxin Crosstalk in the Gynoecial Primordium Ensures Correct Domain Patterning." Plant Physiol **175**(3): 1144-1157.

Muller, D. and O. Leyser (2011). "Auxin, cytokinin and the control of shoot branching." Ann Bot **107**(7): 1203-1212.

Murray, J. D., B. J. Karas, S. Sato, S. Tabata, L. Amyot and K. Szczyglowski (2007). "A Cytokinin Perception Mutant Colonized by Rhizobium in the Absence of Nodule Organogenesis." Science **315**(5808): 101-104.

Nadzieja, M., S. Kelly, J. Stougaard and D. Reid (2018). "Epidermal auxin biosynthesis facilitates rhizobial infection in Lotus japonicus." Plant J **95**(1): 101-111.

Nadzieja, M., J. Stougaard and D. Reid (2019). "A Toolkit for High Resolution Imaging of Cell Division and Phytohormone Signaling in Legume Roots and Root Nodules." Frontiers in Plant Science **10**(1000).

Newcomb, W. (1976). "A correlated light and electron microscopic study of symbiotic growth and differentiation in Pisum sativum root nodules." Canadian Journal of Botany **54**(18): 2163-2186.

Ng, J. L., S. Hassan, T. T. Truong, C. H. Hocart, C. Laffont, F. Frugier and U. Mathesius (2015). "Flavonoids and Auxin Transport Inhibitors Rescue Symbiotic Nodulation

in the Medicago truncatula Cytokinin Perception Mutant cre1." Plant Cell **27**(8): 2210-2226.

Ng, J. L. P. and U. Mathesius (2018). "Acropetal Auxin Transport Inhibition Is Involved in Indeterminate But Not Determinate Nodule Formation." Frontiers in plant science **9**: 169-169.

Nizampatnam, N. R., S. J. Schreier, S. Damodaran, S. Adhikari and S. Subramanian (2015). "microRNA160 dictates stage-specific auxin and cytokinin sensitivities and directs soybean nodule development." Plant J **84**(1): 140-153.

Oldroyd, G. E. (2013). "Speak, friend, and enter: signalling systems that promote beneficial symbiotic associations in plants." Nat Rev Microbiol **11**(4): 252-263.

Oldroyd, G. E., J. D. Murray, P. S. Poole and J. A. Downie (2011). "The rules of engagement in the legume-rhizobial symbiosis." Annu Rev Genet **45**: 119-144.

Op den Camp, R. H., S. De Mita, A. Lillo, Q. Cao, E. Limpens, T. Bisseling and R. Geurts (2011). "A phylogenetic strategy based on a legume-specific whole genome duplication yields symbiotic cytokinin type-A response regulators." Plant Physiol **157**(4): 2013-2022.

Parizotto, E. A., P. Dunoyer, N. Rahm, C. Himber and O. Voinnet (2004). "In vivo investigation of the transcription, processing, endonucleolytic activity, and functional relevance of the spatial distribution of a plant miRNA." Genes & development **18**(18): 2237-2242.

Penmetsa, R. V. and D. R. Cook (1997). "A Legume Ethylene-Insensitive Mutant Hyperinfected by Its Rhizobial Symbiont." Science **275**(5299): 527-530.

Penmetsa, R. V., P. Uribe, J. Anderson, J. Lichtenzveig, J. C. Gish, Y. W. Nam, E. Engstrom, K. Xu, G. Sckisel, M. Pereira, J. M. Baek, M. Lopez-Meyer, S. R. Long, M. J. Harrison, K. B. Singh, G. B. Kiss and D. R. Cook (2008). "The Medicago truncatula ortholog of Arabidopsis EIN2, sickle, is a negative regulator of symbiotic and pathogenic microbial associations." Plant J **55**(4): 580-595.

Pernisová, M., P. Klíma, J. Horák, M. Válková, J. Malbeck, P. Souček, P. Reichman, K. Hoyerová, J. Dubová, J. Friml, Za, E. žímalová and J. Hejátko (2009). "Cytokinins modulate auxin-induced organogenesis in plants via regulation of the auxin efflux." Proceedings of the National Academy of Sciences **106**(9): 3609-3614.

Plet, J., A. Wasson, F. Ariel, C. Le Signor, D. Baker, U. Mathesius, M. Crespi and F. Frugier (2011). "MtCRE1-dependent cytokinin signaling integrates bacterial and plant cues to coordinate symbiotic nodule organogenesis in Medicago truncatula." Plant J **65**(4): 622-633.

Podlesakova, K., J. Fardoux, D. Patrel, K. Bonaldi, O. Novak, M. Strnad, E. Giraud, L. Spichal and N. Nouwen (2013). "Rhizobial synthesized cytokinins contribute to but are not essential for the symbiotic interaction between photosynthetic Bradyrhizobia and Aeschynomene legumes." Mol Plant Microbe Interact **26**(10): 1232-1238.

Reid, D., M. Nadzieja, O. Novák, A. B. Heckmann, N. Sandal and J. Stougaard (2017). "Cytokinin Biosynthesis Promotes Cortical Cell Responses during Nodule Development." Plant Physiology **175**(1): 361-375.

Reid, D. E., A. B. Heckmann, O. Novák, S. Kelly and J. Stougaard (2016). "CYTOKININ OXIDASE/DEHYDROGENASE3 Maintains Cytokinin Homeostasis during Root and Nodule Development in Lotus japonicus." Plant Physiology **170**(2): 1060-1074.

Relic, B., F. Talmont, J. Kopcinska, W. Golinowski, J. C. Prome and W. J. Broughton (1993). "Biological activity of Rhizobium sp. NGR234 Nod-factors on Macroptilium atropurpureum." Mol Plant Microbe Interact **6**(6): 764-774.

Riou-Khamlichi, C., R. Huntley, A. Jacqmard and J. A. Murray (1999). "Cytokinin activation of Arabidopsis cell division through a D-type cyclin." Science **283**(5407): 1541-1544.

RODRIGUEZ-BARRUECO, C. and F. B. CASTRO (1973). "Cytokinin-induced Pseudonodules on Alnus glutinosa." Physiologia Plantarum $V 29(2).

Roy, S., F. Robson, J. Lilley, C.-W. Liu, X. Cheng, J. Wen, S. Walker, J. Sun, D. Cousins, C. Bone, M. J. Bennett, J. A. Downie, R. Swarup, G. Oldroyd and J. D. Murray (2017). "MtLAX2, a Functional Homologue of the Arabidopsis Auxin Influx Transporter AUX1, Is Required for Nodule Organogenesis." Plant Physiology **174**(1): 326-338.

Sablowski, R. (2007). "The dynamic plant stem cell niches." Curr Opin Plant Biol **10**(6): 639-644.

Santelia, D., V. Vincenzetti, E. Azzarello, L. Bovet, Y. Fukao, P. Düchtig, S. Mancuso, E. Martinoia and M. Geisler (2005). "MDR-like ABC transporter AtPGP4 is involved in auxin-mediated lateral root and root hair development." FEBS Letters **579**(24): 5399-5406.

Santi, C., D. Bogusz and C. Franche (2013). "Biological nitrogen fixation in non-legume plants." Ann Bot **111**(5): 743-767.

Shen, C., R. Yue, T. Sun, L. Zhang, L. Xu, S. Tie, H. Wang and Y. Yang (2015). "Genome-wide identification and expression analysis of auxin response factor gene family in Medicago truncatula." Front Plant Sci **6**: 73.

Skoog, F. and C. O. Miller (1957). "Chemical regulation of growth and organ formation in plant tissues cultured in vitro." Symp Soc Exp Biol **11**: 118-130.

Smet, W., I. Sevilem, M. A. de Luis Balaguer, B. Wybouw, E. Mor, S. Miyashima, B. Blob, P. Roszak, T. B. Jacobs, M. Boekschoten, G. Hooiveld, R. Sozzani, Y. Helariutta and B. De Rybel (2019). "DOF2.1 Controls Cytokinin-Dependent Vascular Cell Proliferation Downstream of TMO5/LHW." Curr Biol **29**(3): 520-529.e526.

Stahl, Y. and R. Simon (2010). "Plant primary meristems: shared functions and regulatory mechanisms." Curr Opin Plant Biol **13**(1): 53-58.

Staswick, P. E., B. Serban, M. Rowe, I. Tiryaki, M. T. Maldonado, M. C. Maldonado and W. Suza (2005). "Characterization of an Arabidopsis enzyme family that conjugates amino acids to indole-3-acetic acid." Plant Cell **17**(2): 616-627.

Su, Y. H., Y. B. Liu and X. S. Zhang (2011). "Auxin-cytokinin interaction regulates meristem development." Mol Plant **4**(4): 616-625.

Subach, O. M., P. J. Cranfill, M. W. Davidson and V. V. Verkhusha (2011). "An enhanced monomeric blue fluorescent protein with the high chemical stability of the chromophore." PLoS One **6**(12): e28674.

Subramanian, S., Y. Fu, R. Sunkar, W. B. Barbazuk, J. K. Zhu and O. Yu (2008). "Novel and nodulation-regulated microRNAs in soybean roots." BMC Genomics **9**: 160.

Suzaki, T., M. Ito and M. Kawaguchi (2013). "Genetic basis of cytokinin and auxin functions during root nodule development." Front Plant Sci **4**: 42.

Suzaki, T., K. Yano, M. Ito, Y. Umehara, N. Suganuma and M. Kawaguchi (2012). "Positive and negative regulation of cortical cell division during root nodule development in Lotus japonicus is accompanied by auxin response." Development **139**(21): 3997-4006.

Swarup, R., E. M. Kramer, P. Perry, K. Knox, H. M. Leyser, J. Haseloff, G. T. Beemster, R. Bhalerao and M. J. Bennett (2005). "Root gravitropism requires lateral root cap and epidermal cells for transport and response to a mobile auxin signal." Nat Cell Biol **7**(11): 1057-1065.

Szczyglowski, K., R. S. Shaw, J. Wopereis, S. Copeland, D. Hamburger, B. Kasiborski, F. B. Dazzo and F. J. de Bruijn (1998). "Nodule Organogenesis and Symbiotic Mutants of the Model Legume Lotus japonicus." Molecular Plant-Microbe Interactions® **11**(7): 684-697.

Takanashi, K., A. Sugiyama and K. Yazaki (2011). "Involvement of auxin distribution in root nodule development of Lotus japonicus." Planta **234**(1): 73-81.

Taylor-Teeples, M., A. Lanctot and J. L. Nemhauser (2016). "As above, so below: Auxin's role in lateral organ development." Dev Biol **419**(1): 156-164.

Teale, W. D., I. A. Paponov and K. Palme (2006). "Auxin in action: signalling, transport and the control of plant growth and development." Nat Rev Mol Cell Biol **7**(11): 847-859.

Tirichine, L., N. Sandal, L. H. Madsen, S. Radutoiu, A. S. Albrektsen, S. Sato, E. Asamizu, S. Tabata and J. Stougaard (2007). "A gain-of-function mutation in a cytokinin receptor triggers spontaneous root nodule organogenesis." Science **315**(5808): 104-107.

Torres, D., I. Benavidez, F. Donadio, E. Mongiardini, S. Rosas, S. Spaepen, J. Vanderleyden, A. Pencik, O. Novak, M. Strnad, J. Frebortova and F. Cassan (2018). "New insights into auxin metabolism in Bradyrhizobium japonicum." Res Microbiol **169**(6): 313-323.

Towe, K. M. (2002). "Evolution of Nitrogen Fixation." Science **295**(5556): 798-799.

Turner, M., N. R. Nizampatnam, M. Baron, S. Coppin, S. Damodaran, S. Adhikari, S. P. Arunachalam, O. Yu and S. Subramanian (2013). "Ectopic expression of miR160 results in auxin hypersensitivity, cytokinin hyposensitivity, and inhibition of symbiotic nodule development in soybean." Plant Physiol **162**(4): 2042-2055.

Ulmasov, T., J. Murfett, G. Hagen and T. J. Guilfoyle (1997). "Aux/IAA proteins repress expression of reporter genes containing natural and highly active synthetic auxin response elements." The Plant cell **9**(11): 1963-1971.

van Noorden, G. E., T. Kerim, N. Goffard, R. Wiblin, F. I. Pellerone, B. G. Rolfe and U. Mathesius (2007). "Overlap of proteome changes in Medicago truncatula in response to auxin and Sinorhizobium meliloti." Plant Physiol **144**(2): 1115-1131.

van Spronsen, P. C., M. Grønlund, C. P. Bras, H. P. Spaink and J. W. Kijne (2001). "Cell Biological Changes of Outer Cortical Root Cells in Early Determinate Nodulation." Molecular Plant-Microbe Interactions® **14**(7): 839-847.

van Zeijl, A., R. H. Op den Camp, E. E. Deinum, T. Charnikhova, H. Franssen, H. J. Op den Camp, H. Bouwmeester, W. Kohlen, T. Bisseling and R. Geurts (2015). "Rhizobium Lipo-chitooligosaccharide Signaling Triggers Accumulation of Cytokinins in Medicago truncatula Roots." Mol Plant **8**(8): 1213-1226.

Vanstraelen, M., M. Baloban, O. Da Ines, A. Cultrone, T. Lammens, V. Boudolf, S. C. Brown, L. De Veylder, P. Mergaert and E. Kondorosi (2009). "APC/C^{CCS52A} complexes control meristem maintenance in the

Arabidopsis root." Proceedings of the National Academy of Sciences **106**(28): 11806-11811.

Vernoux, T., G. Brunoud, E. Farcot, V. Morin, H. Van den Daele, J. Legrand, M. Oliva, P. Das, A. Larrieu, D. Wells, Y. Guédon, L. Armitage, F. Picard, S. Guyomarc'h, C. Cellier, G. Parry, R. Koumproglou, J. H. Doonan, M. Estelle, C. Godin, S. Kepinski, M. Bennett, L. De Veylder and J. Traas (2011). "The auxin signalling network translates dynamic input into robust patterning at the shoot apex." Molecular Systems Biology **7**(1): 508.

Wang, J.-W., L.-J. Wang, Y.-B. Mao, W.-J. Cai, H.-W. Xue and X.-Y. Chen (2005). "Control of root cap formation by MicroRNA-targeted auxin response factors in Arabidopsis." The Plant cell **17**(8): 2204-2216.

Wang, Y., K. Li, L. Chen, Y. Zou, H. Liu, Y. Tian, D. Li, R. Wang, F. Zhao, B. J. Ferguson, P. M. Gresshoff and X. Li (2015). "MicroRNA167-Directed Regulation of the Auxin Response Factors GmARF8a and GmARF8b Is Required for Soybean Nodulation and Lateral Root Development." Plant physiology **168**(3): 984-999.

Wang, Y., W. Yang, Y. Zuo, L. Zhu, A. H. Hastwell, L. Chen, Y. Tian, C. Su, B. J. Ferguson and X. Li (2019). "GmYUC2a mediates auxin biosynthesis during root development and nodulation in soybean." Journal of experimental botany **70**(12): 3165-3176.

Wasson, A. P., F. I. Pellerone and U. Mathesius (2006). "Silencing the flavonoid pathway in Medicago truncatula inhibits root nodule formation and prevents auxin transport regulation by rhizobia." The Plant cell **18**(7): 1617-1629.

Wybouw, B. and B. De Rybel (2019). "Cytokinin - A Developing Story." Trends Plant Sci **24**(2): 177-185.

Yoshida, S., T. Mandel and C. Kuhlemeier (2011). "Stem cell activation by light guides plant organogenesis." Genes & development **25**(13): 1439-1450.

Zhang, W., R. Swarup, M. Bennett, G. E. Schaller and J. J. Kieber (2013). "Cytokinin induces cell division in the quiescent center of the Arabidopsis root apical meristem." Curr Biol **23**(20): 1979-1989.

Zürcher, E., D. Tavor-Deslex, D. Lituiev, K. Enkerli, P. T. Tarr and B. Müller (2013). "A robust and sensitive synthetic sensor to monitor the transcriptional output of the cytokinin signaling network in planta." Plant physiology **161**(3): 1066-1075.